

Master thesis

The role of criticality in hippocampal circuits for short term memory

Student: Jan Erik Bellingrath

Matriculation number: 108022250229

E-mail: jan.bellingrath@ruhr-uni-bochum.de

Date: 05.12.2024

Degree program: Cognitive Science, M.Sc., Ruhr-University Bochum

1st supervisor: Dr. Tristan Manfred Stöber

2nd supervisor: Prof. Dr. Sen Cheng

Abstract

Neuronal dynamics unfold in the close vicinity of a second order phase transition. This distance to criticality is associated with various variations of computationally and cognitively central properties. Balancing these properties, the brain may adaptively and dynamically self-regulate the distance to criticality in a task-dependent manner. Short-term memory is dependent on the information storage and transmission capabilities of neuronal circuits, which may be optimized in close proximity to criticality – amongst other criticality-enabled short-term memory facilitative computational properties, which are reviewed. Recent intracranial evidence associates the hippocampus closely with short-term memory, consistent with two theoretical perspectives on the hippocampus: Specifically, first, the computation of a conjunctive representation on a temporally receding internal timeline encoding *what* happened *when*; and, second, the implementation of hippocampal short-term memory in terms of a nested theta-gamma code. In order to test whether the hippocampus dynamically and adaptively self-regulates the distance to criticality in a short-term memory task, neuronal recordings from the rodent hippocampal subregions CA1 & CA3 are analyzed with a sub-sampling invariant estimator. While an *even* smaller distance to criticality within the short-term memory task is not associated with an increased performance, the hippocampal distance to criticality is – in accord with expectations – dynamically reduced in the working memory task. Given that criticality is associated with *universality* – the idea that macroscopic dynamics are invariant with respect to changes in microscopic realization across diverse systems – the framework of criticality offers some hope regards generalizations across species.

The code for the statistical analysis & visualizations, including an illustrative Jupyter notebook, can be accessed under:
https://github.com/JanBellingrath/hippocampal_distance_to_criticality_working_memory.

Table of contents

ABSTRACT	2
1. INTRODUCTION: CRITICALITY & COMPUTATION	4
2. THE CRITICAL BRAIN HYPOTHESIS & DYNAMIC ADAPTIVE COMPUTATION.....	6
2.1 THE CRITICAL BRAIN HYPOTHESIS	6
2.2 DYNAMIC ADAPTIVE COMPUTATION.....	8
3. SPATIAL WORKING MEMORY AND THE HIPPOCAMPUS: A RECORD OF THE RECENT PAST	11
3.1 WORKING MEMORY AND THE HIPPOCAMPUS.....	12
3.2 THEORETICAL FRAMEWORKS FOR WORKING MEMORY IN THE HIPPOCAMPUS	15
4. SHORT-TERM MEMORY COMPUTATIONS BENEFIT FROM A SMALLER DISTANCE TO CRITICALITY .	18
4.1 AN INFORMATION-THEORETIC PERSPECTIVE.....	18
4.2 DYNAMICALLY FADING MEMORY	21
5. SUMMARY & HYPOTHESES	23
6. METHODS	24
7. RESULTS.....	27
DISCUSSION	37
REFERENCES.....	41
APPENDIX	60

1. Introduction: Criticality & computation

Liquid water transitions into steam at a high temperature and iron magnetizes under a strong magnetic field. These are examples of phase transitions: The large-scale collective behavior of a system composed of a multitude of elements suddenly undergoes a qualitative change, controlled by a certain control-parameter, such as temperature in the case of boiling water. Critical phase transitions abound in diverse domains – from flocking birds (Cavagna et al., 2010) and earthquakes (Carlson & Langer, 1989), to traffic jams (Nagel & Herrmann, 1993) and crumbled paper (Houle & Sethna, 1996) – with criticality possibly being one of the central ways by which complexity emerges in nature (Bak, 2013; Langton, 1990).

The unique properties of critical systems, as (traditionally) studied in statistical physics, form the basis for conjectures that systems near a phase transition have the highest computational capabilities. Intuitively, subcritical regimes are too rigid for complex computation, as perturbations are quickly erased, and information flow is limited. In contrast, disordered regimes are too erratic, with noise and disturbances spreading uncontrollably, hindering effective information processing. Critical states are believed to balance reliability and flexibility: they enable consistent responses to inputs while maintaining the capacity for diverse outcomes (for reviews in a neuroscientific context, see Beggs & Timme, 2012; Cocchi et al., 2017; O’Byrne & Jerbi, 2022; Tian et al., 2022; Wilting & Priesemann, 2019; for a recent book see Beggs, 2022).

An early example linking criticality to computation is Langton's work on cellular automata (CA) (Langton, 1990). Here, the transition function is uniform for all cells, consisting of update rules specifying the resulting state at each cell from the pattern of states of the neighboring cells at the previous time-step (e.g. one update rule from the transition function may be: if all neighboring cells of x_{ij} are active, x_{ij} itself is active at the next time step). Despite their simplicity, these CAs can exhibit nontrivial behaviors. Wolfram classified them into four categories (Wolfram, 1984): The first two classes are "ordered" CAs, evolving into a homogeneous state (i.e. limit points, Class 1) or stable/periodic structures (i.e. limit cycles, Class 2). Class 3 consists of chaotic CAs, which are sensitive to initial conditions (i.e. strange attractors). Class 4 exhibits complex dynamics, with intricate temporal patterns and long transients. Langton (1990) introduced a parameter, λ , to quantify the state distribution in the transition function: when λ is zero, all transitions lead to one state, while for λ close to one, all possible transitions are equally probable. Langton showed that λ acts as a control parameter for CA dynamics, with behavior shifting from ordered to disordered as λ approaches one. The transition occurs near $\lambda \approx 0.5$ and exhibits features of a second-order phase transition, such as critical slowing

down, and an increased correlation length. Intriguingly, the critical value of λ corresponds to Wolfram's Class 4, some of which can perform universal computation, equivalent to a universal Turing machine (see e.g. Cook, 2004). Thus, Langton conjectured that significant computational capabilities emerge at the phase transition; associating the long transients (i.e. critical slowing down) with information transmission through time, and the increased correlation length with information transmission through space.

While these long transients already suggest a certain form of a purely dynamical short-term memory, cellular automata are simple: Indeed, perhaps they are computationally as simple as it can possibly get. While the purpose of this example was simply as an introduction to the field that studies the intersection of criticality and computation, it may be asked – especially with respect to more neuronally realistic models in this context, such as the Ising model, for which there are a number of ways by which it has been applied to neuronal systems (e.g. O'Byrne & Jerbi, 2022 & references therein): How can findings in such simple models of critical systems ever hope to map onto aspects of more complex systems, such as the brain?

Universality – the invariance of macroscopic dynamics with respect to changes in microscopic variables – is an intrinsic feature of all critical systems. The origin of universality is explained by the renormalization group interpretation of criticality (Wilson, 1975), with the renormalization process involving successive coarse graining's of the dynamics of a system (i.e. "zooming out" to describe it in terms of larger composite components). At criticality, this process converges on a fixed point, resulting in classes of systems that, despite different microscopic parameters, exhibit identical large-scale dynamics (Wilson, 1975). A recent study – in the context of neuronal criticality and working memory – provides evidence for this point by simulating stable, chaotic, and critical dynamics on different intrinsic networks of an *in-silico* brain (Suárez et al., 2021). Despite a number of varying structural properties (such as clustering, betweenness, centrality, and modularity), all networks performed best, and equally well, in a working memory task under critical dynamics: "That is, at criticality, memory capacity transcends topological features and becomes more dependent on global network dynamics" (Suárez et al., 2021). Accordingly, the universality of critical systems is epistemologically advantageous: Indeed, philosophy of science perspectives explicitly motivate the distinct explanatory strategy of *minimal model explanations* in relation to precisely this perspective (Batterman & Rice, 2014).

This master thesis investigates a possible relationship between short-term memory and the distance to criticality in the CA1 and CA3 subregions of the hippocampal formation. After an introduction to the emerging field that is concerned with neuronal criticality (section 2), the functional implication of the hippocampus in short-term memory is reviewed (section 3). Subsequently – and based on numerous

in silico and *in vivo* studies – it is argued that short-term memory may benefit from an increased proximity to the critical point (section 4). After a summary & an explication of the hypotheses (section 5), this theoretical background is followed by a presentation of the methods (section 6), the results (section 7) & a discussion (section 8). In the following, terminologically, ‘short-term memory’ is, for pragmatic reasons, equated with ‘working memory’: While working memory is in the cognitive psychological literature often discussed in terms of additional information *modification* (next to temporary storage), it is empirically not straightforward to dissociate these two constructs (Aben et al., 2012). Pragmatically, furthermore, many authors do not strictly distinguish between these terms and discuss identical, or similar, operational or mathematical constructs in terms of varying psychological descriptors. Given that it is undesirable – yet unavoidable, if only one descriptor were used continuously – to discuss already conducted research in terms of *different* psychological descriptors from the authors of that research, the interchanging use here is intended to abstract away from these interpretational ambiguities.

2. The critical brain hypothesis & dynamic adaptive computation

The *critical brain hypothesis* is the idea that large-scale neuronal dynamics are posed at, or near, the boundary of a critical phase transition (for reviews see Beggs & Timme, 2012; Cocchi et al., 2017; O’Byrne & Jerbi, 2022; Tian et al., 2022; Wilting & Priesemann, 2019; for a recent book see Beggs, 2022). In the following, (i) the critical brain hypothesis will be introduced, (ii) empirical evidence concerning this hypothesis reviewed, and (iii) the recently developed framework of *dynamic adaptive computation* (Wilting, Dehning, Neto, et al., 2018) leveraged as an interpretation of the empirical evidence.

2.1 The critical brain hypothesis

Avalanche criticality is the most common type of criticality in the neuroscience literature; being sometimes also called ‘crackling noise’ (Sethna et al., 2001), or ‘the edge of activity propagation’ (Muñoz, 2018). The two separated phases themselves can be seen in terms of the average number of active postsynaptic neurons following the activity of a given presynaptic neuron (this perspective on criticality is known as the branching model (see e.g. Jensen, 1998; Miranda & Herrmann, 1991;

Pruessner, 2012). Intuitively, if this branching parameter, m , is below 1, activity, A , exponentially recedes over time (h denotes external input). On the other hand, if m is above 1, activity exponentially increases:

$$\langle A_{t+1} | A_t \rangle = mA_t + h\Delta t$$

The branching parameter is associated with the intrinsic timescale of the neuronal dynamics: As m increases towards 1 from below, approaching the critical state – and every neuronal event comes on average closer to causing one other neuronal event – the intrinsic timescale increases ever further (theoretically, diverges to infinity), as the activity reverberates ever-longer in the network (e.g. Murray et al., 2014). This increase in the intrinsic timescale is known as critical slowing down (Scheffer et al., 2012).

$$\tau = -\Delta t / \ln(m)$$

Because at this critical point, $m = 1$, activity neither recedes nor explodes; neuronal avalanches (i.e. chains of neuronal activation) come in all sizes (i.e. they are scale-free or scale- invariant). The slope of this power law distribution over avalanche sizes is expected to be -1.5 for critical branching processes (Pruessner, 2012); and indeed, corresponding power-law distributions of avalanche sizes were found in many experiments.

After the original study by Beggs and Plenz (2003a) which found power-law distributed avalanches in the LFPs of cultured slices, subsequent studies *in vitro* revealed similar distributions in LFPs and spiking activity of cultured dissociated neurons and cortical slices (e.g. Mazzoni et al., 2007; Pasquale et al., 2008; Tetzlaff et al., 2010). Power laws were also found in MEG (e.g. Shriki et al., 2013), EEG (e.g.. Jannesari et al., 2020; Linkenkaer-Hansen et al., 2001) and in fMRI (e.g. Fraiman et al., 2009; Tagliazucchi et al., 2012); as well as in calcium and voltage imaging (Bellay et al., 2015; Ponce-Alvarez et al., 2018) and in LFPs from intracranial depth electrodes (e.g. Priesemann et al., 2013). For reviews see (Beggs & Timme, 2012; Cocchi et al., 2017; O’Byrne & Jerbi, 2022; Tian et al., 2022; Wilting & Priesemann, 2019).

However, it has been argued that coarse measures could sample from overlapping populations, and that this may lead to the (false) detection of power-laws, given the enhanced correlation between measurement sites (Neto et al., 2022). Consistently with this concern, many more fine-grained studies of *in vivo* spiking activity often differ from power-laws; revealing slightly subcritical neuronal dynamics instead (for a review see Wilting & Priesemann, 2019). While it has been objected to this finding that it may result from a possible subsampling effect (Priesemann et al., 2009) power laws are expected to persist under random subsampling (Levina & Priesemann, 2017). Furthermore, a number of *noncritical*

processes also lead to power laws (e.g. (Bédard et al., 2006; Priesemann & Shriki, 2018; Touboul & Destexhe, 2010) and power law analyses are inherently ambiguous, requiring a choice of the bin size, threshold, and the number of analyzed neurons or channels.

These difficulties of power-law analyses could be overcome by recently developed ways to infer the distance to criticality from heavily subsampled systems. This subsampling invariant estimator (Spitzner et al., 2021), however – and consistent with the findings of another recently developed approach (Dahmen et al., 2016) – also revealed a slightly subcritical, *reverberating* regime ($0.94 < m < 0.998$) (Wilting & Priesemann, 2018, 2018). Accordingly, and consistent with the systematic problems of power-law analyses – which may, especially on coarse recording modalities, falsely infer a close proximity to criticality by virtue of measurement artifacts – accumulating evidence from *in vivo* spiking activity reveals the brain as poised in a *slightly* subcritical dynamical regime; adding nuance to the original critical brain hypothesis.

2.2 Dynamic adaptive computation

However, a crucial point that distinguishes self-organized criticality from the more conventional criticality in statistical mechanics is that in self-organized criticality, systems tune *themselves* to criticality, without the need for external tuning via a control parameter. In a self-organized critical system, the critical point is an attractor, meaning the system tends to evolve toward that point from a wide range of starting points. (for a review on long-term and short term-plasticity rules that tune and sustain neural networks near the critical regime, see (Zeraati et al., 2021)).

Nevertheless – as reviewed above – the evidence is mixed, indicating that the brain might not self-organize itself towards the critical point *per se*, but rather towards a slightly-subcritical reverberating regime. Different distances to the critical point are associated with a number of variations in computational properties. In the following, empirical evidence on these adaptive and non-adaptive consequences of varying distances to criticality will be reviewed. Subsequently, the framework of dynamic adaptive computation is introduced, which posits that the brain self-regulates neuronal dynamics to *varying* distances to criticality, based on currently experienced task-demands and context (Wilting, Dehning, Neto, et al., 2018).

A closer distance to the critical state makes the system maximally sensitive to perturbations, a phenomenon known as divergent susceptibility (e.g. (Binney et al., 1992)). Relatedly, the dynamic

range – the range of inputs the network is able to differentially respond to – is maximized at criticality (e.g. Kinouchi & Copelli, 2006). Criticality has also been shown to maximize the number of metastable states (Haldeman & Beggs, 2005), computational power in terms of input-output mappings (e.g. Maass et al., 2002) and create an optimal balance of integration and segregation (e.g. Timme et al., 2016) (for reviews see Beggs & Timme, 2012; Cocchi et al., 2017; Tian et al., 2022; Wilting & Priesemann, 2019). More closely connected to working memory, the scale-invariant nature of the neuronal avalanches creates long range correlations in space and time – thereby effectively nullifying the path length between nodes through the network and over time (O’Byrne & Jerbi, 2022). Information-theoretically, furthermore, criticality is closely associated with a maximized information transmission, and capacity. Many of these properties are essential for working memory and will be reviewed in the context of working memory in section 4. As might be expected, it has been argued that evolution may have selected critical dynamics for the advantageous information-processing capabilities it confers (Hidalgo et al., 2014).

However, criticality also maximizes further aspects, which are likely negative for function. For example, the variability of network responses diverges, entailing a reduced specificity (e.g. (Gollo, 2017)) and reliability (e.g. (Wilting, Dehning, Pinheiro Neto, et al., 2018)). Furthermore, supercriticality is associated with instability (e.g. (Priesemann et al., 2014)), and critical slowing down results in a significant delay before a response, which is non-adaptive in tasks in which a fast action is required. Similarly, a high dynamic range may result in an increased interference from non-task-specific inputs. These examples highlight that many of the properties that were – under some circumstances and tasks – computationally adaptive, also have task and context dependent negative consequences. Importantly, furthermore, instead of maximizing particular computational properties, a context and task-specific *sufficient* expression of a given property is more ecologically plausible (Wilting & Priesemann, 2019a). Indeed, networks vary the distance to the critical point in balancing specificity and sensitivity (Gollo, 2017) or representational detail and integration time (Shriki & Yellin, 2016). Essentially, because of the functional relationship between m and associated properties of criticality, where *small* changes in m correspond to *large* changes in, e.g. the neuronal timescale or the network sensitivity, it has been proposed that neuronal networks may actively and adaptively control m , with significant task- and context-dependent changes in the timescale and associated computational properties being resultant (Wilting, Dehning, Neto, et al., 2018; Wilting & Priesemann, 2019). This form of meta-optimization – dynamic adaptive computation – is, due to the small changes that are required in the neuronal efficacy, m , computationally and metabolically resource efficient; in accord with perspectives on global brain functioning that emphasize the importance of efficient resource control (e.g. (Barrett et al., 2016; Barrett & Simmons, 2015)).

Empirically, systematic changes in the distance to criticality are evidenced by changes in the avalanche distribution across the wake-sleep cycle (e.g. Meisel, Bailey, et al., 2017; Meisel, Klaus, et al., 2017; Priesemann et al., 2013; Ribeiro et al., 2010), under changes of consciousness (e.g. Fagerholm et al., 2016, 2018; Fekete et al., 2018) and across varying attentional states (Fagerholm et al., 2015; Tomen et al., 2014). Indeed, the hierarchy of intrinsic neuronal timescales that mirrors the functional processing hierarchy of the brain can – because of the relationship between the timescale and the distance to criticality – be conceived of as a hierarchy of ever-smaller distances to criticality as hierarchical height increases (Wilting & Priesemann, 2019a). Furthermore, it has recently been proposed that psychedelics may move neuronal dynamics very close to the critical state (Carhart-Harris & Friston, 2019; Girn et al., 2023), explaining various aspects of the attested phenomenology and empirically observed neuronal evidence. This (exogenously induced) very close proximity to the critical state also speaks against the domain-general benefits of criticality: Granting possible long-term benefits of psychedelics, intuitively, there are nevertheless situations in which ‘trippin like crazy’ is simply not the most adaptive dynamical regime. Rather, the optimal region-specific distance to criticality is dependent on the task; with the brain actively and adaptively self-regulating the distance to criticality by virtue of resource-efficient changes in the effective neuronal coupling (Wilting & Priesemann, 2019a).

But how long does it take for the brain to self-regulate the distance to criticality? Some experiments evidence a self-regulation over several hours. For instance, after monocular deprivation was used to cause a large distance to criticality in the rodent V1, neuronal dynamics restored critical dynamics after about 24 hours (despite ongoing monocular deprivation) (Ma et al., 2019). Other experiments, however, also evidence self-regulation over extremely short periods. For instance, the presentation of a visual stimulus briefly disrupted critical dynamics in the visual cortex of a turtle; but, strikingly, critical dynamics got restored within about *one second*, even though visual stimulation continued (Shew et al., 2015). Given these drastic difference in the timescales of regulation, distinct neurophysiological mechanisms seem plausible.

And indeed, diverse mechanisms, such as Hebbian rules (de Arcangelis & Herrmann, 2010; de Arcangelis et al., 2006), spike-timing-dependent synaptic plasticity (e.g. Effenberger et al., 2015; Meisel & Gross, 2009), inhibitory plasticity in conjunction with network topology (Ma et al., 2019), short-term synaptic depression in conjunction with spike-dependent threshold increase (Girardi-Schappo et al., 2021), and short-term synaptic plasticity (Levina et al., 2009; Levina, Herrmann, & Geisel, 2007) present a range of possible options in this context of neuronal criticality (i.e. see, e.g., the references in this paragraph).

Yet another mechanism, homeostatic plasticity, intuitively illustrates some relevant considerations in this context. Homeostatic plasticity is considered – building mostly on modelling studies – as one of the primary mechanisms that might tune networks to criticality (for a review see Zeraati et al., 2021). Intuitively, the goal function of homeostatic regulation consists in a value of $m = 1$; with the network tuning itself to the critical point accordingly (Levina, Ernst, et al., 2007; Levina, Herrmann, & Denker, 2007). While a similar mechanism may enable dynamic adaptive computation by virtue of a context and task dependent set point (i.e. *allostatic* plasticity), empirically, homeostatic plasticity operates on longer timescales (minutes to hours) (for a review see (Zenke & Gerstner, 2017)). However, recent perspectives deem some form of ‘rapid compensatory process’ (terminology the authors choose to highlight the difference in time-scale to classic homeostatic plasticity) as necessary in order to prevent runaway excitation on short timescales (Zenke & Gerstner, 2017). Accordingly, generally – and while many implementational details of multiple mechanisms in this context are open for further research – this example highlights what is conceptually implied by the framework of dynamic adaptive computation: A relatively short-timescale mechanism that adjusts the computational properties of neuronal dynamics in a resource efficient way (by virtue of causally regulating m); relative to current representations of task and context.

3. Spatial working memory and the hippocampus: A record of the recent past

“Objects fade out of consciousness slowly. If the present thought is of A B C D E F G, the next one will be of B C D E F G H, and the one after that of C D E F G H I —the lingerings of the past dropping successively away, and the incomings of the future making up the loss. These lingerings of old objects, these incomings of new, are the germs of memory and expectation, the retrospective and the prospective sense of time. They give that continuity to consciousness without which it could not be called a stream.”

—William James, *The Principles of Psychology*

Working memory – the “sketchpad of conscious thought” – is supported by widely distributed neuronal networks (for a review see (Christophel et al., 2017)); reflecting the region-relative temporal persistence of diverse forms of contents – with sensory working memory being preferentially encoded

in sensory regions, conceptual memory preferentially in hierarchically higher regions, etc. The hippocampus is a region in the medial temporal lobe that is functionally implicated in spatial cognition (for a review see (Hartley et al., 2014)). Given that working memory is neuronally highly distributed in this region- and content-specific way, it might be expected that the hippocampus is especially involved in *spatial* working memory. However, the hippocampus (and the medial temporal lobe generally) has not been included in typical traditional models of working memory (Xu, 2017). More recently, however, owing in part to advances in intracranial neural recording techniques, it has been demonstrated that the hippocampus is a central neuronal substrate of working memory (Li et al., 2024). In the following, this hippocampal involvement in working memory will be reviewed. Subsequently, two existing theoretical perspectives on the hippocampal involvement in working memory will be detailed.

3.1. Working memory and the hippocampus

Intracranial neural recordings offer immediate access to neuronal spiking at a temporal resolution of milliseconds, enabling detailed analyses of sequential activity and directional information flow across brain-regions. Working memory, operationally, consists of *persistent* and *content-specific* neuronal activations in the *absence of the respectively initiating stimulus*; and these neuronal reverberations have been found with intracranial neural recordings (for a review, see (Li et al., 2024)). For example (Kamiński et al., 2017), human subjects performed a working memory task that consisted of the successive encoding of up to three visual stimuli, each presented for one second; followed by a 2.5 - 2.8 second delay and a presentation of another visual image, for which the participants had to decide whether they had seen the stimulus before (i.e. the Sternberg task). Neurons in the medial temporal lobe fired in a stimulus specific and persistent manner, forming stable attractors and being predictive of memory content. Strikingly, in this study, relative to the 12.1% of hippocampal cells that were identified as highly selective and sparsely responsive ‘concept cells’ (identified by virtue of the covariance of the firing rate with picture identity), 44.9% exhibited persisted activity during the maintenance period (Kamiński et al., 2017). Consistently, it has also been found that the similarity between encoding and maintenance is higher for identical than for different stimuli (J. Liu et al., 2020). Hippocampal neurons also exhibit increased firing rates with increased working memory loads in the maintenance period of working memory tasks (Boran et al., 2019, 2022). Furthermore – and consistent with a model of hippocampal working memory based on gamma & theta-oscillations ((Lisman & Idiart, 1995); see the next section) – intracranial recordings from the hippocampus have shown significant theta-gamma coupling during working memory maintenance (Axmacher et al., 2010; Daume et al.,

2024); a reduced variability of modulation phases across trials which might prevent content-content interference (Axmacher et al., 2010); as well as potentially sequential order-indexing amplitude varying gamma activity at different theta phases (Yang et al., 2021). In general, intracranial evidence systematically demonstrates a central role of the hippocampal formation in working memory (for a review, see (Li et al., 2024)); revealing not only content-specific stimulus independent persistence of neuronal activations, but also various computational aspects of the involved coding schemes. However, fMRI evidence recently sparked a controversy: As opposed to one recent meta-analysis reporting hippocampal involvement in working memory tasks (Grady, 2020), another recent fMRI meta-analysis claimed that no such systematic involvement could be found (Slotnick, 2022) (for a reply to several commentaries on this analysis, see (Slotnick, 2023)). However, it has been objected (e.g. Li et al., 2024) that fMRI consists of indirect hemodynamic responses with limited temporal resolution (methodologically inferior compared to intracranial evidence); with fMRI in the MTL being furthermore affected by signal dropout (Rua et al., 2018).

Rodent studies show that lesions in the dorsal hippocampus (homologous to the posterior hippocampus in humans) cause severe spatial WM deficit (Hauser et al., 2020). In humans, the evidence for a working memory impairment after lesions to the MTL is mixed and difficult to interpret. For instance, while (Finke et al., 2008) demonstrates working memory deficits with MTL lesions over longer working memory delay-periods (5 seconds), this pattern was not apparent over a shorter, 0.9 second, delay. However, another patient with a hippocampal lesion performed normally on working memory color–shape association and word association tasks (Baddeley et al., 2010). Studies reporting decreased working memory performance after lesions of the MTL are associated with *more* lesioned regions next to the hippocampus (e.g. Finke et al. (2008)) – such that no specific claims about the functional necessity of the hippocampus for working memory are enabled. However, conversely, many studies which report an intact working memory even though the hippocampus is damaged, report only *partial* lesions of the hippocampus (e.g. Baddeley et al. (2010)) – which makes it difficult to rule out the sustenance of functionality within that substrate. Furthermore, damage to other areas in the MTL might causally implicate an impaired information processing within the hippocampus by virtue of ions in inter-regional information flow (such as the medial septum or fornix; see the next section).

As mentioned above, working memory can, on an operational level, be conceived in terms of persistent stimulus-independent and stimulus-selective neuronal activations. A complementary perspective on working memory – focused more on the encoded *content* – is in terms of conjunctive representations of *what* happened *when* (thereby adding temporal information; see also the next section): Specifically, neurophysiologically, populations of so-called “time cells” are hypothesized as essential in constructing

this conjunctive representation (for a review see Eichenbaum, 2014). Time cells are sequentially firing cells found in the hippocampus, being activated during unfilled delay intervals after the presentation of a sufficiently salient stimulus (MacDonald et al., 2011; Pastalkova et al., 2008). General linear model analyses have demonstrated that these temporal sequences are statistically reliably present even after accounting for variations in activation based on speed, head direction & location (MacDonald et al., 2011); with subsequent studies showing that time cells integrate both time as well as distance travelled (Kraus et al., 2013). Importantly, the firing sequence is reliable across trials, and in many cases *specific* to the stimulus that initiated the delay – it is possible to reconstruct both the identity of the stimulus that initiated it (Bright et al., 2020; Taxidis et al., 2020) as well as the starting time of the delay (e.g. Mau et al., 2018). To give an example in this context, (MacDonald et al., 2013), head-fixed (preventing misattributions of findings to behavioral correlates) animals performed a delayed matching to sample task with odor stimuli, wherein the animal, similar to studies elaborated above, receives an odor and after a delay of 3 seconds, has to determine if a subsequently presented odor is identical to the previous odor. Here, it has been found that distinct & selective sequences of firing spanned the delay period for each odor; being consistent with the stimulus specific persistent activation elaborated upon above. In another study, a sequence of five odors was presented, and in the test phase, rats had to report the relative order of two of the odors (Shahbaba et al., 2022). Time cells spanned the presentations of the respective odors (as well as the delays afterwards). The populations changed their order of firing for each successive odor, but for each odor they maintained the same orderly sequence of activations between trials. Statistical tools developed by the authors showed selectivity for odor identity and order and provided the most accurate estimates for correct trials. Interestingly, this sequential and conjunctive coding can also function prospectively: In a study in which animals can choose to go to one of two arms, after starting from two alternate possibilities, the time cell sequences are specific relative to the goal arm which is selected, independent of the start arm (Gill et al., 2011). While studies on time cells in the hippocampus have initially, and predominantly, focused on the hippocampal area CA1, time-cells have also been found in CA3 (Salz et al., 2016). Interestingly, it has been found that hippocampal representations reliably change across *several minutes*. For instance, (Manns et al., 2007) inferred population vectors for several temporally separated tasks, observing reliable changes not only within each task, but also across the tasks; with more temporally proximate tasks having more similar population vectors. Similar results (i.e. gradually changing activity over thousands of seconds) have been found in spatial exploration (Hyman et al., 2012; Mankin et al., 2012). To summarize, while evidence from fMRI and lesioning studies is not entirely conclusive, methodologically superior intracranial measurements reveal stimulus-specific persistent activations in the absence of the initiating stimulus over extended periods; providing

evidence for theoretical proposals of working memory in the hippocampus which are discussed in the following.

3.2 Theoretical frameworks for working memory in the hippocampus

A *minimally necessary* criterium for a short-term memory on the neuronal level of description is a sequential activation of a number of neuronal units. Indeed, if the *branching parameter* of that neuronal sequence was too low, the content could – by definition – not self-sustain itself over time, with working memory being lost. Intuitively, by this perspective, a closer distance to criticality is advantageous for working memory. Given, furthermore, that interference between distinct elements in working memory is to be avoided, it might be hypothesized that the sequentially activated chains of neuronal activity are unique to each stimulus. Because it takes some time to traverse the chain of neurons, the encoded information might not only be relative to the stimulus – i.e. encoding a *what* – but also temporally relative – i.e. encoding a *when*. Independent of the relationship to criticality mentioned above, this neuro-computational hypothesis of temporally-relative stimulus-specific sequential activations is known under the name of synfire chains; constructing a distributed representation of *what happened when* (e.g. Goldman, 2009; Hayon et al., 2005; Rajan et al., 2016). These chains of sequentially activated neurons could in principle account for the existence of time cells (Itskov et al., 2011). While intuitive, synfire chains entail a number of links in the chain that increases linearly with the duration of the longest retained interval (Howard & Eichenbaum, 2013), which might become neuronally implausible given the retainment of information in the hippocampus over extended time-periods, mentioned above. Furthermore, the representations of temporal history that are constructed by synfire chains are not scale-invariant, in contrast with evidence from intracranial recordings (see more below; for a review touching upon this point see also (Howard & Eichenbaum, 2013)). Nevertheless, synfire chains are a concrete neuro-computational proposal of short-term memory in terms of a temporally receding and dynamically reverberating conjunctive representation of *what happened when*.

As mentioned earlier, working memory is highly distributed across brain regions, and present on multiple levels across the functional hierarchy; with the content being retained being relative to the general functional role of each circuit. While in the field of working memory research, numerous concrete functional level accounts of working memory exist (for a recent book see (Logie et al., 2020)), in the following, emphasis will be laid on two specific proposals focused on the hippocampal neurophysiological literature.

Short-term memory buffers (Shiffrin & Atkinson, 1969) are a classic cognitive psychological hypothesis for short-term memory; being constituted by a fixed number of slots to hold recently presented information. Short-term memory buffers have originally often been conceptualized as being interference-based (Waugh & Norman, 1965); with the stored content being unchanged by the passage of time per se, yet incrementally updated by incoming stimuli (with the oldest item dropping out of the buffer, and every item “shifting” its location). In this way the memory buffer forms an ordinal representation of the past. In a proposal of an implementation of a short-term memory buffer in terms of brain oscillations, individual slots correspond to neurons firing in (and thereby constituting) one gamma cycle; with the capacity of the buffer corresponding to the number of gamma cycles fitting in one theta cycle (Lisman & Idiart, 1995; Lisman & Jensen, 2013; Lisman & Redish, 2009): there are four to eight gamma cycles embedded within one theta-cycle; consistent with the well-known result that working memory has a capacity limit (span) of 7 ± 2 (Miller, 1956). Consistently, the ratio of gamma to theta has been demonstrated to correlate with the working memory span (Kamiński et al., 2011).

Furthermore, intracranial neural recordings from the hippocampus have demonstrated significant coupling between gamma activity and theta phase in the hippocampus during the maintenance of multiple WM items (Axmacher et al., 2010; Daume et al., 2024); with the order of sequential information being potentially indexed by a varying gamma activity at different theta phases (as demonstrated in a sequential odor task (Yang et al., 2021)). While theta oscillations can be generated by intrinsic hippocampal mechanisms – as documented, by, e.g., experiments on hippocampal slices ((Fellous & Sejnowski, 2000) – another important influence on the generation of theta rhythms is the medial septal nucleus (by virtue of cholinergic and GABAergic neurons imposing a drive on hippocampal neurons (King et al., 1998)). Inactivations of the medial septal nucleus, which reduce theta oscillations, negatively impact spatial working memory; and, conversely, pacing the septum or hippocampus with theta oscillations can facilitate working memory performance (e.g. Shirvalkar et al., 2010; Siegle & Wilson, 2014). However, this theta-gamma ordinal working memory representation does not explicitly encode information about *when*, specifically, a given event occurred, and would be potentially functionally disadvantageous due to the hard constraints imposed on working memory capacity; with the latter being inconsistent with empirical evidence on scale-invariant effects observed in working memory (such as recency effects across widely different timescales, see e.g. (Howard et al., 2008; Howard & Kahana, 1999)).

Another recent computational cognitive neuroscience theory describes a mechanism for computing a temporally explicit scale-invariant representation of temporal history leading up to the present moment (Howard et al., 2014; Howard & Eichenbaum, 2013; Shankar & Howard, 2012). It should be

noted that this latter perspective is, at least in part, not necessarily in conflict with the importance to the theta-gamma code implied by the above perspective but may be operative on a different level of description. To motivate this account – given that there are no receptors for time, it may be asked with respect to this *explicit* construction of a temporal history (as opposed to a non-temporal ordinal representation, as above): How can this latent dimension be constructed?

External signals are time-varying functions, unfolding over a temporal domain. However, while physical time is the domain within which neuronal processing unfolds, and which an external observer can use to describe neuronal sequences (see also (Buzsáki & Tingley, 2018)), physical time itself cannot be causally efficacious in the brain. To make an analogy regards the proposed mechanism by Howard et. al., of how the brain is able to construct this latent dimension, consider inverse operations in mathematics; with the simplest examples being subtraction as the inverse of addition, or division being the inverse of multiplication. The inverse of a given operation “undoes” that very operation. Howard et. al. considers a mathematical transform (and its inverse) that results in the conversion of whole functions to other functions, with changed domains. Specifically, the guiding idea is that if there were a transform of the external signal (unfolding over the *time-domain*) that results in a neuronally plausible encoding in, e.g. the *frequency domain* (e.g. neuronal firing rates), that a subsequent explicit computation of the inverse of this transformation could “undo” this operation: thereby reverting back to a neuronally instantiated explicit encoding over a *temporal domain* (i.e. a temporal history). The sought mathematical transformation is the Laplace Transform and its inverse, with the inverse reconstructing the temporal history.

In terms of neuronal implementation, the method relies on two populations of cells. A population of stimulus-specific cells that shows exponentially decaying persistent firing with a variety of rate constants (in the mathematical limit of the presence of all possible rate constants, this population would uniquely specify one temporal history in the second population of cells); and a second population of cells, with each cell being connected to all the cells from the first population with weights that approximate the inverse Laplace transform (for details, see (Liu et al., 2019)). And, indeed, subsequent work found evidence for the presence of the first population of cells, characterized by a high degree of heterogeneity in exponential decay rates (from a few hundred ms to several s) as the initiating event recedes in the past, in the lateral EC (Bright et al., 2020; Tsao et al., 2018). This is consistent with biophysical findings of slowly inactivating currents in EC, as observed in, e.g., slice experiments (Egorov et al., 2002). Different cells in the second population encode different points in the reconstructed temporal history, similarly to the different slots in the classic memory buffer; with the main difference being the presence of an explicit encoding of the temporal timeline itself.

Furthermore, Howard et al's theory mathematically entails a specific scale-invariant scaling of the representation of the temporal history (Shankar & Howard, 2012); thereby accounting for empirical evidence in this domain (for a review in this context, see (Howard & Eichenbaum, 2013)). Indeed, neurophysiological evidence conforming to this specific scaling has recently been confirmed on recordings of time-cells (Cao et al., 2022).

4. Short-term memory computations benefit from a smaller distance to criticality

As mentioned above, the classic *critical brain hypothesis* is closely tied to and motivated by numerous computationally adaptive properties occurring near a branching parameter of $m = 1$ (for reviews see Beggs & Timme, 2012; Cocchi et al., 2017; O'Byrne & Jerbi, 2022; Tian et al., 2022; Wilting & Priesemann, 2019; for a recent book see Beggs, 2022). In the following, a number of conceptually distinct (though functionally and dynamically intertwined) ways by which a smaller distance to criticality is adaptive for short-term memory is presented.

4.1 An information-theoretic perspective

In the context of short-term memory, one central computational advantage of criticality concerns a maximized information transmission and capacity (for an introduction to information theory see (Cover, 1999); and as applied to neuroscience, see, e.g., Rieke and others (1997)). Greenfield and Lecar already showed in 2001 that the mutual information between different neurons in a model of a neural network peaks at criticality (Greenfield & Lecar, 2001); mirroring earlier work on cellular automata that demonstrated a maximized mutual information between cells at criticality (Li et al., 1990). (Beggs & Plenz, 2003b) had similar findings in a feed-forward neural network model. By systematically changing the excitation-inhibition ratio in a network model and in *in vitro* cortex cultures, (Shew et al., 2011) similarly discovered that both information capacity (i.e. Shannon entropy) and the information transmission (i.e. mutual information) are maximized at that particular value of the excitation-inhibition ratio at which power law distributed neuronal avalanches emerge. (Shew et al., 2011) used these results to correctly predict *in vivo* information capacity in awake macaque monkeys; obtaining a close correspondence between model and experiment. This increased information capacity is consistent with earlier work by (Stewart & Plenz, 2006) who varied dopamine tone in cortex slices, revealing that a maximum diversity of activity patterns co-emerged with critical signatures.

Furthermore, (Fagerholm et al., 2016) – concerned with the limited spatial coverage and resolution of previous experimental techniques; overcoming them by using genetically encoded voltage imaging in layer 2/3 pyramidal cells from mice cortex with $< 100 \mu\text{m}$ spatial resolution – found that, as mice recovered from anesthesia, cortical mutual information (for now on simply called information transmission) and Shannon entropy (from now on called information capacity) increased. This increase in information capacity and transmission (as well as region-specific variability) was accounted for by the extent to which the dynamics became scale-free (i.e. critical). Conversely, learning and synaptic plasticity rules which optimize mutual information result in networks that evince signatures of criticality (e.g. (Tanaka et al., 2009)). Accordingly, generally, given that an increased information capacity and an increased information transmission are adaptive for working memory (by entailing the potential for *more* information in working memory to be *reliably* sustained), and ensue in the vicinity of criticality, it is expected that the brain self-regulates itself closer to the critical regime in working memory tasks. Indeed, a recent study that investigated two information-theoretic fingerprints of working memory (i.e., in their words, ‘intrinsic memory’ (i.e. active information storage; a generalization of mutual information that includes the whole temporal history as predictive information (as opposed to only one distinct time-step)), and ‘memory capacity’ (i.e. the integral of the time-lagged mutual information) revealed that both increase as the reservoir approximated criticality (Cramer et al., 2020).

However, information is not a monolithic entity but consists of distinct contributions that can be analyzed through an information decomposition. Specifically, (partial) information decomposition provides a formal framework to disentangle synergistic, unique, and redundant information in empirical data (for a review, see (Luppi et al., 2024)). Intuitively, the XOR function illustrates how information jointly exists in a manner not decomposable into individual components, representing pure synergy (the output can only be known given the *joint* state of the two inputs; one input state alone is not sufficient). Redundant information, on the other hand, pertains to shared information across elements of a system (i.e. duplicated information present in more than one source), while unique information reflects contributions specific to individual components. Synergistic information provides a computational advantage by allowing a system to exploit combinations and interactions among its components (i.e. ‘integration by cooperation’ (Luppi et al., 2024)): It results in the systems complete informational content exceeding the sum of its individual parts. Furthermore, synergistic information is behaviorally meaningful: For instance, performance of artificial neural networks in multimodal tasks critically depends on synergistic neurons (i.e. the removal of synergistic neurons impairs performance most) (Proca et al., 2022). Indeed – and consistent with this integrative role – a number of studies implicate the presence of synergy most strongly in multimodal association cortices

(Luppi et al., 2022; Varley et al., 2023) (i.e. those locations where information from multiple processing streams converge (Deco et al., 2021; Mesulam, 1998; Sydnor et al., 2021) with a NeuroSynth meta-analysis of over 15 000 neuroimaging studies showing that high-redundancy regions activate to modality-specific tasks as opposed to high-synergy regions – which are activated by more complex, and integrative, forms of cognition (Yarkoni et al., 2011). Synergistic computation is also central in spatial working memory. Conjunctive representations of *what* and *when* are only adaptive if both of these informational atoms are present. Intuitively, if only the exact time can be recalled when *something* happened, this provides too little information for the execution of an appropriate response. Conversely, if only the event itself can be recalled, but independent of information pertaining to its temporal recency, behavior will be impaired in tasks dependent upon that information. Accordingly, conjunctive representations of *what* and *when* – central in working memory – necessitate informational *synergy*: It is only upon knowing both pieces of information together, that successful performance is unlocked (similar to the XOR-gate). Interestingly, a closer proximity to criticality may facilitate the presence of synergistic information. For instance, a recurrent neuronal network, implemented on a neuromorphic chip, tunes itself based on local learning rules to the critical point (as evidenced by characteristic critical phenomena, such as an increasing timescale, power-laws, etc.), given low external input (Cramer et al., 2020): The authors found that the proximity to the critical point is facilitative of synergistic information. Another recent study has ‘reversed the script’ (Varley & Bongard, 2024): Instead of treating synergistic information as a dependent variable, they used evolutionary optimization to evolve Boolean networks to varying dynamical regimes (e.g. synergistic, random, high statistical complexity). This study, too, found that a high degree of synergy co-occurs with a high timescale. This is consistent with another study, leveraging the Kuramoto-model, which has shown that synergistic information dominates at longer timescales (i.e. critical slowing down), being maximized at the phase-transition of coupled oscillators (Mediano et al., 2022). This relationship is also empirically mirrored in terms of an increase of synergistic information with a higher intrinsic neuronal timescale: High-synergy brain regions, such as those in the default mode and fronto-parietal networks, exhibit longer intrinsic timescales and complex activity patterns (Luppi et al., 2022). Furthermore, models of fMRI signals indicate that synergy becomes more prominent at extended timescales (Mediano et al., 2022). Accordingly, if the presence of synergistic information increases at higher timescales, and intrinsic neuronal timescales increase near criticality, a dynamical regime in a closer vicinity to the critical point likely promotes synergistic information, facilitating complex cognitive functions: specifically, in this context, synergistic information from the joint state of *what* & *when* on a temporally receding internal timeline computed in the hippocampus, necessary for the performance in a (spatial) working memory task.

In general, there are two main information-theoretic reasons why a closer distance to the critical point might be advantageous in a (spatial) working memory task. First, the critical regime has been shown to maximize information capacity and information transmission – facilitating the reliable sustenance of more information. Second, the task-mandated conjunctive nature of spatial working memory necessitates the presence of synergistic information; and a closer proximity to the critical point has shown to be facilitative of synergistic information.

4.2 Dynamically fading memory

The intrinsic neuronal timescale – which, as elaborated above, diverges at the critical point – is conceptually closely related to the optimized information sustenance; effectively endowing the system through reverberating activity with a purely dynamical short-term memory (Wilting, Dehning, Pinheiro Neto, et al., 2018). Put in other words, the long timescale at the critical point (i.e. critical slowing down) enables the system to retain maximum information about the history of its own dynamics.

In simulations of neural networks, this became historically first evident in the framework of reservoir computing, and specifically, echo-state networks (Jaeger et al., 2007; Maass et al., 2002). An echo-state network is a recurrent neural network with randomly initialized weights in its reservoir (recurrent part), which are typically not trained (Jaeger, 2001, 2007). The only aspect of the network that is trained is a linear decoder (readout layer), which takes as input the reservoir states (i.e. the latent states of the network at a given time). Intuitively, the central idea of the echo-state network consists of projecting the input into a high-dimensional dynamic space through the reservoir's nonlinear dynamics, potentially making complex temporal patterns more linearly separable. The linear decoder is trained to extract relevant patterns from these reservoir states, effectively leveraging the richness of the high-dimensional space. Echo-state networks have been used predominantly in time-series forecasting problems, such as weather or financial forecasting. Indeed, because they can memorize and non-linearly transform present and past information in their latent state, reservoirs can function as universal approximators for dynamic systems (Maass & Markram, 2004). The edge of criticality is obtained in an echo-state network by scaling the largest eigenvalue of the weight matrix of the reservoir to (close to) 1. (Bertschinger & Natschläger, 2004) showed that networks were able to exhibit long memories at the critical transition between a stable (ordered) and an unstable (chaotic) dynamic regime; and this finding of an increased memory in proximity to the edge of chaos was also shown in subsequent studies (Büsing et al., 2010; Legenstein & Maass, 2007; Maass et al., 2004). To give a more detailed example: A recent study reconstructed human brain connectomes using diffusion-weighted imaging; and implemented these connectomes using reservoir computing. Memory capacity was

quantified as the average correlation between inputs to the reservoir and time delayed states of a linear model (which was trained in a supervised manner), taking input from the reservoir states; with a high correlation indexing a high memory and vice versa. It was shown that the performance in this memory task was maximized for critical dynamics (Suárez et al., 2021).

However, as mentioned earlier, while edge of chaos criticality and avalanche criticality are commonly assumed to co-exist, and many properties of criticality, such as, e.g., critical slowing down, is present in diverse forms of criticality (Scheffer et al., 2012); edge of chaos criticality and avalanche criticality are measured in distinct ways and *might* refer to different phenomena; with a general link still being missing (e.g. see Del Papa et al., 2019).

However, a recent study, using self-organizing recurrent neural networks (SORNs) and the avalanche criticality framework showed mathematically similar properties compared to systems tuned to edge of chaos criticality (Del Papa et al., 2019). SORNs are composed of neurons whose synaptic weights evolve through biologically inspired plasticity rules (Lazar et al., 2009; Zheng et al., 2013). Interestingly, SORNs – which were initially researched in the context of sequence learning (Lazar et al., 2009) – are able to generate distributions of synaptic efficacies and fluctuations thereof as found in the hippocampus (Zheng et al., 2013). SORNs can also create synfire chains (Zheng & Triesch, 2014; see above). A recent study on SORNs has shown that the so-called fading memory time scale – the average number of time steps over which past input tokens to the network can be classified from the network with an accuracy of at least 90 % – is maximized in that regime in which avalanche criticality occurs (Del Papa et al., 2019). Interestingly – and relating to the still unknown relationship between edge of chaos and avalanche criticality – the fading memory time scale in this study increased approximately logarithmically with the network size; a comparable scaling to the one observed in networks operating at the edge of chaos.

In the human brain, working memory is also closely related to criticality (and critical slowing down). For instance, it has been shown that individual neurons that evince a high intrinsic timescale constitute a robust neuronal working memory correlate (Cavanagh et al., 2018); consistent with findings documenting that high intrinsic timescale neurons encode relatively more task-relevant information (Wasmuht et al., 2018). Furthermore, a recent study investigated the relationship of whole brain avalanche criticality with fluid intelligence and working memory – demonstrating that the neuronal dynamics of human participants that have a higher intelligence and a better working memory are closer to criticality.

5. Summary & Hypotheses

Recent intracranial evidence – both in terms of the methodologically classic ‘persistent & stimulus independent selective activation’ working memory studies & in terms of more hippocampus-specific evidence, centered on theta-gamma codes and time-cells – robustly demonstrates hippocampal involvement in working memory (see section 3.1 & 3.2). This is consistent with two theoretical perspectives on working memory in the hippocampus; many of the specific predictions of which have been tested and validated both neurophysiologically and psychologically (see section 3.2). This master thesis investigates a possible relationship between (spatial) working memory and the distance to criticality of hippocampal neuronal population dynamics. Given that mainly the hippocampal subregions CA1 & CA3 have been associated with informational sustenance & time cells, the proposed relationship between criticality and working memory will be investigated in these subregions, specifically. The original *critical brain hypothesis* – positing that the brain is operating at a second order phase transition due to numerous computationally optimized properties – has found only mixed empirical support; in part caused by methodological difficulties (see section 2.1). What has, over the more recent years, found significant empirical support, however, is the presence of a slightly subcritical, *reverberating*, dynamical regime. Indeed, the brain might self-regulate the distance to criticality in a resource-efficient manner, balancing both adaptive and non-adaptive computational properties relative to the processing demands induced by a given task and context (for a review, see (Wilting & Priesemann, 2019a); see section 2.2). In the context of working memory, the presence of neuronal dynamics in closer proximity to the critical state might be adaptive for a number of reasons. First, a closer distance to criticality increases information storage and information transmission capabilities of neuronal circuits. Second, a closer distance to criticality facilitates the presence of synergistic information (e.g. information about the *joint* state of “what” and “when”); mandated by successful working memory performance (see section 4.1 for the information-theoretic perspective, generally). Third, the increased intrinsic neuronal timescale – possibly corresponding to a purely dynamical form of short-term memory – might facilitate an increased memory capacity; in accord with studies on reservoir computing evidencing this relationship (see section 4.2). And while there are also additional related properties of critical systems, such as diverging correlations in space and time, which might be advantageous for short-term memory; and cognitive neuroscience studies that already attest a relationship between working memory and criticality; the hypothesis that a reduced distance to criticality is facilitative for working memory tasks in the hippocampus has not yet been investigated. More specifically, two distinct effects might be hypothesized in this context. First – given the functional advantages of a closer distance to criticality for working memory and the empirically attested capabilities of the brain to dynamically *self-regulate* the distance to criticality (see section 2.2) – it is

expected that the distance to criticality is smaller in a working memory task, compared to a control task. While this *between-task effect* would be operative over extended timescales, it is possible that an effect over smaller timescales is also present. Indeed, studies exist which evidence such a dynamic self-regulation over extremely short time-periods. For instance, the presentation of a visual stimulus briefly disrupted critical dynamics in the visual cortex of a turtle; but, strikingly, got restored within about *one second*, even though visual stimulation continued (Shew et al., 2015). And while the concrete neuronal plasticity rules which might mediate these rapid changes are still under investigation, it has been argued that some form of set-point relative ‘rapid compensatory process’ is generally necessary in order to prevent runaway excitation on short time scales (see section 2.2; for a review see (Zenke & Gerstner, 2017); for a review on long-term and short term-plasticity rules that tune and sustain neural networks near the critical regime, see (Zeraati et al., 2021)). Accordingly – and even though, in the context of working memory, as of yet, no study has functionally implicated a reduced distance to criticality *in vivo* over such small timescales – a *within-task effect* is also possible. Specifically, it might be the case that in the working memory task itself, a transiently *even closer* distance to criticality is facilitative of an increased task performance. These two hypotheses (i.e. the *between-task* & the *within-task* effect) are investigated in this master thesis.

6. Methods

This master thesis has analyzed openly available data obtained by the Loren Frank group (Karlsson, Carr, Frank (2015)). This data set consists of 11 male Long Evans rats (500–700 g, 4–9 months old) which were trained on a W-track spatial alternation task. The W-maze were 76 × 76 cm, with 7-cm-wide track sections. Animals alternate between 20 min rest sessions in a rest box and 15 min run sessions on the W-shaped track. The animals sleep before these alternating blocks, with data being recorded (i.e. sleep sessions). The track is equipped with a reward well at each arm end. Animals are rewarded on the track at the ends of an arm if and only if that arm is the next correct arm in the sequence. Correctness is based on the following rules: If the animal is in an outer arm, it must next visit the center arm (‘inbound trial’). If the animal is in the center arm, it has to subsequently visit the less recently visited outer arm (‘outbound trial’). The outbound trials test short-term memory by virtue of presupposing memory of the last visit to an outer arm. The resulting sequence is, accordingly (starting from the center arm): center, left, center, right, center, left, etc. The simple structure of this set-up and task enables a *minimal* testbed for the hypotheses – effectively experimentally controlling for alternate hypotheses. Animals were not constrained in their choice of the arms or in their movements. Only data from CA1 and CA3 was used in this study (see section 3.1 & 3.2 for

neurophysiological findings on hippocampal working memory as predominantly located within these regions).

Spike time series were constructed using commonly used and openly available code from the Frank lab, specifically available for this (kind of) dataset (https://github.com/Eden-Kramer-Lab/loren_frank_data_processing/tree/master/loren_frank_data_processing). The subsampling invariant estimator of the distance to criticality (Wilting & Priesemann, 2018) – which is described in the following, starting from the construct validity of the branching model – operates on these time series.

The branching model is a generic model of how activity spreads in a network. While the branching model abstracts away from a high degree of neuronal complexity – such as the distinction between inhibitory and excitatory connections – it captures the *effective* propagation of activity. Indeed, the branching model reproduces statistical characteristic of networks with inhibition (Dahmen et al., 2019) and is more generally in accord with experimentally observed features of neural networks, such as Fano factors, inter-spike interval distributions, spectra and – most centrally – an exponential decay of the autocorrelation function (Dahmen et al., 2019; Murray et al., 2014; Wilting, Dehning, Pinheiro Neto, et al., 2018; Wilting & Priesemann, 2019b). While it is a non-trivial problem to enable unbiased and reliable inferences about population-level parameters from highly subsampled systems, given that a typical intracranial recording may (traditionally) only sample from a couple dozen of neurons, it has been shown that inferences about the branching parameter m can be obtained in a *subsampling invariant* manner (Wilting & Priesemann, 2018). The autocorrelation function at k different time-lags can be estimated from the activity as:

$$C(k) = \frac{\sum_{t=1}^{T-k} (A_t - \bar{A}_t)(A_{t+k} - \bar{A}_{t+k})}{\sum_{t=1}^{T-k} (A_t - \bar{A}_t)(A_t - \bar{A}_t)}$$

For a stationary branching process, the autocorrelation of A_t follows $C(k) \propto m^k$. Accordingly, by fitting an exponential the branching parameter m can be estimated:

$$\begin{aligned} f(k) &= Bm^k + D \\ &= B \exp(-\frac{k\Delta t}{\tau}) + D \end{aligned}$$

The offset D accounts for long timescales that do not decay over the recording time. B represents the degree to which the autocorrelation is biased by subsampling (which is partialized out); and the last equality above was used to express the estimation of the autocorrelation in terms of the intrinsic timescale.

As mentioned, there are three distinct behavioral modes: task epochs, rest epochs & sleep epochs. This master thesis investigates whether there is a *between-task* (i.e. between-epoch) effect, i.e. whether there is a difference in the distance to criticality in the working memory task relative to a control condition. However, it is methodologically essential to deploy the appropriate control condition – given that a possible alternative explanation could, in principle, always be that it is – *contra* to the hypothesis – not the case that the distance to criticality *decreases* in the working memory task, but that it *increases* in the control condition (for some unknown, alternate reason). Hence, it would be optimal if already conducted independent analyses of the same dataset were available which can be used to establish the correct control condition. And indeed, (Garg, 2023) used various measures of the distance to criticality on the same dataset (not in the context of working memory); comparing wake (i.e. rest & task) to sleep. It was found that neuronal dynamics in the hippocampus are, for the different methods, either similar, or closer to criticality, in sleep epochs, compared to wake epochs. Accordingly, if the rest epochs were chosen as the control condition, it might be the case that it is not the working memory task which leads to a decreased distance to criticality, but the resting state which is associated with an increase in the distance to criticality. In order to methodologically control for this alternative explanation, here, sleep epochs are chosen as the control condition (because they were already isolated, they form a stable baseline).

Concerning the *within-task* effect, in order to detect a possible association between the performance in the working memory task and the distance to criticality, it would be optimal to infer the relevant metrics for the episode that precedes a single outbound task (and over which the working memory has to be sustained), specifically. However, the specific episode of the task over which the animal retains the working memory is unclear, comprising, maximally the whole epoch starting from the last decision point from the last outbound task, which has to be reversed in the next outbound trial and therefore remembered, to the subsequent decision point. However, it is also possible that the animal discovers a *minimal* strategy based on the specificity of afferent proprioceptive input at the *last* point at which this information is available: The direction in which the animal turns (in the inbound trial) changes based on the direction where it came from; thereby uniquely determining the next outbound choice to be made. However, the temporal window over which a unique branching parameter/intrinsic neuronal timescale is inferred cannot be too short: A bias of the estimated quantities is otherwise

induced – there is a tradeoff between the magnitude of the bias and the length of the temporal interval (Spitzner et al., 2021). Based on this tradeoff, and based on the uncertainty about (i) the strategy the animal deploys and (ii) the timescales of regulation of the distance to criticality (see section 2.2), in this study, the metrics were inferred for 30s time-intervals. The bin size that was chosen was 5 ms, similar to previous work with the estimator (e.g. Hagemann et al., 2021); being chosen to reflect the spike-propagation time between neuronal elements. The neuronal time series were pooled by the area (here, CA1 and CA3), and it was not assumed that the neuronal activity is stationary across trials (trial separated method (Spitzner et al., 2021)).

7. Results

In order to obtain a statistical evaluation of changes in the distance to criticality as the animals perform the working memory task, two *mixed effects models* with animal as the random factor, the state (working memory task or control), area (CA1 or CA3) and state-area interactions as the predictors, and branching factor/intrinsic neuronal timescale as the dependent variable have been built (while branching factor and the intrinsic neuronal timescale are analytically related, they emphasize different aspects of the distance to criticality and might have differing statistical consequences – mandating independent analyses in terms of both variables (i.e. in terms of two models)). Mixed effects models presuppose independence of observations; and even though the identity of each animal was included as a random factor it might be the case that (i) *within area* observations are not independent over time (i.e. across subsequent 30 s intervals), or that (ii) *between area* observations are not independent (i.e. at the same or (iii) across subsequent 30s intervals). Accordingly, in order to test for independence across areas, time (for both areas), and areas & time (for both directionalities), 10 statistical tests were conducted to control for all possible relationships (i.e. five possible relationships for branching factor & for the timescale, each). A non-parametric approach (permutation-testing) was chosen because (i) parametric tests typically presuppose (i) distributional assumptions (e.g. normality – which is not fulfilled), and (ii) independence of observations (which is, in part, precisely what is in question, so it cannot be presupposed), and (iii) the synthetic data generation approach of permutation testing induces a more realistic statistical baseline that incorporates the actual observed distribution in the null-hypothesis (compared to, e.g., simple point estimates as in t-tests). More specifically, for each of the above relationships, the average (auto-)correlation was calculated over the complete dataset (i.e. all animals, days and epochs). Subsequently, for each relationship, 1000 synthetic average (auto-)correlations were generated based on shuffled 30-s time-chunks over the whole dataset (this preserves the individual distributions but destroys (auto)-correlations). Two-tailed p-values were

calculated as the fraction of synthetic means which had an absolute value greater than the absolute value of the empirical mean. It turned out that out of the 10 tests (2 models x 5 tests), 9 tests were insignificant – suggesting that there is no violation of the assumption of independence across areas, time, and areas & time; enabling a formulation of the mixed model as specified above. While one test – the correlation across areas at the same 30 s interval – revealed a significant interaction for the branching factor, this was not evident in the model with the intrinsic neuronal timescale. Given that in total, 20 tests were performed (10 for each set of models (concerning one hypothesis, each); for the second two models see below), this may also result from multiple testing. Figures 1 & 3 visualize the results of the tests, and Figures 2, 4, 5 & 6 depict the statistical outcomes.

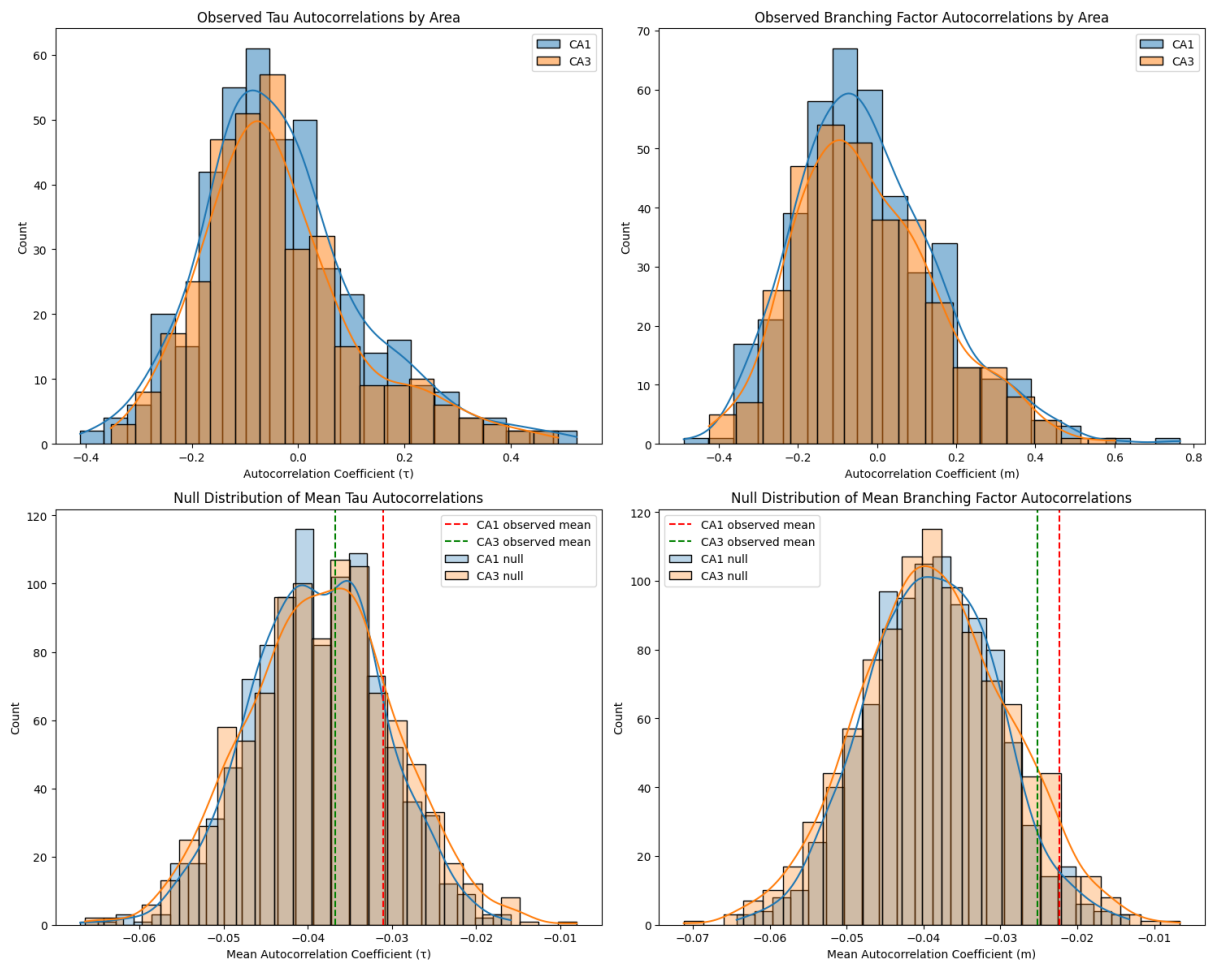


Figure 1. (Top) Distribution over mean autocorrelations (for data from animal-day-epoch combinations) of intrinsic neuronal timescale and branching factor. (Bottom) Mean autocorrelations (for the *complete* data set) of CA1 & CA3 relative to a null-distribution over *means* obtained from synthetically generated autocorrelations (shuffled time-chunks within each animal-day-epoch combination; with the whole dataset being permuted 1000 times).

Within-Area Autocorrelation Analysis Results

Area	Measure	Observed Mean	Null Mean	p-value	CI 95%
CA1	Neural Timescale	-0.031	-0.039	8.430e-01	[-0.054, -0.023]
CA1	Branching Factor	-0.022	-0.039	9.730e-01	[-0.055, -0.022]
CA3	Neural Timescale	-0.037	-0.038	5.510e-01	[-0.054, -0.021]
CA3	Branching Factor	-0.025	-0.039	9.390e-01	[-0.057, -0.022]

Figure 2. Results of the within-area autocorrelation analysis. Across all areas and measures, no significant autocorrelation is present in subsequent 30 s intervals.

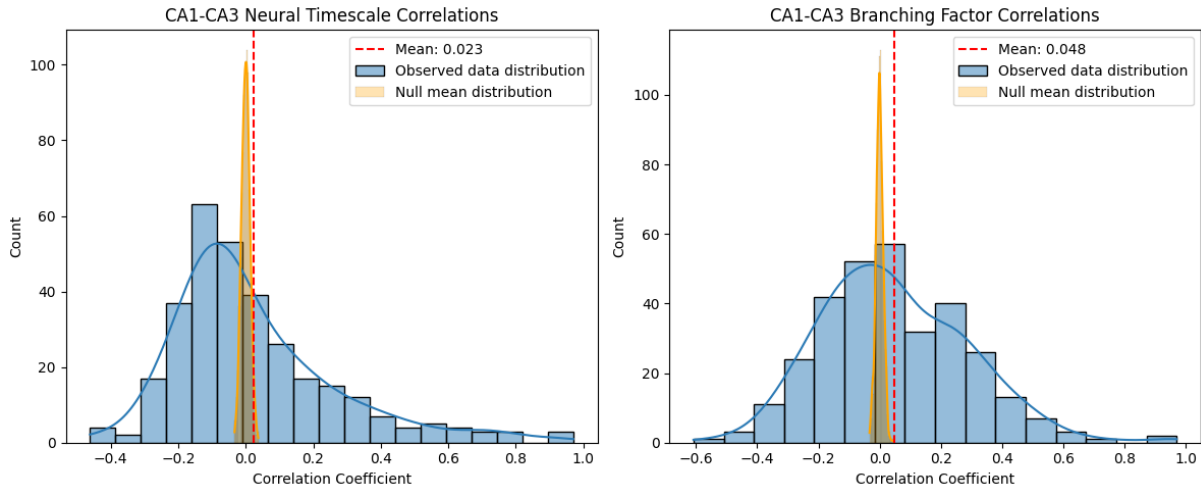


Figure 3. Distribution over correlation coefficients of neuronal timescale (left) and branching factor (right) between CA1 and CA3 for temporally simultaneous time-chunks. The synthetically generated distribution over means under the null-hypothesis is superimposed, together with the empirical mean of the observed distribution for the complete dataset.

CA1-CA3 Correlation Analysis Results (Between-Task)

Measure	Observed Mean	Null Mean	p-value	CI 95%
Neural Timescale	0.023	-0.000	5.600e-02	[-0.022, 0.025]
Branching Factor	0.048	0.001	0.000e+00	[-0.023, 0.025]

Figure 4. Results of the inter-area correlation analysis (see the text for discussion).

Between-Area Analysis Results (CA3_to_CAI)

Measure	Observed Mean	Null Mean	p-value	CI 95%
Neural Timescale	-0.006	0.001	5.840e-01	[-0.020, 0.024]
Branching Factor	-0.007	-0.000	5.420e-01	[-0.023, 0.022]

Figure 5. Results of the temporally directed inter-area correlation analysis from CA3 to CA1.

Between-Area Analysis Results (CA1_to_CA3)

Measure	Observed Mean	Null Mean	p-value	CI 95%
Neural Timescale	-0.013	-0.000	2.950e-01	[-0.024, 0.025]
Branching Factor	0.002	-0.000	8.650e-01	[-0.023, 0.024]

Figure 6. Results of the temporally directed inter-area correlation analysis from CA1 to CA3.

Consistently, both models reveal that the hippocampal distance to criticality in CA1 & CA3 is reduced when the animals perform the working memory task (see Figure 7 & 10). An interaction effect between area and task condition was not consistently evident: While for the model with branching factor as a dependent variable, the branching factor in the working memory task was even higher for CA1, as opposed to CA3; this effect was not evident in the model with the intrinsic neuronal timescale as the dependent variable (see Figure 8 & 10).

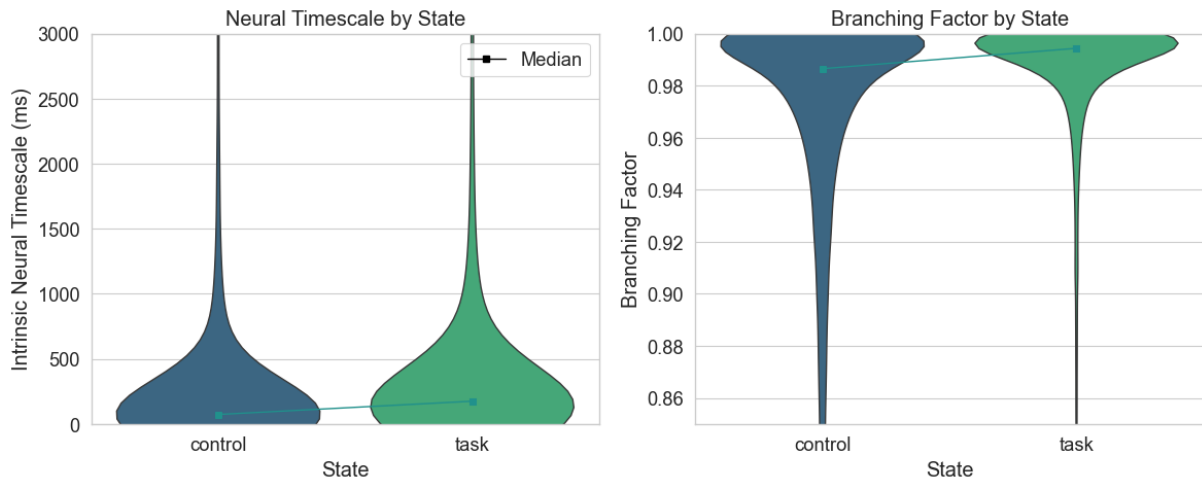


Figure 7. Violin-plot of the intrinsic neuronal timescale and the branching factor for the working memory task and the control condition. The distribution of both intrinsic neuronal timescale and branching factor is highly skewed, such that the median is displayed.

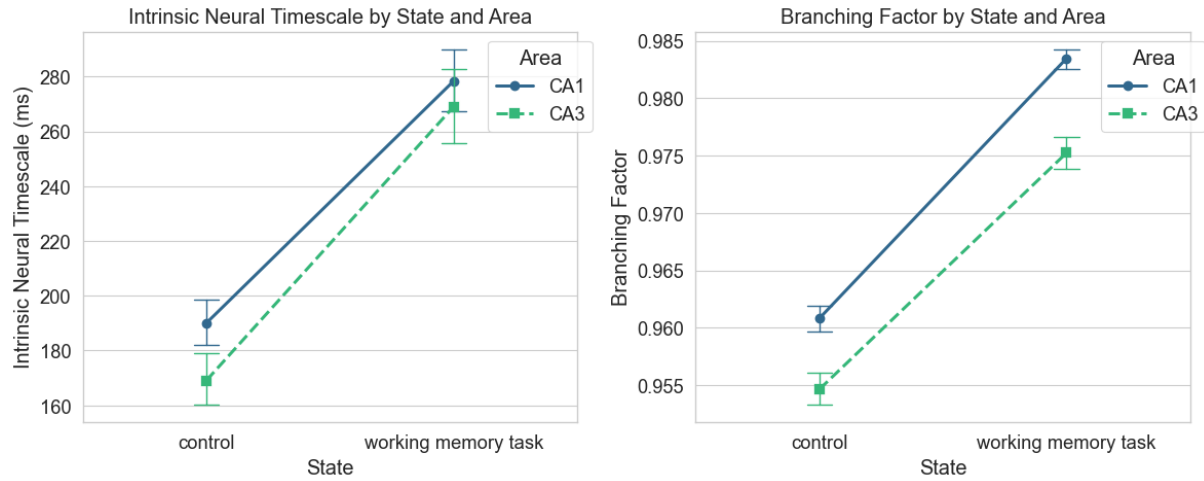


Figure 8. Interaction on intrinsic neuronal timescale and branching factor between state and hippocampal subarea. The interaction on intrinsic timescale for state & area is unsignificant, whereas the interaction on branching factor for state and area is significant – with the branching factor in CA1 being, relative to CA3, higher in the working memory task.

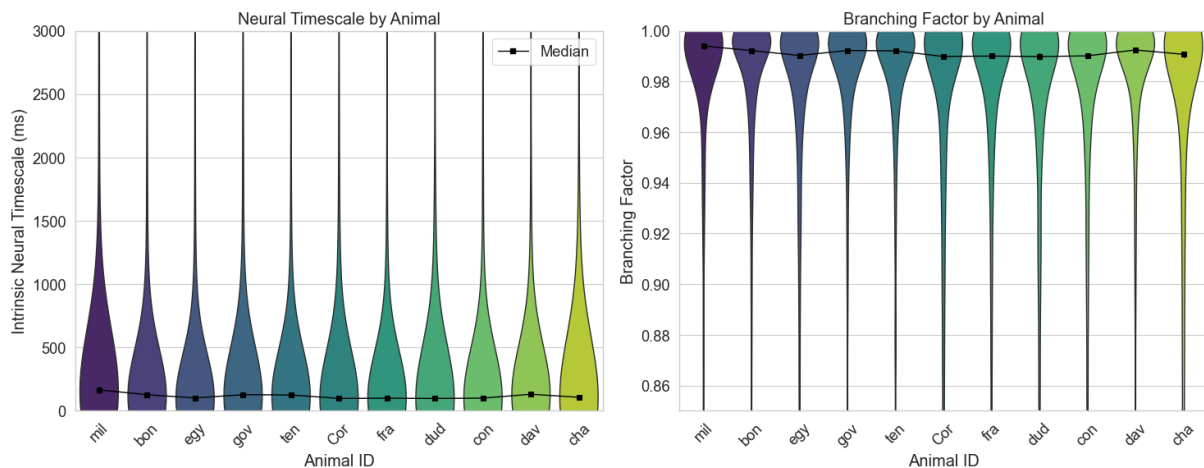


Figure 9. Intrinsic neuronal timescale and branching factor for the 11 animals that were included in the analysis.

Mixed Effects Model Results (Between-Task)						
Measure	Parameter	Coefficient	Std. Error	z-value	p-value	CI 95%
Branching Factor	Intercept	0.960	0.002	475.690	0.000e+00	[0.956, 0.964]
Branching Factor	state[T.working memory task]	0.023	0.001	26.422	7.559e-154	[0.021, 0.024]
Branching Factor	area[T.CA3]	-0.005	0.001	-6.399	1.562e-10	[-0.007, -0.004]
Branching Factor	state[T.working memory task]:area[T.CA3]	-0.003	0.001	-2.054	3.998e-02	[-0.005, -0.000]
Branching Factor	Group Var	0.020	0.009	2.162	3.060e-02	[0.002, 0.038]
Branching Factor	Random Effect (Animal)	0.006	--	--	--	--
Neural Timescale	Intercept	188.497	6.186	30.472	6.101e-204	[176.372, 200.621]
Neural Timescale	state[T.working memory task]	89.023	7.383	12.057	1.771e-33	[74.552, 103.493]
Neural Timescale	area[T.CA3]	-18.551	6.997	-2.651	8.021e-03	[-32.265, -4.837]
Neural Timescale	state[T.working memory task]:area[T.CA3]	11.018	11.041	0.998	3.183e-01	[-10.622, 32.658]
Neural Timescale	Group Var	0.001	0.001	1.388	1.651e-01	[-0.000, 0.003]
Neural Timescale	Random Effect (Animal)	13.456	--	--	--	--

Figure 10. Results of the two mixed effects model analyses over all animals, investigating the relationship between the distance to criticality with the enactment of a working memory task (compared to a control task), as well as a possible interaction with the hippocampal subarea (CA1 & CA3).

Given that it is possible that certain structures vary significantly between individual animals, individual analyses of all single animal were also performed (i.e. 2 mixed effect models for each animal, which – apart from the absence of the random-factor (i.e. animals) – were identically constructed to the models described above). These models served to (i) validate the effects attested by the group level analysis, and (ii) discern any possible effects pertaining to only a subset of animals. Despite potentially over-conservative Bonferroni-correction, the modulation of the distance to criticality during the working memory task was present in 18/22 models (i.e. 11/11 in the model with branching factor; and 7/11 in the model with timescale). An interaction effect, however, was only evident in 5/22 animals. More specifically, and apart from seven animals which did not show any interaction effect, only one animal showed a closer distance to criticality for CA3 in the working memory task for both models; two animals only in the model with the branching factor; and one animal showed the effect in the *opposite* direction, with CA1 having a closer distance to criticality in the working memory task. The results of an example animal (“Conley”) are shown in Figure 11 & 12; and Bonferroni-corrected p-values over the individual-animal analyses are shown in Figure 13. More detailed results and visualizations for all animals can be found in the Appendix.

Animal: con

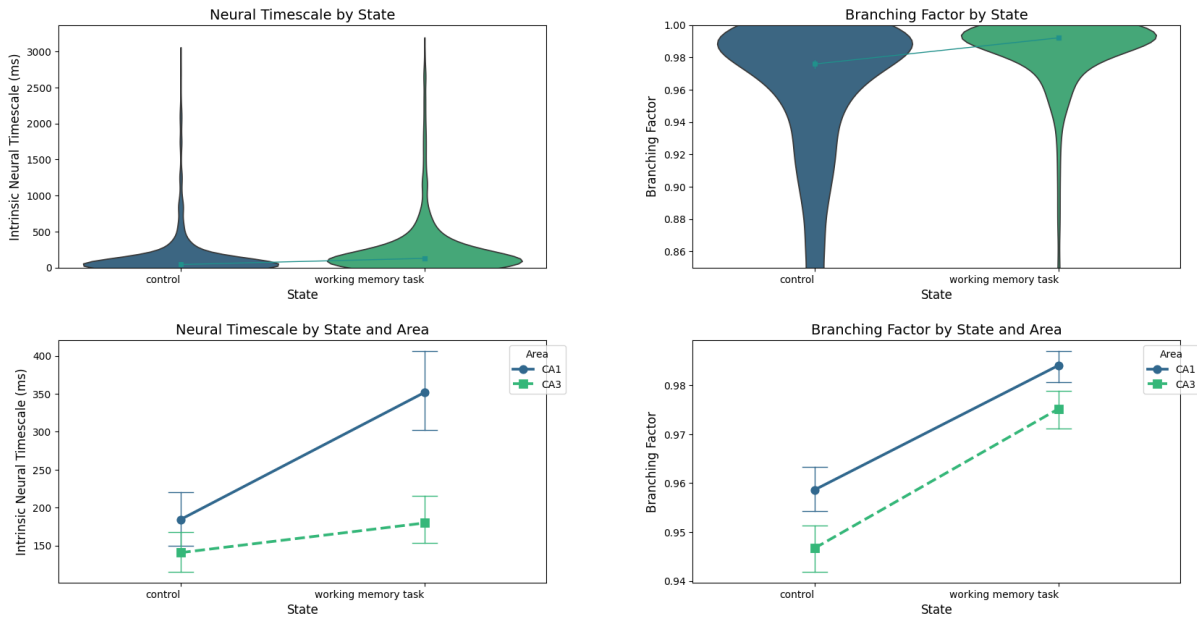


Figure 11. Exemplary visualization of the results for a single animal (“Conley”)

Between-Task Analysis Results for Animal con

Measure	Predictor	Coefficient (SE)	z-value	p-value (Bonferroni-corrected) [uncorrected]	CI 95%
Neural Timescale	Intercept	184.447 (387.617)	0.476	> 1 [0.634]	[-575.269, 944.162]
Neural Timescale	state[T.working memory task]	167.357 (26.033)	6.429	< 0.001 [< 0.001]	[116.333, 218.381]
Neural Timescale	area[T.CA3]	-43.729 (23.996)	-1.822	0.752 [0.068]	[-90.759, 3.302]
Neural Timescale	state[T.working memory task];area[T.CA3]	-128.320 (36.591)	-3.507	0.005 [< 0.001]	[-200.037, -56.602]
Neural Timescale	Group Var	1.000 (-)	--	-- [--]	[--, --]
Neural Timescale	Group Var	149948.906 (-)	--	-- [--]	[--, --]
Branching Factor	Intercept	0.959 (0.046)	20.856	< 0.001 [< 0.001]	[0.869, 1.049]
Branching Factor	state[T.working memory task]	0.025 (0.003)	8.234	< 0.001 [< 0.001]	[0.019, 0.031]
Branching Factor	area[T.CA3]	-0.012 (0.003)	-4.190	< 0.001 [< 0.001]	[-0.017, -0.006]
Branching Factor	state[T.working memory task];area[T.CA3]	0.003 (0.004)	0.703	> 1 [0.482]	[-0.005, 0.012]
Branching Factor	Group Var	1.000 (-)	--	-- [--]	[--, --]
Branching Factor	Group Var	0.002 (-)	--	-- [--]	[--, --]

Figure 12. Exemplary results of the linear model analysis for a single animal (“Conley”).

Summary of Bonferroni-corrected Significant Results for Between-Task Analysis

Measure	Predictor	Significant Results (Bonferroni-corrected)
Neural Timescale	Intercept	0/11
Neural Timescale	state(reference=control)[T.working memory task]	7/11
Neural Timescale	area[T.CA3]	1/11
Neural Timescale	state(reference=control)[T.working memory task] × area[T.CA3]	3/11
Branching Factor	Intercept	11/11
Branching Factor	state(reference=control)[T.working memory task]	11/11
Branching Factor	area[T.CA3]	7/11
Branching Factor	state(reference=control)[T.working memory task] × area[T.CA3]	2/11

Figure 13. Summary of the linear model analysis of all individual animals (predictors: state (i.e. working memory task/control) area (i.e. CA1/CA3), and interactions; dependent variable: neural timescale or branching factor (a separate model was built for each). Bonferroni-adjusted p-values reveal a consistent variation of the neuronal timescale and the branching factor across states: The distance to criticality is – for 18/22 models of the 11 animals and for all animals for the model with the branching factor – reduced during the performance in the working memory task.

In order to test a possible relationship between the distance to criticality and the performance in the working memory task *within* the time the animals performed this task (second hypothesis), a similar mixed model approach was used. Specifically – and following the above-mentioned consistency analysis across two separate models relative to one dependent variable, each (i.e. branching factor and intrinsic neuronal timescale) – these dependent variables were predicted by task performance, area, and their interaction (i.e. three independent variables); with animal being the random factor. Task performance, as elaborated above, was subdivided into three (relative) performance categories:

0, 0.5, & 1 – reflecting the relative number of the working memory involving outbound trials the animal performed successfully. Even though the data that was used to investigate this relationship is a subset of the data from the first hypothesis (see above), the independency across areas, time, and areas & time was investigated similarly via a non-parametric permutation-analysis (see the results in the Appendix); in order to exclude possible characteristics of the data that are only evinced by a subset of the data (and which would undermine the independence assumption presupposed by the mixed effects models).

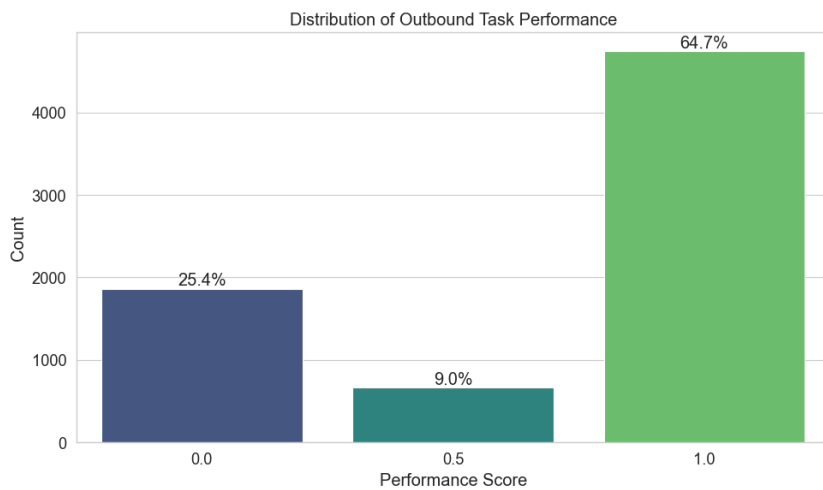


Figure 14. Relative performance (i.e. number of correct outbound trials relative to all trials in 30 s) of all animals over all days and epochs in the working memory task (i.e. outbound task). The number of trials per 30 s interval was at most 2, and the animals performed the task optimally 64.7 % of the time.

Across both mixed effects models on the group-level analysis, all possible effects pertaining to a relationship between relative performance and the distance to criticality, as well as all possible interaction effects of relative performance and area on the distance to criticality, remained insignificant (see Figures 15, 16 & 17).

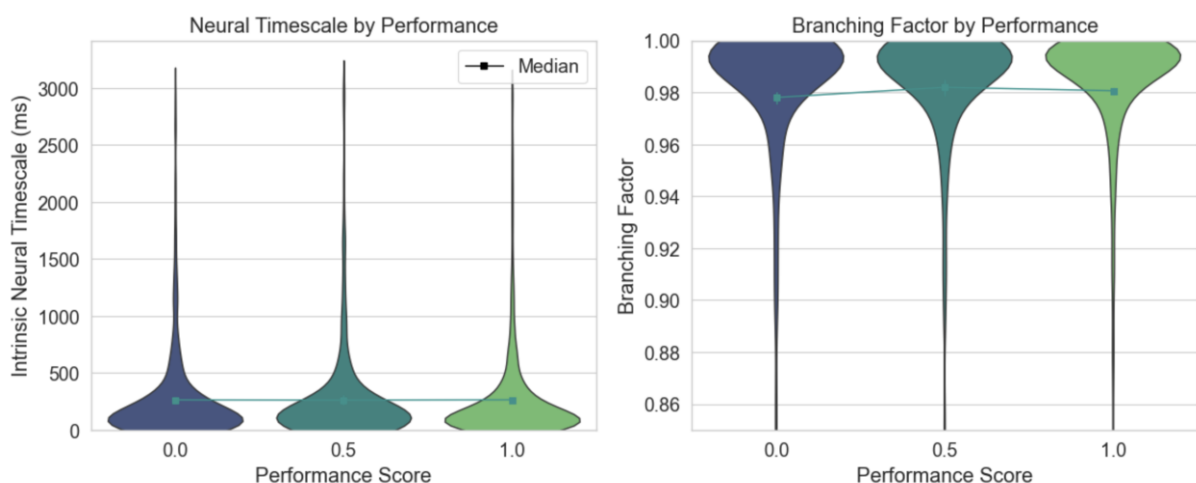


Figure 15. Intrinsic neuronal timescale and branching factor relative to performance categories.

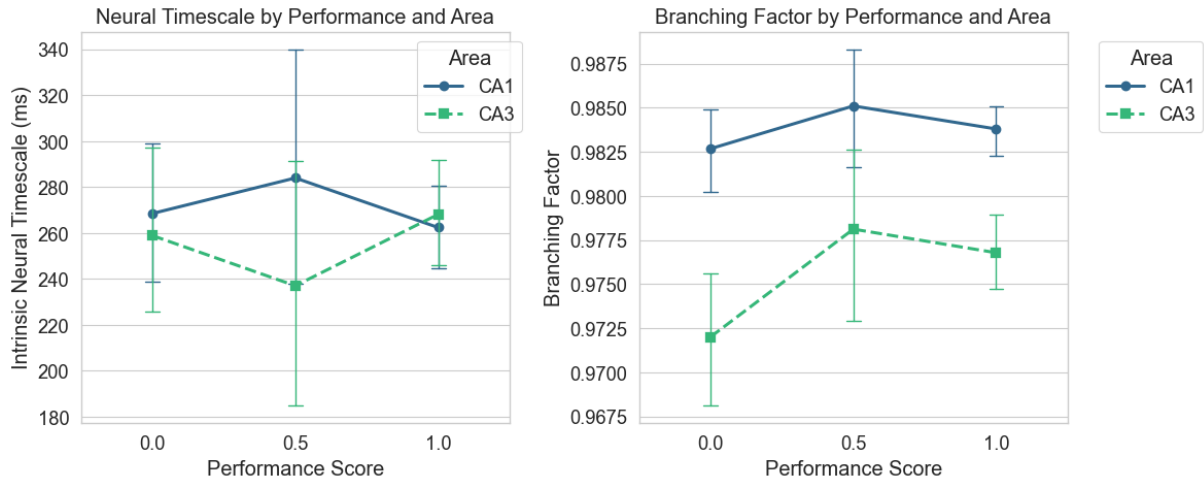


Figure 16. Intrinsic neuronal timescale and branching factor relative to performance categories and areas.

Mixed Effects Model Results (Within-Task)						
Measure	Parameter	Coefficient	Std. Error	z-value	p-value	CI 95%
Branching Factor	Intercept	0.983	0.003	374.839	0.000e+00	[0.978, 0.988]
Branching Factor	outbound_performance[T.0.5]	-0.000	0.003	-0.129	8.974e-01	[-0.005, 0.005]
Branching Factor	outbound_performance[T.1.0]	-0.001	0.002	-0.355	7.230e-01	[-0.004, 0.003]
Branching Factor	area[T.CA3]	-0.011	0.002	-5.543	2.968e-08	[-0.015, -0.007]
Branching Factor	outbound_performance[T.0.5]:area[T.CA3]	0.004	0.004	0.996	3.193e-01	[-0.004, 0.011]
Branching Factor	outbound_performance[T.1.0]:area[T.CA3]	0.003	0.002	1.503	1.328e-01	[-0.001, 0.008]
Branching Factor	Group Var	0.039	0.021	1.881	5.992e-02	[-0.002, 0.080]
Branching Factor	Random Effect (Animal)	0.007	--	--	--	--
Neural Timescale	Intercept	272.285	95.276	2.858	4.265e-03	[85.547, 459.023]
Neural Timescale	outbound_performance[T.0.5]	12.622	30.826	0.409	6.822e-01	[-47.796, 73.039]
Neural Timescale	outbound_performance[T.1.0]	-12.348	18.759	-0.658	5.104e-01	[-49.115, 24.419]
Neural Timescale	area[T.CA3]	-12.477	23.681	-0.527	5.983e-01	[-58.890, 33.937]
Neural Timescale	outbound_performance[T.0.5]:area[T.CA3]	-37.427	45.703	-0.819	4.128e-01	[-127.004, 52.150]
Neural Timescale	outbound_performance[T.1.0]:area[T.CA3]	15.122	27.893	0.542	5.877e-01	[-39.547, 69.792]
Neural Timescale	Group Var	0.462	nan	nan	nan	[nan, nan]
Neural Timescale	Random Effect (Animal)	281.958	--	--	--	--

Figure 17. Results of the two mixed effects model analyses over all animals, investigating the relationship between the distance to criticality with the performance in a working memory task (outbound trials), as well as possible interactions with the hippocampal subarea (CA1 & CA3).

Given that it is possible that significant variance exists between individual animals, individual analyses of all single animal were also performed (i.e. 2 mixed effect models for each animal, which – apart from the absence of inclusion of the random-factor (i.e. animals) – were identically constructed to the models described above). These models served to (i) validate the absence of effects attested by the group level analysis, and (ii) to discern any possible effects pertaining only to a subset of animals. These animal-specific analyses consistently demonstrated the absence of effects pertaining to a relationship between relative performance and the distance to criticality, as well as all interaction effects with the area. For an overview of the Bonferroni-corrected relative significance per predictor for all animals,

see Figure 20. For an example analysis of a single animal, see Figure 18 & 19; for all other analyses of all other animals, see the Appendix. The code for the statistical analyses & visualizations, is open source: https://github.com/JanBellingrath/hippocampal_distance_to_criticality_working_memory.

Animal: con

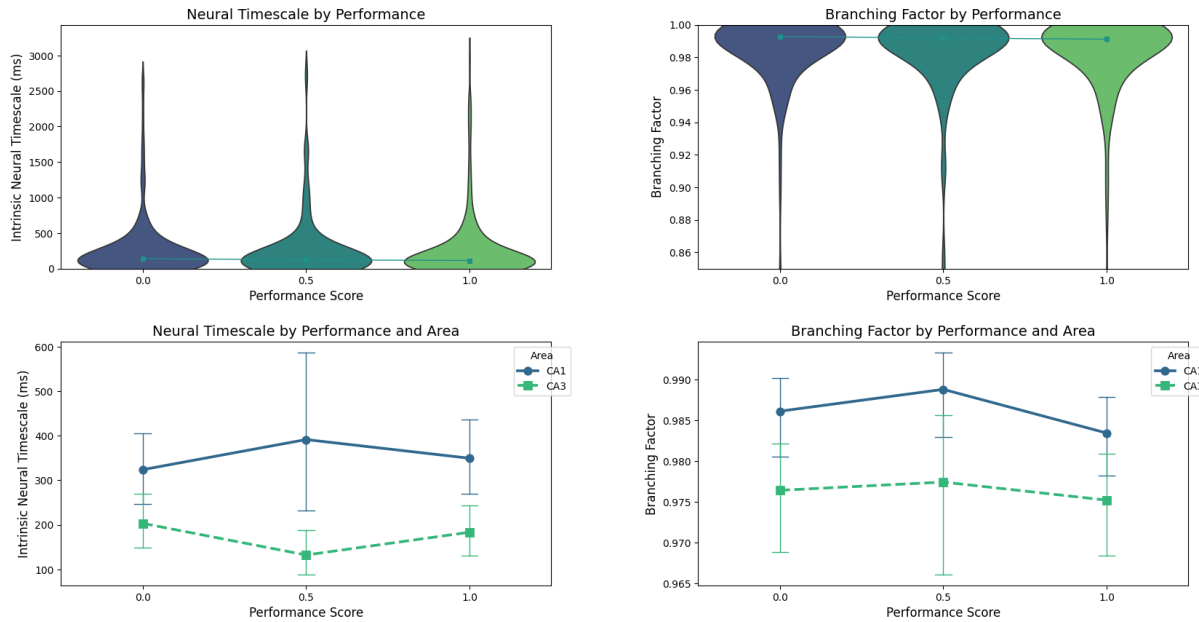


Figure 18. Exemplary visualization of the results of the linear model analysis for a single animal ("Conley").

Within-Task Analysis Results for Animal con

Measure	Predictor	Coefficient (SE)	z-value	p-value (Bonferroni-corrected) [uncorrected]	CI 95%
Neural Timescale	Intercept	323.981 (423.880)	0.764	> 1 [0.445]	[-506.808, 1154.769]
Neural Timescale	C(performance_cat, Treatment(reference='0.0'))[T.0.5]	67.613 (77.296)	0.875	> 1 [0.382]	[-83.885, 219.111]
Neural Timescale	C(performance_cat, Treatment(reference='0.0'))[T.1.0]	25.668 (51.397)	0.499	> 1 [0.617]	[-75.069, 126.405]
Neural Timescale	area[T.CA3]	-120.735 (54.601)	-2.211	0.243 [0.027]	[-227.752, -13.718]
Neural Timescale	C(performance_cat, Treatment(reference='0.0'))[T.0.5]:area[T.CA3]	-138.693 (107.722)	-1.288	> 1 [0.198]	[-349.823, 72.437]
Neural Timescale	C(performance_cat, Treatment(reference='0.0'))[T.1.0]:area[T.CA3]	-45.600 (73.873)	-0.617	> 1 [0.537]	[-190.389, 99.190]
Neural Timescale	Group Var	1.000 (-)	--	-- [-]	[-, -]
Neural Timescale	Group Var	178270.239 (-)	--	-- [-]	[-, -]
Branching Factor	Intercept	0.986 (0.033)	30.055	< 0.001 [< 0.001]	[0.922, 1.050]
Branching Factor	C(performance_cat, Treatment(reference='0.0'))[T.0.5]	0.003 (0.006)	0.447	> 1 [0.655]	[-0.009, 0.014]
Branching Factor	C(performance_cat, Treatment(reference='0.0'))[T.1.0]	-0.003 (0.004)	-0.674	> 1 [0.500]	[-0.010, 0.005]
Branching Factor	area[T.CA3]	-0.010 (0.004)	-2.297	0.194 [0.022]	[-0.018, -0.001]
Branching Factor	C(performance_cat, Treatment(reference='0.0'))[T.0.5]:area[T.CA3]	-0.002 (0.008)	-0.200	> 1 [0.842]	[-0.018, 0.015]
Branching Factor	C(performance_cat, Treatment(reference='0.0'))[T.1.0]:area[T.CA3]	0.001 (0.006)	0.258	> 1 [0.797]	[-0.010, 0.013]
Branching Factor	Group Var	1.000 (-)	--	-- [-]	[-, -]
Branching Factor	Group Var	0.001 (-)	--	-- [-]	[-, -]

Figure 19. Exemplary depiction of the results of the linear model for a single animal (predictors: area, performance categories & interaction between area and performance categories; dependent variable: neural timescale or branching factor (a separate model was built for each)).

Summary of Bonferroni-corrected Significant Results for Within-Task Analysis

Measure	Predictor	Significant Results (Bonferroni-corrected)
Neural Timescale	Intercept	0/9
Neural Timescale	performance(reference=0.0)[T.0.5]	0/9
Neural Timescale	performance(reference=0.0)[T.1.0]	0/9
Neural Timescale	area[T.CA3]	0/9
Neural Timescale	performance(reference=0.0)[T.0.5] × area[T.CA3]	0/9
Neural Timescale	performance(reference=0.0)[T.1.0] × area[T.CA3]	0/9
Branching Factor	Intercept	9/9
Branching Factor	performance(reference=0.0)[T.0.5]	0/9
Branching Factor	performance(reference=0.0)[T.1.0]	0/9
Branching Factor	area[T.CA3]	3/9
Branching Factor	performance(reference=0.0)[T.0.5] × area[T.CA3]	0/9
Branching Factor	performance(reference=0.0)[T.1.0] × area[T.CA3]	0/9

Figure 20. Summary of the linear model analyses for all individual animals. Bonferroni-adjusted p-values, consistently across all animals, predictors, and dependent variables, reveal no associations between performance and distance to criticality.

Discussion

This master thesis investigates a possible relationship between working memory and the distance to the critical state. Working memory (equated for pragmatic reasons with short-term memory; see page 6) is neuronally widely distributed, with the specific encoded content being processed in a region-relative manner (e.g. sensory regions encode sensory working memory; hierarchically higher regions encode more conceptual working memory content; etc. (for a review see (Christophel et al., 2017)). As predicted by two theoretical perspectives on hippocampal functioning (see section 3.2) and evidenced by numerous recently conducted intracranial studies (see sections 3.1 & 3.2) – the hippocampus is functionally implicated in working memory. Indeed, given its important functional role in spatial cognition (for a review see (Hartley et al., 2014)), the hippocampus may be especially involved in spatial working memory. A closer distance to the critical state may be expected to be facilitative for working memory for a number of reasons. Concerning computationally adaptive information-theoretic properties that have been evidenced to ensue in the vicinity of criticality, an increased information-storage capacity and an increased information transmission are especially central in the context of working memory (see section 4.1). Furthermore, given the conjunctive encoding in hippocampal working memory – i.e. an encoding of *what* happened *when* on a temporally receding internal timeline (Howard et al., 2014; Shankar & Howard, 2012) – is conceptually necessary for successful performance in the working memory task (i.e. the presence of one of those pieces of information alone is not sufficient); the presence of higher-order synergistic information (i.e. information only revealed by the

joint state of “what” and “when”) is adaptive for working memory performance. Given that previous work revealed an increase of synergistic information as the distance to the critical point decreases, working memory encodings are expected to profit from a closer distance to criticality (see section 4.1). Furthermore – next to recent human neuroimaging work, which directly demonstrated a relationship between working memory and a closer distance to criticality – numerous *in silico* studies in the context of reservoir computing attest to the presence of an increased dynamical memory at the critical phase transition (see section 4.2). On the most general level, *critical slowing down* (the long transients that ensue in the vicinity to criticality) itself may be read as a purely dynamical form of working memory. This is also in accord with the diverging correlation length through time at the critical point; enabling this very informational persistence. Using a W-track spatial alternation task with 11 rodents, and a subsampling invariant estimator that inferred the proximity to criticality from the hippocampal subregions CA1 and CA3 – which are empirically most closely associated with short-term memory encodings (see section 3) – this relationship was tested in terms of two concrete hypotheses. The first hypothesis concerned an increased proximity to criticality for a working memory task relative to a control condition. The second hypothesis investigated whether *within* the working memory task, an *even* closer distance to criticality is associated with an increased performance. While it was found that an even smaller distance to criticality within the working memory task is *not* associated with an increased performance, the hippocampal distance to criticality is – in accord with expectations – dynamically reduced in the working memory task. This finding holds both on a global level (i.e. analyzed collectively with the data from all animals), and on an individual-animal level of analysis: Indeed, despite a potentially over-conservative Bonferroni-correction, this modulation of the distance to criticality was present in 18/22 individual-animal level models (i.e. it was found across 11/11 animals in the model with branching factor as the dependent variable; and across 7/11 animals in the model with intrinsic neuronal timescale). Accordingly, neuronal dynamics in the hippocampus are endogenously regulated towards the critical state during the performance of a working memory task. Equally consistently, the *within-task* effect – i.e. the relationship between the distance to criticality and the task performance – was not found on both a global and an individual-animal level of analysis. Indeed, on the individual-animal level analysis, only 5/22 models revealed a significant effect, and this effect was *neither* directionally consistent across animals, *nor* evident across both models for individual animals except for one. Apart from the most parsimonious explanation that there simply is no such regulation over these very small timescales, two alternative explanations for this finding exist – one based on a methodological limitation of the subsampling invariant estimator of the distance to criticality as specifically paired with the W-track spatial alternation task; and another one based on the level of difficulty of the task – as specifically seen through the lens of the framework of dynamic adaptive computation (Wilting, Dehning, Neto, et al., 2018). As elaborated above (section 6) statistical

inferences concerning the distance to criticality become biased for temporal windows that become shorter. This study was based on 30 s temporal windows, which – while already inducing some bias – were hypothesized to optimize the tradeoff between the bias in estimation and a sufficiently temporally fine-grained analysis. While it is possible that the animal sustains the relevant information in its short-term memory across an entire task-iteration – perhaps also because the task is relatively easy (see Figure 14) – it is also possible that the animals predominantly use the *last perceptible cue* that uniquely determines the next correct choice. Here, specifically, this concerns the point at which the animal turns from one of the outer arms to the middle-most arm (in the inbound trial): The animal can infer from the proprioceptive afferents received by turning its body to the inner arm the outbound arm it came from. However, if the animals only actively self-sustain information in working memory from that last perceptible cue onwards, *and* if it were possible for the brain to regulate the distance to criticality over such small timescales (which is itself to a large degree an open question; see section 2.2), a reduced distance to criticality would only be expected in this part of the task (i.e. from turning into the inner arm, to the subsequent choice-point out of the inner arm). However, given that this interval is temporally only a small fraction of the 30 s temporal windows the analysis was based upon, the systematic measurement bias of the estimator that would be induced might become problematic. A second consideration, based on the difficulty-level of the task, as seen through the lens of the framework of dynamic adaptive computation (Wilting, Dehning, Neto, et al., 2018), is that the task was simply too easy: The animals are in the highest performance category 64.7% of the time (see Figure 14). Perhaps, accordingly, the distance to criticality does not have to be *further* reduced in order to sustain the information in working memory, because the generated dynamical regime – which is *already* closer to criticality in the working memory task, compared to a control – is already sufficient for satisfactory task performance. From this perspective, this effect might only be evident for more difficult tasks that impose higher demands on working memory. This is also in accord with previous simulation studies, that document the adaptivity of close-to-critical dynamics only for more complex tasks (Cramer et al., 2020). Indeed, this study found that less complex tasks might even be facilitated by an increased distance to criticality by virtue of the increased response-reliability that it enables (see also section 2.2). Accordingly, it is possible that multiple opposing effects balance each other out in the observed dynamical regime (i.e. response-reliability and storage & transmission capacity). Generally, this perspective is consistent with the framework of dynamic adaptive computation; being focused not on the *maximization* of particular computational properties, but on a *sufficient* expression thereof under competing requirements and resource constraints. However, apart from this possibility of a balancing of effects in an easier-than-optimal task, the most parsimonious explanation is that the neuronal distance to criticality is simply *not* regulated relative to the processing-requirements induced by a task on such a *small* timescale. As elaborated in section 2.2., empirical evidence on, e.g., set-point

(i.e. task) relative neuronal regulatory processes on small timescales – while predicted on a theoretical basis and presupposed in many modelling studies – remain empirically speculative. To summarize, this master thesis has evaluated the hypothesis that an increased proximity to criticality in the rodent hippocampus is adaptive in the context of a working memory task. This hypothesis is supported by numerous computational and dynamical properties adaptive for working memory that ensue in the vicinity of criticality; as well as cognitive neuroscience studies and *in silico* simulations. While it was found that an even smaller distance to criticality within the working memory task is *not* associated with an increased performance, the hippocampal distance to criticality is – in accord with expectations – dynamically reduced in the working memory task. These findings can be understood in terms of the framework of dynamic adaptive computation; with the brain self-regulating the distance to criticality in a task dependent manner in order to obtain *sufficiently* optimized (as opposed to maximized) computational properties. Given that criticality is associated with *universality* – the idea that macroscopic dynamics are invariant with respect to changes in microscopic realization across diverse systems – the framework of criticality offers some hope regards generalizations across species.

The code for the statistical analysis & visualizations, including an illustrative Jupyter notebook, can be accessed under:
https://github.com/JanBellingrath/hippocampal_distance_to_criticality_working_memory.

References

- Aben, B., Stapert, S., & Blokland, A. (2012). About the Distinction between Working Memory and Short-Term Memory. *Frontiers in Psychology*, 3.
<https://doi.org/10.3389/fpsyg.2012.00301>
- Axmacher, N., Henseler, M. M., Jensen, O., Weinreich, I., Elger, C. E., & Fell, J. (2010). Cross-frequency coupling supports multi-item working memory in the human hippocampus. *Proceedings of the National Academy of Sciences*, 107(7), 3228–3233. <https://doi.org/10.1073/pnas.0911531107>
- Baddeley, A., Allen, R., & Vargha-Khadem, F. (2010). Is the hippocampus necessary for visual and verbal binding in working memory? *Neuropsychologia*, 48(4), 1089–1095.
<https://doi.org/10.1016/j.neuropsychologia.2009.12.009>
- Bak, P. (2013). *How nature works: The science of self-organized criticality*. Springer Science & Business Media.
<https://books.google.de/books?hl=de&lr=&id=x8nSBwAAQBAJ&oi=fnd&pg=PP10&ots=wY0awrSavx&sig=sWdjw802N97XIY5Q8rwU0h52fpc>
- Barrett, L. F., Quigley, K. S., & Hamilton, P. (2016). An active inference theory of allostasis and interoception in depression. *Philosophical Transactions of the Royal Society B: Biological Sciences*, 371(1708), 20160011.
<https://doi.org/10.1098/rstb.2016.0011>
- Barrett, L. F., & Simmons, W. K. (2015). Interoceptive predictions in the brain. *Nature Reviews Neuroscience*, 16(7), Article 7. <https://doi.org/10.1038/nrn3950>
- Batterman, R. W., & Rice, C. C. (2014). Minimal model explanations. *Philosophy of Science*, 81(3), 349–376.
- Bédard, C., Kröger, H., & Destexhe, A. (2006). Does the \$1/f\$ Frequency Scaling of Brain Signals Reflect Self-Organized Critical States? *Physical Review Letters*, 97(11), 118102. <https://doi.org/10.1103/PhysRevLett.97.118102>
- Beggs, J. M. (2022). *The Cortex and the Critical Point: Understanding the Power of Emergence*. MIT Press.
- Beggs, J. M., & Plenz, D. (2003a). Neuronal Avalanches in Neocortical Circuits. *Journal of Neuroscience*, 23(35), 11167–11177. <https://doi.org/10.1523/JNEUROSCI.23-35-11167.2003>

- Beggs, J. M., & Plenz, D. (2003b). Neuronal Avalanches in Neocortical Circuits. *Journal of Neuroscience*, 23(35), 11167–11177. <https://doi.org/10.1523/JNEUROSCI.23-35-11167.2003>
- Beggs, J., & Timme, N. (2012). Being Critical of Criticality in the Brain. *Frontiers in Physiology*, 3. <https://www.frontiersin.org/articles/10.3389/fphys.2012.00163>
- Bellay, T., Klaus, A., Seshadri, S., & Plenz, D. (2015). Irregular spiking of pyramidal neurons organizes as scale-invariant neuronal avalanches in the awake state. *eLife*, 4, e07224. <https://doi.org/10.7554/eLife.07224>
- Bertschinger, N., & Natschläger, T. (2004). Real-Time Computation at the Edge of Chaos in Recurrent Neural Networks. *Neural Computation*, 16(7), 1413–1436. Neural Computation. <https://doi.org/10.1162/089976604323057443>
- Binney, J. J., Dowrick, N. J., Fisher, A. J., & Newman, M. E. J. (1992). *The Theory of Critical Phenomena: An Introduction to the Renormalization Group*. Oxford University Press.
- Boran, E., Fedele, T., Klaver, P., Hilfiker, P., Stieglitz, L., Grunwald, T., & Sarnthein, J. (2019). Persistent hippocampal neural firing and hippocampal-cortical coupling predict verbal working memory load. *Science Advances*, 5(3), eaav3687. <https://doi.org/10.1126/sciadv.aav3687>
- Boran, E., Hilfiker, P., Stieglitz, L., Sarnthein, J., & Klaver, P. (2022). Persistent neuronal firing in the medial temporal lobe supports performance and workload of visual working memory in humans. *NeuroImage*, 254, 119123. <https://doi.org/10.1016/j.neuroimage.2022.119123>
- Bright, I. M., Meister, M. L. R., Cruzado, N. A., Tiganj, Z., Buffalo, E. A., & Howard, M. W. (2020). A temporal record of the past with a spectrum of time constants in the monkey entorhinal cortex. *Proceedings of the National Academy of Sciences*, 117(33), 20274–20283. <https://doi.org/10.1073/pnas.1917197117>
- Büsing, L., Schrauwen, B., & Legenstein, R. (2010). Connectivity, Dynamics, and Memory in Reservoir Computing with Binary and Analog Neurons. *Neural Computation*, 22(5), 1272–1311. <https://doi.org/10.1162/neco.2009.01-09-947>
- Buzsáki, G., & Tingley, D. (2018). Space and Time: The Hippocampus as a Sequence Generator. *Trends in Cognitive Sciences*, 22(10), 853–869. <https://doi.org/10.1016/j.tics.2018.07.006>

- Cao, R., Bladon, J. H., Charczynski, S. J., Hasselmo, M. E., & Howard, M. W. (2022). Internally generated time in the rodent hippocampus is logarithmically compressed. *eLife*, 11, e75353. <https://doi.org/10.7554/eLife.75353>
- Carhart-Harris, R. L., & Friston, K. J. (2019). REBUS and the Anarchic Brain: Toward a Unified Model of the Brain Action of Psychedelics. *Pharmacological Reviews*, 71(3), 316–344. <https://doi.org/10.1124/pr.118.017160>
- Carlson, J. M., & Langer, J. S. (1989). Properties of earthquakes generated by fault dynamics. *Physical Review Letters*, 62(22), 2632–2635.
<https://doi.org/10.1103/PhysRevLett.62.2632>
- Cavagna, A., Cimarelli, A., Giardina, I., Parisi, G., Santagati, R., Stefanini, F., & Viale, M. (2010). Scale-free correlations in starling flocks. *Proceedings of the National Academy of Sciences*, 107(26), 11865–11870.
<https://doi.org/10.1073/pnas.1005766107>
- Cavanagh, S. E., Towers, J. P., Wallis, J. D., Hunt, L. T., & Kennerley, S. W. (2018). Reconciling persistent and dynamic hypotheses of working memory coding in prefrontal cortex. *Nature Communications*, 9(1), 3498. <https://doi.org/10.1038/s41467-018-05873-3>
- Christophel, T. B., Klink, P. C., Spitzer, B., Roelfsema, P. R., & Haynes, J.-D. (2017). The Distributed Nature of Working Memory. *Trends in Cognitive Sciences*, 21(2), 111–124. <https://doi.org/10.1016/j.tics.2016.12.007>
- Cocchi, L., Gollo, L. L., Zalesky, A., & Breakspear, M. (2017). Criticality in the brain: A synthesis of neurobiology, models and cognition. *Progress in Neurobiology*, 158, 132–152. <https://doi.org/10.1016/j.pneurobio.2017.07.002>
- Cover, T. M. (1999). *Elements of information theory*. John Wiley & Sons.
- Cramer, B., Stöckel, D., Kreft, M., Wibral, M., Schemmel, J., Meier, K., & Priesemann, V. (2020). Control of criticality and computation in spiking neuromorphic networks with plasticity. *Nature Communications*, 11(1), 2853.
<https://doi.org/10.1038/s41467-020-16548-3>
- Dahmen, D., Diesmann, M., & Helias, M. (2016). *Distributions of covariances as a window into the operational regime of neuronal networks* (No. arXiv:1605.04153). arXiv.
<https://doi.org/10.48550/arXiv.1605.04153>

- Dahmen, D., Grün, S., Diesmann, M., & Helias, M. (2019). Second type of criticality in the brain uncovers rich multiple-neuron dynamics. *Proceedings of the National Academy of Sciences*, 116(26), 13051–13060.
<https://doi.org/10.1073/pnas.1818972116>
- Daume, J., Kamiński, J., Schjetnan, A. G. P., Salimpour, Y., Khan, U., Kyzar, M., Reed, C. M., Anderson, W. S., Valiante, T. A., Mamelak, A. N., & Rutishauser, U. (2024). Control of working memory by phase–amplitude coupling of human hippocampal neurons. *Nature*, 629(8011), 393–401. <https://doi.org/10.1038/s41586-024-07309-z>
- de Arcangelis, L., & Herrmann, H. J. (2010). Learning as a phenomenon occurring in a critical state. *Proceedings of the National Academy of Sciences*, 107(9), 3977–3981.
<https://doi.org/10.1073/pnas.0912289107>
- de Arcangelis, L., Perrone-Capano, C., & Herrmann, H. J. (2006). Self-Organized Criticality Model for Brain Plasticity. *Physical Review Letters*, 96(2), 028107.
<https://doi.org/10.1103/PhysRevLett.96.028107>
- Deco, G., Vidaurre, D., & Kringelbach, M. L. (2021). Revisiting the global workspace orchestrating the hierarchical organization of the human brain. *Nature Human Behaviour*, 5(4), 497–511. <https://doi.org/10.1038/s41562-020-01003-6>
- Del Papa, B., Priesemann, V., & Triesch, J. (2019). *Fading Memory, Plasticity, and Criticality in Recurrent Networks* (pp. 95–115). https://doi.org/10.1007/978-3-030-20965-0_6
- Department of Computation and Neural Systems, Caltech, Mail Stop 136-93, Pasadena, California 91125, USA, & Cook, M. (2004). Universality in Elementary Cellular Automata. *Complex Systems*, 15(1), 1–40.
<https://doi.org/10.25088/ComplexSystems.15.1.1>
- Effenberger, F., Jost, J., & Levina, A. (2015). Self-organization in Balanced State Networks by STDP and Homeostatic Plasticity. *PLOS Computational Biology*, 11(9), e1004420.
<https://doi.org/10.1371/journal.pcbi.1004420>
- Egorov, A. V., Hamam, B. N., Fransén, E., Hasselmo, M. E., & Alonso, A. A. (2002). Graded persistent activity in entorhinal cortex neurons. *Nature*, 420(6912), 173–178.
<https://doi.org/10.1038/nature01171>

- Eichenbaum, H. (2014). Time cells in the hippocampus: A new dimension for mapping memories. *Nature Reviews Neuroscience*, 15(11), Article 11. <https://doi.org/10.1038/nrn3827>
- Fagerholm, E. D., Dinov, M., Knöpfel, T., & Leech, R. (2018). The characteristic patterns of neuronal avalanches in mice under anesthesia and at rest: An investigation using constrained artificial neural networks. *PLOS ONE*, 13(5), e0197893. <https://doi.org/10.1371/journal.pone.0197893>
- Fagerholm, E. D., Lorenz, R., Scott, G., Dinov, M., Hellyer, P. J., Mirzaei, N., Leeson, C., Carmichael, D. W., Sharp, D. J., Shew, W. L., & Leech, R. (2015). Cascades and Cognitive State: Focused Attention Incurs Subcritical Dynamics. *Journal of Neuroscience*, 35(11), 4626–4634. <https://doi.org/10.1523/JNEUROSCI.3694-14.2015>
- Fagerholm, E. D., Scott, G., Shew, W. L., Song, C., Leech, R., Knöpfel, T., & Sharp, D. J. (2016). Cortical Entropy, Mutual Information and Scale-Free Dynamics in Waking Mice. *Cerebral Cortex*, 26(10), 3945–3952. <https://doi.org/10.1093/cercor/bhw200>
- Fekete, T., Omer, D. B., O’Hashi, K., Grinvald, A., van Leeuwen, C., & Shriki, O. (2018). Critical dynamics, anesthesia and information integration: Lessons from multi-scale criticality analysis of voltage imaging data. *NeuroImage*, 183, 919–933. <https://doi.org/10.1016/j.neuroimage.2018.08.026>
- Fellous, J.-M., & Sejnowski, T. J. (2000). Cholinergic induction of oscillations in the hippocampal slice in the slow (0.5–2 Hz), theta (5–12 Hz), and gamma (35–70 Hz) bands. *Hippocampus*, 10(2), 187–197. [https://doi.org/10.1002/\(SICI\)1098-1063\(2000\)10:2<187::AID-HIPO8>3.0.CO;2-M](https://doi.org/10.1002/(SICI)1098-1063(2000)10:2<187::AID-HIPO8>3.0.CO;2-M)
- Finke, C., Braun, M., Ostendorf, F., Lehmann, T.-N., Hoffmann, K.-T., Kopp, U., & Ploner, C. J. (2008). The human hippocampal formation mediates short-term memory of colour–location associations. *Neuropsychologia*, 46(2), 614–623. <https://doi.org/10.1016/j.neuropsychologia.2007.10.004>
- Garg, P. (2023). Mixed signatures for subcritical dynamics in rodent hippocampus during sleep and awake epochs. <https://doi.org/10.1101/2023.10.30.564597>
- Gill, P. R., Mizumori, S. J. Y., & Smith, D. M. (2011). Hippocampal episode fields develop with learning. *Hippocampus*, 21(11), 1240–1249. <https://doi.org/10.1002/hipo.20832>

- Girardi-Schappo, M., Galera, E. F., Carvalho, T. T. A., Brochini, L., Kamiji, N. L., Roque, A. C., & Kinouchi, O. (2021). A unified theory of E/I synaptic balance, quasicritical neuronal avalanches and asynchronous irregular spiking. *Journal of Physics: Complexity*, 2(4), 045001. <https://doi.org/10.1088/2632-072X/ac2792>
- Girn, M., Rosas, F. E., Daws, R. E., Gallen, C. L., Gazzaley, A., & Carhart-Harris, R. L. (2023). A complex systems perspective on psychedelic brain action. *Trends in Cognitive Sciences*, 27(5), 433–445. <https://doi.org/10.1016/j.tics.2023.01.003>
- Goldman, M. S. (2009). Memory without Feedback in a Neural Network. *Neuron*, 61(4), 621–634. <https://doi.org/10.1016/j.neuron.2008.12.012>
- Gollo, L. L. (2017). Coexistence of critical sensitivity and subcritical specificity can yield optimal population coding. *Journal of The Royal Society Interface*, 14(134), 20170207. <https://doi.org/10.1098/rsif.2017.0207>
- Grady, C. L. (2020). Meta-analytic and functional connectivity evidence from functional magnetic resonance imaging for an anterior to posterior gradient of function along the hippocampal axis. *Hippocampus*, 30(5), 456–471. <https://doi.org/10.1002/hipo.23164>
- Greenfield, E., & Lecar, H. (2001). Mutual information in a dilute, asymmetric neural network model. *Physical Review E*, 63(4), 041905. <https://doi.org/10.1103/PhysRevE.63.041905>
- Hagemann, A., Wilting, J., Samimizad, B., Mormann, F., & Priesemann, V. (2021). Assessing criticality in pre-seizure single-neuron activity of human epileptic cortex. *PLOS Computational Biology*, 17(3), e1008773. <https://doi.org/10.1371/journal.pcbi.1008773>
- Haldeman, C., & Beggs, J. M. (2005). Critical Branching Captures Activity in Living Neural Networks and Maximizes the Number of Metastable States. *Physical Review Letters*, 94(5), 058101. <https://doi.org/10.1103/PhysRevLett.94.058101>
- Hartley, T., Lever, C., Burgess, N., & O’Keefe, J. (2014). Space in the brain: How the hippocampal formation supports spatial cognition. *Philosophical Transactions of the Royal Society B: Biological Sciences*, 369(1635), 20120510. <https://doi.org/10.1098/rstb.2012.0510>
- Hauser, J., Llano López, L. H., Feldon, J., Gargiulo, P. A., & Yee, B. K. (2020). Small lesions of the dorsal or ventral hippocampus subregions are associated with distinct

- impairments in working memory and reference memory retrieval, and combining them attenuates the acquisition rate of spatial reference memory. *Hippocampus*, 30(9), 938–957. <https://doi.org/10.1002/hipo.23207>
- Hayon, G., Abeles, M., & Lehmann, D. (2005). A Model for Representing the Dynamics of a System of Synfire Chains. *Journal of Computational Neuroscience*, 18(1), 41–53. <https://doi.org/10.1007/s10827-005-5479-1>
- Hidalgo, J., Grilli, J., Suweis, S., Muñoz, M. A., Banavar, J. R., & Maritan, A. (2014). Information-based fitness and the emergence of criticality in living systems. *Proceedings of the National Academy of Sciences*, 111(28), 10095–10100. <https://doi.org/10.1073/pnas.1319166111>
- Houle, P. A., & Sethna, J. P. (1996). Acoustic emission from crumpling paper. *Physical Review E*, 54(1), 278–283. <https://doi.org/10.1103/PhysRevE.54.278>
- Howard, M. W., & Eichenbaum, H. (2013). THEORETICAL REVIEW The Hippocampus, Time, and Memory Across Scales. *Journal of Experimental Psychology. General*, 142(4), 1211. <https://doi.org/10.1037/a0033621>
- Howard, M. W., & Kahana, M. J. (1999). Contextual variability and serial position effects in free recall. *Journal of Experimental Psychology: Learning, Memory, and Cognition*, 25(4), 923–941. <https://doi.org/10.1037/0278-7393.25.4.923>
- Howard, M. W., MacDonald, C. J., Tiganj, Z., Shankar, K. H., Du, Q., Hasselmo, M. E., & Eichenbaum, H. (2014). A Unified Mathematical Framework for Coding Time, Space, and Sequences in the Hippocampal Region. *The Journal of Neuroscience*, 34(13), 4692–4707. <https://doi.org/10.1523/JNEUROSCI.5808-12.2014>
- Howard, M. W., Youker, T. E., & Venkatadass, V. S. (2008). The persistence of memory: Contiguity effects across hundreds of seconds. *Psychonomic Bulletin & Review*, 15(1), 58–63. <https://doi.org/10.3758/PBR.15.1.58>
- Hyman, J. M., Ma, L., Balaguer-Ballester, E., Durstewitz, D., & Seamans, J. K. (2012). Contextual encoding by ensembles of medial prefrontal cortex neurons. *Proceedings of the National Academy of Sciences*, 109(13), 5086–5091. <https://doi.org/10.1073/pnas.1114415109>
- Itskov, V., Curto, C., Pastalkova, E., & Buzsáki, G. (2011). Cell Assembly Sequences Arising from Spike Threshold Adaptation Keep Track of Time in the Hippocampus.

- Journal of Neuroscience*, 31(8), 2828–2834.
<https://doi.org/10.1523/JNEUROSCI.3773-10.2011>
- Jaeger, H. (2001). *Short term memory in echo state networks*.
<https://doi.org/10.24406/publica-fhg-291107>
- Jaeger, H. (2007). Echo state network. *Scholarpedia*, 2(9), 2330.
<https://doi.org/10.4249/scholarpedia.2330>
- Jaeger, H., Maass, W., & Principe, J. (2007). Special issue on echo state networks and liquid state machines. *Neural Networks*, 20(3), 287–289.
<https://doi.org/10.1016/j.neunet.2007.04.001>
- Jannesari, M., Saeedi, A., Zare, M., Ortiz-Mantilla, S., Plenz, D., & Benasich, A. A. (2020). Stability of neuronal avalanches and long-range temporal correlations during the first year of life in human infants. *Brain Structure and Function*, 225(3), 1169–1183. <https://doi.org/10.1007/s00429-019-02014-4>
- Jensen, H. J. (1998). *Self-Organized Criticality: Emergent Complex Behavior in Physical and Biological Systems*. Cambridge University Press.
- Kamiński, J., Brzezicka, A., & Wróbel, A. (2011). Short-term memory capacity (7 ± 2) predicted by theta to gamma cycle length ratio. *Neurobiology of Learning and Memory*, 95(1), 19–23. <https://doi.org/10.1016/j.nlm.2010.10.001>
- Kamiński, J., Sullivan, S., Chung, J. M., Ross, I. B., Mamelak, A. N., & Rutishauser, U. (2017). Persistently active neurons in human medial frontal and medial temporal lobe support working memory. *Nature Neuroscience*, 20(4), 590–601.
<https://doi.org/10.1038/nn.4509>
- King, C., Recce, M., & O’Keefe, J. (1998). The rhythmicity of cells of the medial septum/diagonal band of Broca in the awake freely moving rat: Relationships with behaviour and hippocampal theta. *European Journal of Neuroscience*, 10(2), 464–477. <https://doi.org/10.1046/j.1460-9568.1998.00026.x>
- Kinouchi, O., & Copelli, M. (2006). Optimal dynamical range of excitable networks at criticality. *Nature Physics*, 2(5), 348–351. <https://doi.org/10.1038/nphys289>
- Kraus, B. J., Robinson, R. J., White, J. A., Eichenbaum, H., & Hasselmo, M. E. (2013). Hippocampal “Time Cells”: Time versus Path Integration. *Neuron*, 78(6), 1090–1101. <https://doi.org/10.1016/j.neuron.2013.04.015>

- Langton, C. G. (1990). Computation at the edge of chaos: Phase transitions and emergent computation. *Physica D: Nonlinear Phenomena*, 42(1), 12–37.
[https://doi.org/10.1016/0167-2789\(90\)90064-V](https://doi.org/10.1016/0167-2789(90)90064-V)
- Lazar, A., Pipa, G., & Triesch, J. (2009). SORN: A self-organizing recurrent neural network. *Frontiers in Computational Neuroscience*, 3.
<https://doi.org/10.3389/neuro.10.023.2009>
- Legenstein, R., & Maass, W. (2007). Edge of chaos and prediction of computational performance for neural circuit models. *Neural Networks*, 20(3), 323–334.
<https://doi.org/10.1016/j.neunet.2007.04.017>
- Levina, A., Ernst, U., & Michael Herrmann, J. (2007). Criticality of avalanche dynamics in adaptive recurrent networks. *Neurocomputing*, 70(10), 1877–1881.
<https://doi.org/10.1016/j.neucom.2006.10.056>
- Levina, A., Herrmann, J. M., & Denker, M. (2007). Critical branching processes in neural networks. *PAMM*, 7(1), 1030701–1030702.
<https://doi.org/10.1002/pamm.200700029>
- Levina, A., Herrmann, J. M., & Geisel, T. (2007). Dynamical synapses causing self-organized criticality in neural networks. *Nature Physics*, 3(12), 857–860.
<https://doi.org/10.1038/nphys758>
- Levina, A., Herrmann, J. M., & Geisel, T. (2009). Phase Transitions towards Criticality in a Neural System with Adaptive Interactions. *Physical Review Letters*, 102(11), 118110. <https://doi.org/10.1103/PhysRevLett.102.118110>
- Levina, A., & Priesemann, V. (2017). Subsampling scaling. *Nature Communications*, 8(1), Article 1. <https://doi.org/10.1038/ncomms15140>
- Li, J., Cao, D., Li, W., Sarnthein, J., & Jiang, T. (2024). Re-evaluating human MTL in working memory: Insights from intracranial recordings. *Trends in Cognitive Sciences*.
<https://doi.org/10.1016/j.tics.2024.07.008>
- Li, W., Packard, N. H., & Langton, C. G. (1990). Transition phenomena in cellular automata rule space. *Physica D: Nonlinear Phenomena*, 45(1), 77–94.
[https://doi.org/10.1016/0167-2789\(90\)90175-O](https://doi.org/10.1016/0167-2789(90)90175-O)
- Linkenkaer-Hansen, K., Nikouline, V. V., Palva, J. M., & Ilmoniemi, R. J. (2001). Long-Range Temporal Correlations and Scaling Behavior in Human Brain Oscillations. *Journal*

- of Neuroscience*, 21(4), 1370–1377. <https://doi.org/10.1523/JNEUROSCI.21-04-01370.2001>
- Lisman, J. E., & Idiart, M. A. P. (1995). Storage of 7 ± 2 Short-Term Memories in Oscillatory Subcycles. *Science*, 267(5203), 1512–1515.
<https://doi.org/10.1126/science.7878473>
- Lisman, J. E., & Jensen, O. (2013). The Theta-Gamma Neural Code. *Neuron*, 77(6), 1002–1016. <https://doi.org/10.1016/j.neuron.2013.03.007>
- Lisman, J., & Redish, A. d. (2009). Prediction, sequences and the hippocampus. *Philosophical Transactions of the Royal Society B: Biological Sciences*, 364(1521), 1193–1201.
<https://doi.org/10.1098/rstb.2008.0316>
- Liu, J., Zhang, H., Yu, T., Ni, D., Ren, L., Yang, Q., Lu, B., Wang, D., Heinen, R., Axmacher, N., & Xue, G. (2020). Stable maintenance of multiple representational formats in human visual short-term memory. *Proceedings of the National Academy of Sciences*, 117(51), 32329–32339. <https://doi.org/10.1073/pnas.2006752117>
- Liu, Y., Tiganj, Z., Hasselmo, M. E., & Howard, M. W. (2019). A neural microcircuit model for a scalable scale-invariant representation of time. *Hippocampus*, 29(3), 260–274.
<https://doi.org/10.1002/hipo.22994>
- Logie, R., Camos, V., & Cowan, N. (2020). *Working Memory: The state of the science*. Oxford University Press.
- Luppi, A. I., Mediano, P. A. M., Rosas, F. E., Holland, N., Fryer, T. D., O'Brien, J. T., Rowe, J. B., Menon, D. K., Bor, D., & Stamatakis, E. A. (2022). A synergistic core for human brain evolution and cognition. *Nature Neuroscience*, 25(6), 771–782.
<https://doi.org/10.1038/s41593-022-01070-0>
- Luppi, A. I., Rosas, F. E., Mediano, P. A. M., Menon, D. K., & Stamatakis, E. A. (2024). Information decomposition and the informational architecture of the brain. *Trends in Cognitive Sciences*, 28(4), 352–368.
<https://doi.org/10.1016/j.tics.2023.11.005>
- Ma, Z., Turrigiano, G. G., Wessel, R., & Hengen, K. B. (2019). Cortical Circuit Dynamics Are Homeostatically Tuned to Criticality In Vivo. *Neuron*, 104(4), 655-664.e4.
<https://doi.org/10.1016/j.neuron.2019.08.031>
- Maass, W., Legenstein, R., & Bertschinger, N. (2004). Methods for Estimating the Computational Power and Generalization Capability of Neural Microcircuits.

- Advances in Neural Information Processing Systems*, 17.
<https://proceedings.neurips.cc/paper/2004/hash/9ff7c9eb9d37f434db778f59178012da-Abstract.html>
- Maass, W., & Markram, H. (2004). On the computational power of circuits of spiking neurons. *Journal of Computer and System Sciences*, 69(4), 593–616.
<https://doi.org/10.1016/j.jcss.2004.04.001>
- Maass, W., Natschläger, T., & Markram, H. (2002). Real-Time Computing Without Stable States: A New Framework for Neural Computation Based on Perturbations. *Neural Computation*, 14(11), 2531–2560. Neural Computation.
<https://doi.org/10.1162/089976602760407955>
- MacDonald, C. J., Carrow, S., Place, R., & Eichenbaum, H. (2013). Distinct Hippocampal Time Cell Sequences Represent Odor Memories in Immobilized Rats. *Journal of Neuroscience*, 33(36), 14607–14616. <https://doi.org/10.1523/JNEUROSCI.1537-13.2013>
- MacDonald, C. J., Lepage, K. Q., Eden, U. T., & Eichenbaum, H. (2011). Hippocampal “Time Cells” Bridge the Gap in Memory for Discontiguous Events. *Neuron*, 71(4), 737–749. <https://doi.org/10.1016/j.neuron.2011.07.012>
- Mankin, E. A., Sparks, F. T., Slayyeh, B., Sutherland, R. J., Leutgeb, S., & Leutgeb, J. K. (2012). Neuronal code for extended time in the hippocampus. *Proceedings of the National Academy of Sciences*, 109(47), 19462–19467.
<https://doi.org/10.1073/pnas.1214107109>
- Manns, J. R., Howard, M. W., & Eichenbaum, H. (2007). Gradual Changes in Hippocampal Activity Support Remembering the Order of Events. *Neuron*, 56(3), 530–540.
<https://doi.org/10.1016/j.neuron.2007.08.017>
- Mau, W., Sullivan, D. W., Kinsky, N. R., Hasselmo, M. E., Howard, M. W., & Eichenbaum, H. (2018). The same hippocampal CA1 population simultaneously codes temporal information over multiple timescales. *Current Biology*, 28(10), 1499–1508.
- Mazzoni, A., Broccard, F. D., Garcia-Perez, E., Bonifazi, P., Ruaro, M. E., & Torre, V. (2007). On the Dynamics of the Spontaneous Activity in Neuronal Networks. *PLOS ONE*, 2(5), e439. <https://doi.org/10.1371/journal.pone.0000439>
- Mediano, P. A. M., Rosas, F. E., Farah, J. C., Shanahan, M., Bor, D., & Barrett, A. B. (2022). Integrated information as a common signature of dynamical and information-

- processing complexity. *Chaos: An Interdisciplinary Journal of Nonlinear Science*, 32(1), 013115. <https://doi.org/10.1063/5.0063384>
- Meisel, C., Bailey, K., Achermann, P., & Plenz, D. (2017). Decline of long-range temporal correlations in the human brain during sustained wakefulness. *Scientific Reports*, 7(1), 11825. <https://doi.org/10.1038/s41598-017-12140-w>
- Meisel, C., & Gross, T. (2009). Adaptive self-organization in a realistic neural network model. *Physical Review E*, 80(6), 061917. <https://doi.org/10.1103/PhysRevE.80.061917>
- Meisel, C., Klaus, A., Vyazovskiy, V. V., & Plenz, D. (2017). The Interplay between Long- and Short-Range Temporal Correlations Shapes Cortex Dynamics across Vigilance States. *Journal of Neuroscience*, 37(42), 10114–10124.
<https://doi.org/10.1523/JNEUROSCI.0448-17.2017>
- Mesulam, M. M. (1998). From sensation to cognition. *Brain*, 121(6), 1013–1052.
<https://doi.org/10.1093/brain/121.6.1013>
- Miller, G. (1956). Human memory and the storage of information. *IRE Transactions on Information Theory*, 2(3), 129–137. IRE Transactions on Information Theory.
<https://doi.org/10.1109/TIT.1956.1056815>
- Miranda, E. N., & Herrmann, H. J. (1991). Self-organized criticality with disorder and frustration. *Physica A: Statistical Mechanics and Its Applications*, 175(3), 339–344. [https://doi.org/10.1016/0378-4371\(91\)90235-5](https://doi.org/10.1016/0378-4371(91)90235-5)
- Muñoz, M. A. (2018). Colloquium: Criticality and dynamical scaling in living systems. *Reviews of Modern Physics*, 90(3), 031001.
<https://doi.org/10.1103/RevModPhys.90.031001>
- Murray, J. D., Bernacchia, A., Freedman, D. J., Romo, R., Wallis, J. D., Cai, X., Padoa-Schioppa, C., Pasternak, T., Seo, H., Lee, D., & Wang, X.-J. (2014). A hierarchy of intrinsic timescales across primate cortex. *Nature Neuroscience*, 17(12), 1661–1663.
<https://doi.org/10.1038/nn.3862>
- Nagel, K., & Herrmann, H. J. (1993). Deterministic models for traffic jams. *Physica A: Statistical Mechanics and Its Applications*, 199(2), 254–269.
[https://doi.org/10.1016/0378-4371\(93\)90006-P](https://doi.org/10.1016/0378-4371(93)90006-P)
- Neto, J. P., Spitzner, F. P., & Priesemann, V. (2022). Sampling effects and measurement overlap can bias the inference of neuronal avalanches. *PLOS Computational Biology*, 18(11), e1010678. <https://doi.org/10.1371/journal.pcbi.1010678>

- O'Byrne, J., & Jerbi, K. (2022). How critical is brain criticality? *Trends in Neurosciences*, 45(11), 820–837. <https://doi.org/10.1016/j.tins.2022.08.007>
- Pasquale, V., Massobrio, P., Bologna, L. L., Chiappalone, M., & Martinoia, S. (2008). Self-organization and neuronal avalanches in networks of dissociated cortical neurons. *Neuroscience*, 153(4), 1354–1369.
<https://doi.org/10.1016/j.neuroscience.2008.03.050>
- Pastalkova, E., Itskov, V., Amarasingham, A., & Buzsáki, G. (2008). Internally Generated Cell Assembly Sequences in the Rat Hippocampus. *Science*, 321(5894), 1322–1327.
<https://doi.org/10.1126/science.1159775>
- Ponce-Alvarez, A., Jouary, A., Privat, M., Deco, G., & Sumbre, G. (2018). Whole-Brain Neuronal Activity Displays Crackling Noise Dynamics. *Neuron*, 100(6), 1446–1459.e6. <https://doi.org/10.1016/j.neuron.2018.10.045>
- Priesemann, V., Munk, M. H., & Wibral, M. (2009). Subsampling effects in neuronal avalanche distributions recorded in vivo. *BMC Neuroscience*, 10(1), 40.
<https://doi.org/10.1186/1471-2202-10-40>
- Priesemann, V., & Shriki, O. (2018). Can a time varying external drive give rise to apparent criticality in neural systems? *PLOS Computational Biology*, 14(5), e1006081.
<https://doi.org/10.1371/journal.pcbi.1006081>
- Priesemann, V., Valderrama, M., Wibral, M., & Quyen, M. L. V. (2013). Neuronal Avalanches Differ from Wakefulness to Deep Sleep – Evidence from Intracranial Depth Recordings in Humans. *PLOS Computational Biology*, 9(3), e1002985.
<https://doi.org/10.1371/journal.pcbi.1002985>
- Priesemann, V., Wibral, M., Valderrama, M., Pröpper, R., Le Van Quyen, M., Geisel, T., Triesch, J., Nikolić, D., & Munk, M. H. J. (2014). Spike avalanches in vivo suggest a driven, slightly subcritical brain state. *Frontiers in Systems Neuroscience*, 8.
<https://doi.org/10.3389/fnsys.2014.00108>
- Proca, A. M., Rosas, F. E., Luppi, A. I., Bor, D., Crosby, M., & Mediano, P. A. M. (2022). *Synergistic information supports modality integration and flexible learning in neural networks solving multiple tasks* (No. arXiv:2210.02996). arXiv.
<https://doi.org/10.48550/arXiv.2210.02996>
- Pruessner, G. (2012). *Self-Organised Criticality: Theory, Models and Characterisation*. Cambridge University Press.

- Rajan, K., Harvey, C. D., & Tank, D. W. (2016). Recurrent Network Models of Sequence Generation and Memory. *Neuron*, 90(1), 128–142.
<https://doi.org/10.1016/j.neuron.2016.02.009>
- Ribeiro, T. L., Copelli, M., Caixeta, F., Belchior, H., Chialvo, D. R., Nicolelis, M. A. L., & Ribeiro, S. (2010). Spike Avalanches Exhibit Universal Dynamics across the Sleep-Wake Cycle. *PLOS ONE*, 5(11), e14129. <https://doi.org/10.1371/journal.pone.0014129>
- Rua, C., Wastling, S. J., Costagli, M., Symms, M. R., Biagi, L., Cosottini, M., Del Guerra, A., Tosetti, M., & Barker, G. J. (2018). Improving fMRI in signal drop-out regions at 7 T by using tailored radio-frequency pulses: Application to the ventral occipito-temporal cortex. *Magnetic Resonance Materials in Physics, Biology and Medicine*, 31(2), 257–267. <https://doi.org/10.1007/s10334-017-0652-x>
- Salz, D. M., Tiganj, Z., Khasnabish, S., Kohley, A., Sheehan, D., Howard, M. W., & Eichenbaum, H. (2016). Time Cells in Hippocampal Area CA3. *Journal of Neuroscience*, 36(28), 7476–7484. <https://doi.org/10.1523/JNEUROSCI.0087-16.2016>
- Scheffer, M., Carpenter, S. R., Lenton, T. M., Bascompte, J., Brock, W., Dakos, V., van de Koppel, J., van de Leemput, I. A., Levin, S. A., van Nes, E. H., Pascual, M., & Vandermeer, J. (2012). Anticipating Critical Transitions. *Science*, 338(6105), 344–348. <https://doi.org/10.1126/science.1225244>
- Sethna, J. P., Dahmen, K. A., & Myers, C. R. (2001). Crackling noise. *Nature*, 410(6825), 242–250. <https://doi.org/10.1038/35065675>
- Shahbaba, B., Li, L., Agostinelli, F., Saraf, M., Cooper, K. W., Haghverdian, D., Elias, G. A., Baldi, P., & Fortin, N. J. (2022). Hippocampal ensembles represent sequential relationships among an extended sequence of nonspatial events. *Nature Communications*, 13(1), 787. <https://doi.org/10.1038/s41467-022-28057-6>
- Shankar, K. H., & Howard, M. W. (2012). A Scale-Invariant Internal Representation of Time. *Neural Computation*, 24(1), 134–193. https://doi.org/10.1162/NECO_a_00212
- Shew, W. L., Clawson, W. P., Pobst, J., Karimipanah, Y., Wright, N. C., & Wessel, R. (2015). Adaptation to sensory input tunes visual cortex to criticality. *Nature Physics*, 11(8), 659–663. <https://doi.org/10.1038/nphys3370>
- Shew, W. L., Yang, H., Yu, S., Roy, R., & Plenz, D. (2011). Information Capacity and Transmission Are Maximized in Balanced Cortical Networks with Neuronal

- Avalanches. *Journal of Neuroscience*, 31(1), 55–63.
<https://doi.org/10.1523/JNEUROSCI.4637-10.2011>
- Shiffrin, R. M., & Atkinson, R. C. (1969). Storage and retrieval processes in long-term memory. *Psychological Review*, 76(2), 179–193.
<https://doi.org/10.1037/h0027277>
- Shirvalkar, P. R., Rapp, P. R., & Shapiro, M. L. (2010). Bidirectional changes to hippocampal theta–gamma comodulation predict memory for recent spatial episodes. *Proceedings of the National Academy of Sciences*, 107(15), 7054–7059.
<https://doi.org/10.1073/pnas.0911184107>
- Shriki, O., Alstott, J., Carver, F., Holroyd, T., Henson, R. N. A., Smith, M. L., Coppola, R., Bullmore, E., & Plenz, D. (2013). Neuronal Avalanches in the Resting MEG of the Human Brain. *Journal of Neuroscience*, 33(16), 7079–7090.
<https://doi.org/10.1523/JNEUROSCI.4286-12.2013>
- Shriki, O., & Yellin, D. (2016). Optimal Information Representation and Criticality in an Adaptive Sensory Recurrent Neuronal Network. *PLOS Computational Biology*, 12(2), e1004698. <https://doi.org/10.1371/journal.pcbi.1004698>
- Siegle, J. H., & Wilson, M. A. (2014). Enhancement of encoding and retrieval functions through theta phase-specific manipulation of hippocampus. *eLife*, 3, e03061.
<https://doi.org/10.7554/eLife.03061>
- Slotnick, S. D. (2022). Does working memory activate the hippocampus during the late delay period? *Cognitive Neuroscience*, 13(3–4), 182–207.
<https://doi.org/10.1080/17588928.2022.2075842>
- Slotnick, S. D. (2023). No convincing evidence the hippocampus is associated with working memory. *Cognitive Neuroscience*, 14(3), 96–106.
<https://doi.org/10.1080/17588928.2023.2223919>
- Spitzner, F. P., Dehning, J., Wilting, J., Hagemann, A., Neto, J. P., Zierenberg, J., & Priesemann, V. (2021). MR. Estimator, a toolbox to determine intrinsic timescales from subsampled spiking activity. *PLOS ONE*, 16(4), e0249447.
<https://doi.org/10.1371/journal.pone.0249447>
- Stewart, C. V., & Plenz, D. (2006). Inverted-U Profile of Dopamine–NMDA-Mediated Spontaneous Avalanche Recurrence in Superficial Layers of Rat Prefrontal Cortex.

Journal of Neuroscience, 26(31), 8148–8159.

<https://doi.org/10.1523/JNEUROSCI.0723-06.2006>

Suárez, L. E., Richards, B. A., Lajoie, G., & Misic, B. (2021). Learning function from structure in neuromorphic networks. *Nature Machine Intelligence*, 3(9), 771–786.

<https://doi.org/10.1038/s42256-021-00376-1>

Sydnor, V. J., Larsen, B., Bassett, D. S., Alexander-Bloch, A., Fair, D. A., Liston, C., Mackey, A. P., Milham, M. P., Pines, A., Roalf, D. R., Seidlitz, J., Xu, T., Raznahan, A., & Satterthwaite, T. D. (2021). Neurodevelopment of the association cortices: Patterns, mechanisms, and implications for psychopathology. *Neuron*, 109(18), 2820–2846. <https://doi.org/10.1016/j.neuron.2021.06.016>

Tagliazucchi, E., Balenzuela, P., Fraiman, D., & Chialvo, D. R. (2012). Criticality in Large-Scale Brain fMRI Dynamics Unveiled by a Novel Point Process Analysis. *Frontiers in Physiology*, 3. <https://doi.org/10.3389/fphys.2012.00015>

Tanaka, T., Kaneko, T., & Aoyagi, T. (2009). Recurrent Infomax Generates Cell Assemblies, Neuronal Avalanches, and Simple Cell-Like Selectivity. *Neural Computation*, 21(4), 1038–1067. <https://doi.org/10.1162/neco.2008.03-08-727>

Taxidis, J., Pnevmatikakis, E. A., Dorian, C. C., Mylavarapu, A. L., Arora, J. S., Samadian, K. D., Hoffberg, E. A., & Golshani, P. (2020). Differential Emergence and Stability of Sensory and Temporal Representations in Context-Specific Hippocampal Sequences. *Neuron*, 108(5), 984-998.e9.

<https://doi.org/10.1016/j.neuron.2020.08.028>

Tetzlaff, C., Okujeni, S., Egert, U., Wörgötter, F., & Butz, M. (2010). Self-Organized Criticality in Developing Neuronal Networks. *PLOS Computational Biology*, 6(12), e1001013. <https://doi.org/10.1371/journal.pcbi.1001013>

Tian, Y., Tan, Z., Hou, H., Li, G., Cheng, A., Qiu, Y., Weng, K., Chen, C., & Sun, P. (2022). Theoretical foundations of studying criticality in the brain. *Network Neuroscience*, 6(4), 1148–1185. https://doi.org/10.1162/netn_a_00269

Timme, N. M., Marshall, N. J., Bennett, N., Ripp, M., Lautzenhisler, E., & Beggs, J. M. (2016). Criticality Maximizes Complexity in Neural Tissue. *Frontiers in Physiology*, 7. <https://doi.org/10.3389/fphys.2016.00425>

- Tomen, N., Rotermund, D., & Ernst, U. (2014). Marginally subcritical dynamics explain enhanced stimulus discriminability under attention. *Frontiers in Systems Neuroscience*, 8. <https://doi.org/10.3389/fnsys.2014.00151>
- Touboul, J., & Destexhe, A. (2010). Can Power-Law Scaling and Neuronal Avalanches Arise from Stochastic Dynamics? *PLOS ONE*, 5(2), e8982. <https://doi.org/10.1371/journal.pone.0008982>
- Tsao, A., Sugar, J., Lu, L., Wang, C., Knierim, J. J., Moser, M.-B., & Moser, E. I. (2018). Integrating time from experience in the lateral entorhinal cortex. *Nature*, 561(7721), 57–62. <https://doi.org/10.1038/s41586-018-0459-6>
- Varley, T. F., & Bongard, J. (2024). Evolving higher-order synergies reveals a trade-off between stability and information-integration capacity in complex systems. *Chaos: An Interdisciplinary Journal of Nonlinear Science*, 34(6), 063127. <https://doi.org/10.1063/5.0200425>
- Varley, T. F., Pope, M., Faskowitz, J., & Sporns, O. (2023). Multivariate information theory uncovers synergistic subsystems of the human cerebral cortex. *Communications Biology*, 6(1), Article 1. <https://doi.org/10.1038/s42003-023-04843-w>
- Wasmuht, D. F., Spaak, E., Buschman, T. J., Miller, E. K., & Stokes, M. G. (2018). Intrinsic neuronal dynamics predict distinct functional roles during working memory. *Nature Communications*, 9(1), 3499. <https://doi.org/10.1038/s41467-018-05961-4>
- Waugh, N. C., & Norman, D. A. (1965). Primary memory. *Psychological Review*, 72(2), 89–104. <https://doi.org/10.1037/h0021797>
- Wilson, K. G. (1975). The renormalization group: Critical phenomena and the Kondo problem. *Reviews of Modern Physics*, 47(4), 773–840. <https://doi.org/10.1103/RevModPhys.47.773>
- Wilting, J., Dehning, J., Neto, J. P., Rudelt, L., Wibral, M., Zierenberg, J., & Priesemann, V. (2018). Dynamic Adaptive Computation: Tuning network states to task requirements. *Frontiers in Systems Neuroscience*, 12, 55. <https://doi.org/10.3389/fnsys.2018.00055>
- Wilting, J., Dehning, J., Pinheiro Neto, J., Rudelt, L., Wibral, M., Zierenberg, J., & Priesemann, V. (2018). Operating in a Reverberating Regime Enables Rapid Tuning of Network

- States to Task Requirements. *Frontiers in Systems Neuroscience*, 12.
- <https://doi.org/10.3389/fnsys.2018.00055>
- Wilting, J., & Priesemann, V. (2018). Inferring collective dynamical states from widely unobserved systems. *Nature Communications*, 9(1), 2325.
<https://doi.org/10.1038/s41467-018-04725-4>
- Wilting, J., & Priesemann, V. (2019a). 25 years of criticality in neuroscience—Established results, open controversies, novel concepts. *Current Opinion in Neurobiology*, 58, 105–111. <https://doi.org/10.1016/j.conb.2019.08.002>
- Wilting, J., & Priesemann, V. (2019b). Between Perfectly Critical and Fully Irregular: A Reverberating Model Captures and Predicts Cortical Spike Propagation. *Cerebral Cortex*, 29(6), 2759–2770. <https://doi.org/10.1093/cercor/bhz049>
- Wolfram, S. (1984). Universality and complexity in cellular automata. *Physica D: Nonlinear Phenomena*, 10(1), 1–35. [https://doi.org/10.1016/0167-2789\(84\)90245-8](https://doi.org/10.1016/0167-2789(84)90245-8)
- Xu, Y. (2017). Reevaluating the Sensory Account of Visual Working Memory Storage. *Trends in Cognitive Sciences*, 21(10), 794–815.
<https://doi.org/10.1016/j.tics.2017.06.013>
- Yang, A. I., Dikecligil, G. N., Jiang, H., Das, S. R., Stein, J. M., Schuele, S. U., Rosenow, J. M., Davis, K. A., Lucas, T. H., & Gottfried, J. A. (2021). The what and when of olfactory working memory in humans. *Current Biology*, 31(20), 4499–4511.e8.
<https://doi.org/10.1016/j.cub.2021.08.004>
- Yarkoni, T., Poldrack, R. A., Nichols, T. E., Van Essen, D. C., & Wager, T. D. (2011). Large-scale automated synthesis of human functional neuroimaging data. *Nature Methods*, 8(8), 665–670. <https://doi.org/10.1038/nmeth.1635>
- Zenke, F., & Gerstner, W. (2017). Hebbian plasticity requires compensatory processes on multiple timescales. *Philosophical Transactions of the Royal Society B: Biological Sciences*, 372(1715), 20160259. <https://doi.org/10.1098/rstb.2016.0259>
- Zeraati, R., Priesemann, V., & Levina, A. (2021). Self-Organization Toward Criticality by Synaptic Plasticity. *Frontiers in Physics*, 9.
<https://doi.org/10.3389/fphy.2021.619661>
- Zheng, P., Dimitrakakis, C., & Triesch, J. (2013). Network Self-Organization Explains the Statistics and Dynamics of Synaptic Connection Strengths in Cortex. *PLOS*

Computational Biology, 9(1), e1002848.

<https://doi.org/10.1371/journal.pcbi.1002848>

Zheng, P., & Triesch, J. (2014). Robust development of synfire chains from multiple plasticity mechanisms. *Frontiers in Computational Neuroscience*, 8.

<https://doi.org/10.3389/fncom.2014.00066>

Appendix

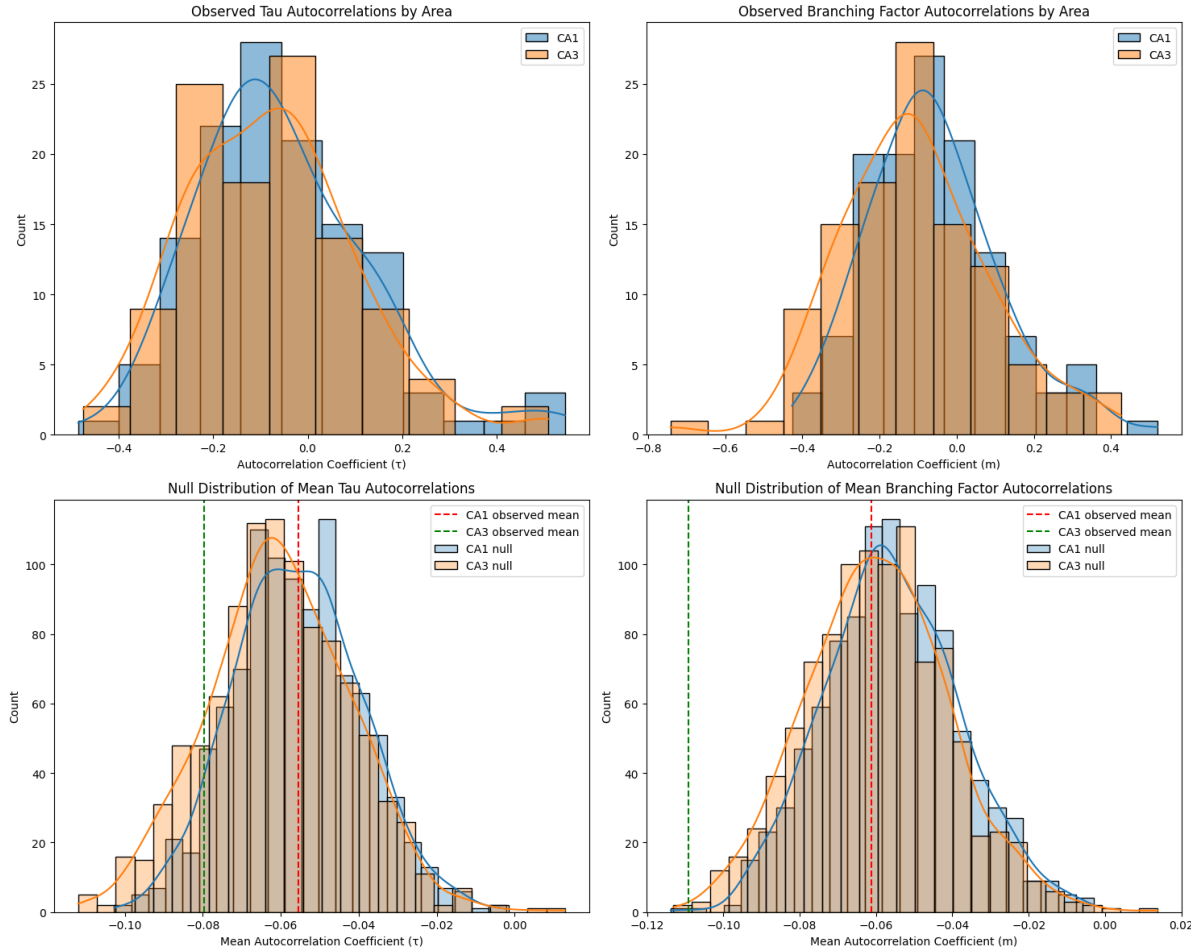


Figure 21. (Top) Distribution over mean autocorrelations (for individual animal-day-epoch combinations of those parts of the data where the animal is in the working memory task) of intrinsic neuronal timescale and branching factor. (Bottom) Mean autocorrelations (for the part of the dataset where the animal is in the working memory task) of CA1 & CA3 relative to a null-distribution over means obtained from synthetically generated autocorrelations (shuffled time-chunks within each animal-day-epoch combination; with the partial dataset being permuted 1000 times).

Within-Area Autocorrelation Analysis Results

Area	Measure	Observed Mean	Null Mean	p-value	CI 95%
CA1	Neural Timescale	-0.055	-0.054	4.750e-01	[-0.088, -0.020]
CA1	Branching Factor	-0.061	-0.056	3.770e-01	[-0.090, -0.023]
CA3	Neural Timescale	-0.080	-0.061	1.620e-01	[-0.096, -0.025]
CA3	Branching Factor	-0.109	-0.059	3.000e-03	[-0.099, -0.020]

Figure 22. Results of the within-area autocorrelation analysis.

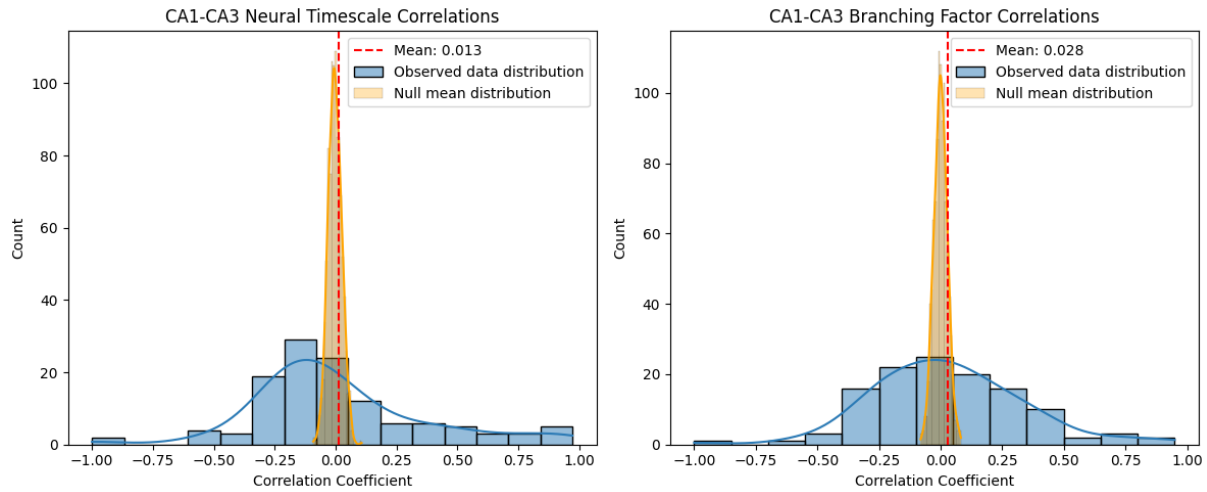


Figure 23. Distribution over correlation coefficients of neuronal timescale (left) and branching factor (right) between CA1 and CA3 for temporally simultaneous time-chunks in the subset of the data where the animals perform the working memory task. The synthetically generated distribution over means under the null-hypothesis is superimposed, together with the empirical mean of the observed distribution for the subset of the data where the animals perform the working memory task.

CA1-CA3 Correlation Analysis Results (Within-Task)

Measure	Observed Mean	Null Mean	p-value	CI 95%
Neural Timescale	0.013	-0.001	6.660e-01	[-0.054, 0.055]
Branching Factor	0.028	0.000	2.920e-01	[-0.053, 0.056]

Figure 24. Results of the temporally simultaneous inter-area correlation analysis from CA3 to CA1 in the subset of the data where the animals perform the working memory task.

Within-Task Analysis Results (CA1_to_CA3)

Measure	Observed Mean	Null Mean	p-value	CI 95%
Neural Timescale	0.009	-0.000	7.060e-01	[-0.049, 0.048]
Branching Factor	-0.010	-0.000	6.880e-01	[-0.052, 0.054]

Figure 25. Results of the temporally directed inter-area correlation analysis from CA1 to CA3 in the subset of the data where the animals perform the working memory task.

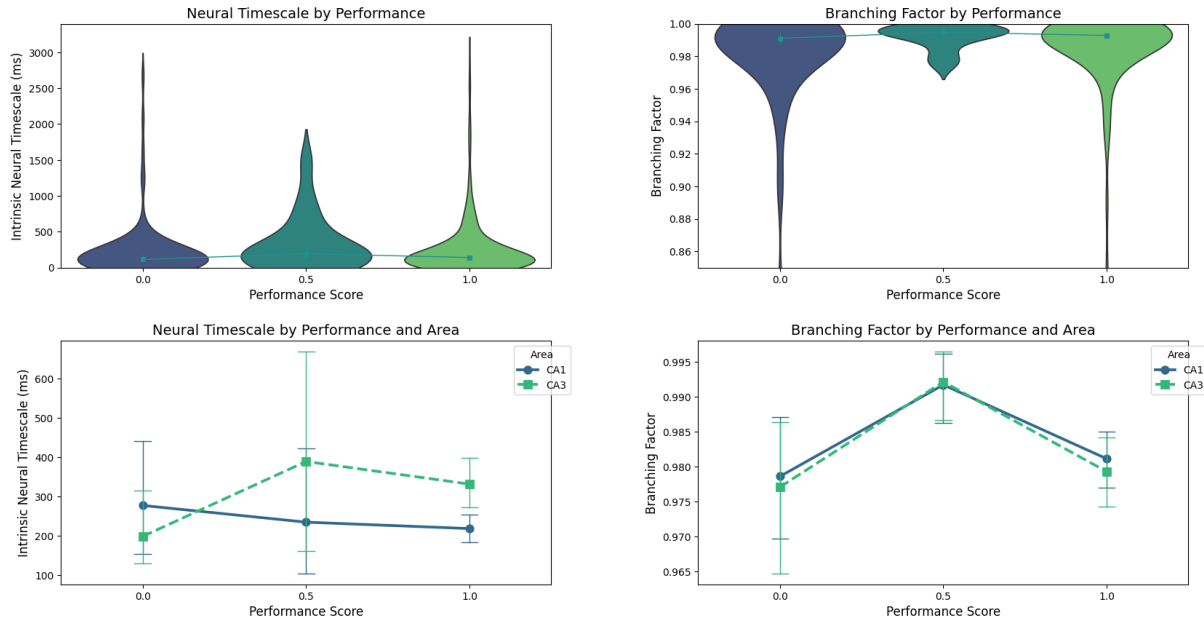
Within-Task Analysis Results (CA3_to_CA1)

Measure	Observed Mean	Null Mean	p-value	CI 95%
Neural Timescale	0.001	0.000	9.710e-01	[-0.050, 0.051]
Branching Factor	-0.020	-0.001	4.190e-01	[-0.049, 0.049]

Figure 26. Results of the temporally directed inter-area correlation analysis from CA3 to CA1 in the subset of the data where the animals perform the working memory task.

Within-task individual animal analysis

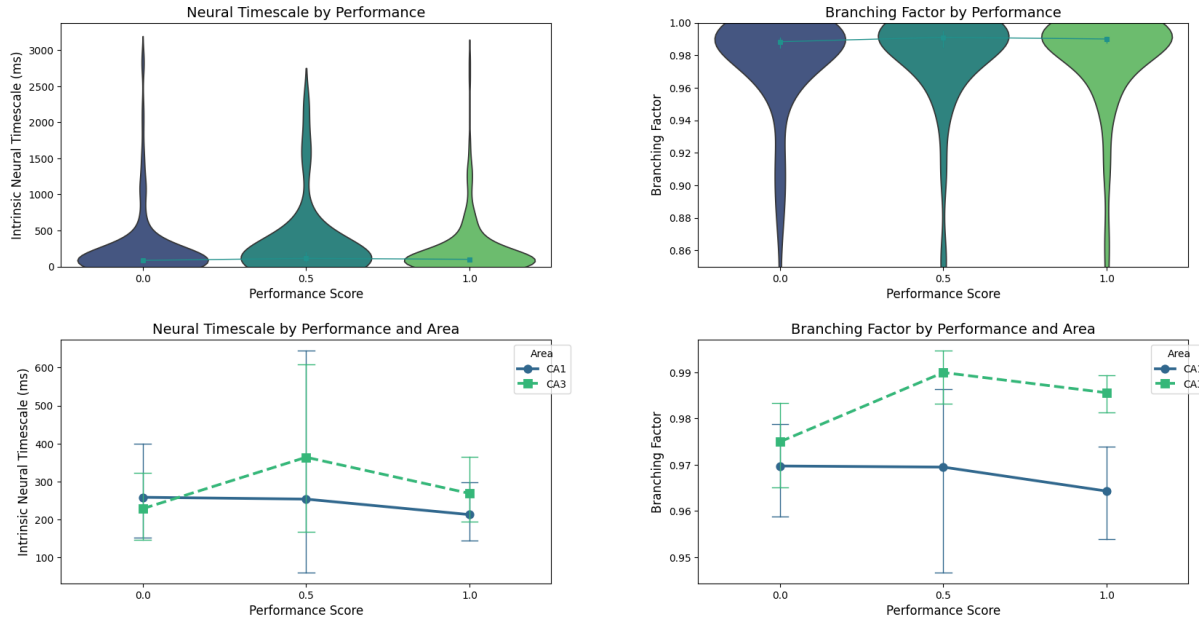
Animal: fra



Within-Task Analysis Results for Animal fra

Measure	Predictor	Coefficient (SE)	z-value	p-value [Bonferroni-corrected] [uncorrected]	CI 95%
Neural Timescale	Intercept	277.046 (414.456)	0.668	> 1 [0.504]	[-535.273, 1089.366]
Neural Timescale	C(performance_cat, Treatment(reference='0.0'))[T.0.5]	-42.516 (179.465)	-0.237	> 1 [0.813]	[-394.261, 309.229]
Neural Timescale	C(performance_cat, Treatment(reference='0.0'))[T.1.0]	-58.806 (70.535)	-0.834	> 1 [0.404]	[-197.052, 79.439]
Neural Timescale	area[T.CA3]	-78.616 (85.045)	-0.924	> 1 [0.355]	[-245.300, 88.069]
Neural Timescale	C(performance_cat, Treatment(reference='0.0'))[T.0.5]:area[T.CA3]	232.944 (224.436)	1.038	> 1 [0.299]	[-206.942, 672.829]
Neural Timescale	C(performance_cat, Treatment(reference='0.0'))[T.1.0]:area[T.CA3]	191.710 (92.690)	2.068	0.348 [0.039]	[10.041, 373.380]
Neural Timescale	Group Var	1.000 (11509075.232)	0.000	> 1 [1.000]	[-22557371.950, 22557373.950]
Neural Timescale	Group Var	167479.740 (-)	--	-- [-]	[-, -]
Branching Factor	Intercept	0.979 (0.037)	26.244	< 0.001 [< 0.001]	[0.905, 1.052]
Branching Factor	C(performance_cat, Treatment(reference='0.0'))[T.0.5]	0.013 (0.016)	0.811	> 1 [0.417]	[-0.019, 0.045]
Branching Factor	C(performance_cat, Treatment(reference='0.0'))[T.1.0]	0.003 (0.006)	0.398	> 1 [0.691]	[-0.010, 0.015]
Branching Factor	area[T.CA3]	-0.002 (0.008)	-0.200	> 1 [0.842]	[-0.017, 0.013]
Branching Factor	C(performance_cat, Treatment(reference='0.0'))[T.0.5]:area[T.CA3]	0.002 (0.020)	0.097	> 1 [0.923]	[-0.038, 0.042]
Branching Factor	C(performance_cat, Treatment(reference='0.0'))[T.1.0]:area[T.CA3]	-0.000 (0.008)	-0.036	> 1 [0.971]	[-0.017, 0.016]
Branching Factor	Group Var	1.000 (11509089.409)	0.000	> 1 [1.000]	[-22557399.736, 22557401.736]
Branching Factor	Group Var	0.001 (-)	--	-- [-]	[-, -]

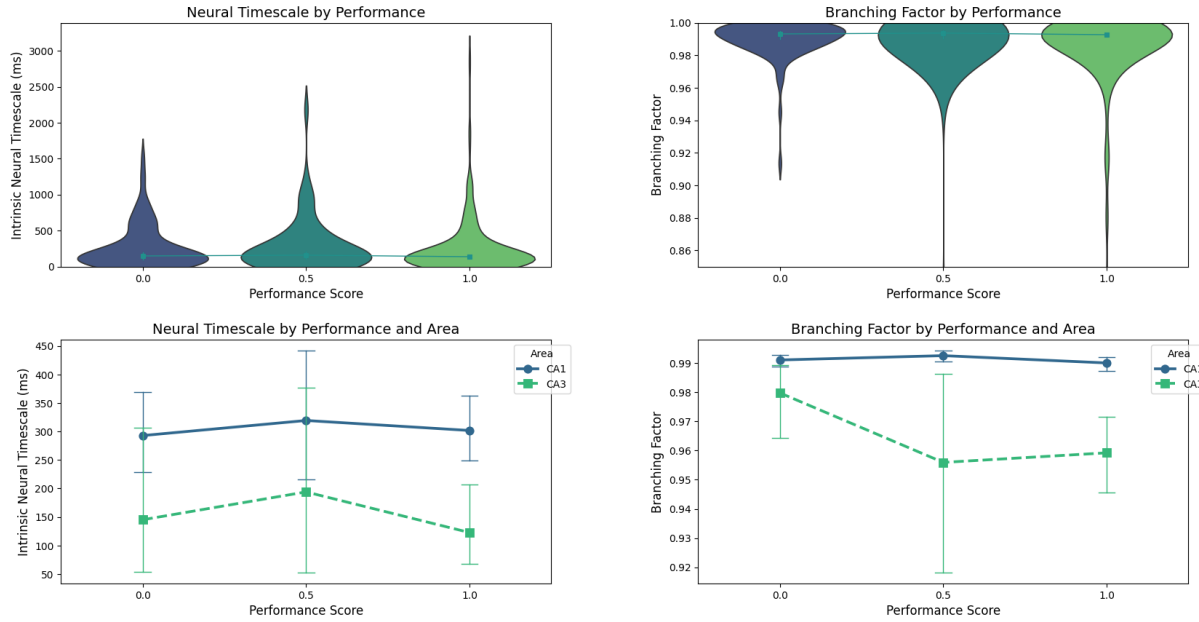
Animal: dud



Within-Task Analysis Results for Animal dud

Measure	Predictor	Coefficient (SE)	z-value	p-value (Bonferroni-corrected) [uncorrected]	CI 95%
Neural Timescale	Intercept	258.700 (445.016)	0.581	> 1 [0.561]	[-613.515, 1130.916]
Neural Timescale	C(performance_cat, Treatment(reference='0.0'))[T.0.5]	-4.817 (125.168)	-0.038	> 1 [0.969]	[-250.142, 240.509]
Neural Timescale	C(performance_cat, Treatment(reference='0.0'))[T.1.0]	-45.618 (68.381)	-0.667	> 1 [0.505]	[-179.642, 88.406]
Neural Timescale	area[T.CA3]	-30.002 (72.671)	-0.413	> 1 [0.680]	[-172.434, 112.430]
Neural Timescale	C(performance_cat, Treatment(reference='0.0'))[T.0.5]:area[T.CA3]	140.243 (172.632)	0.812	> 1 [0.417]	[-198.108, 478.595]
Neural Timescale	C(performance_cat, Treatment(reference='0.0'))[T.1.0]:area[T.CA3]	85.840 (96.596)	0.889	> 1 [0.374]	[-103.485, 275.166]
Neural Timescale	Group Var	1.000 (1604.2086.839)	0.000	> 1 [1.000]	[-31441911.442, 31441913.442]
Neural Timescale	Group Var	195398.697 (-)	--	-- [-]	[-, -]
Branching Factor	Intercept	0.970 (0.038)	25.334	< 0.001 [< 0.001]	[0.895, 1.045]
Branching Factor	C(performance_cat, Treatment(reference='0.0'))[T.0.5]	-0.000 (0.011)	-0.022	> 1 [0.983]	[-0.021, 0.021]
Branching Factor	C(performance_cat, Treatment(reference='0.0'))[T.1.0]	-0.005 (0.006)	-0.922	> 1 [0.356]	[-0.017, 0.006]
Branching Factor	area[T.CA3]	0.005 (0.006)	0.838	> 1 [0.402]	[-0.007, 0.017]
Branching Factor	C(performance_cat, Treatment(reference='0.0'))[T.0.5]:area[T.CA3]	0.015 (0.015)	1.025	> 1 [0.306]	[-0.014, 0.044]
Branching Factor	C(performance_cat, Treatment(reference='0.0'))[T.1.0]:area[T.CA3]	0.016 (0.008)	1.930	0.483 [0.054]	[-0.000, 0.032]
Branching Factor	Group Var	1.000 (1604.2087.710)	0.000	> 1 [1.000]	[-31441913.149, 31441915.149]
Branching Factor	Group Var	0.001 (-)	--	-- [-]	[-, -]

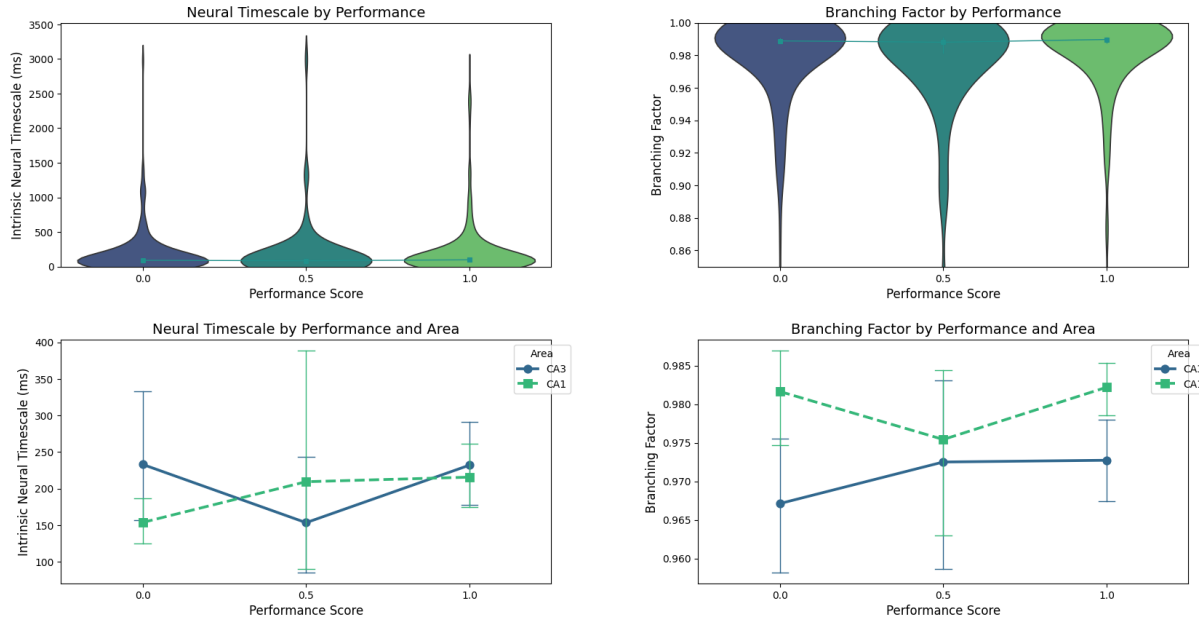
Animal: gov



Within-Task Analysis Results for Animal gov

Measure	Predictor	Coefficient (SE)	z-value	p-value (Bonferroni-corrected) [uncorrected]	CI 95%
Neural Timescale	Intercept	292.762 (366.194)	0.799	> 1 [0.424]	[-424.966, 1010.490]
Neural Timescale	C(performance_cat, Treatment(reference='0.0'))[T.0.5]	26.430 (68.431)	0.386	> 1 [0.699]	[-107.692, 160.552]
Neural Timescale	C(performance_cat, Treatment(reference='0.0'))[T.1.0]	8.909 (49.268)	0.181	> 1 [0.857]	[-87.654, 105.472]
Neural Timescale	area[CA3]	-147.594 (122.381)	-1.206	> 1 [0.228]	[-387.457, 92.270]
Neural Timescale	C(performance_cat, Treatment(reference='0.0'))[T.0.5]:area[CA3]	22.341 (170.142)	0.131	> 1 [0.896]	[-311.131, 355.812]
Neural Timescale	C(performance_cat, Treatment(reference='0.0'))[T.1.0]:area[CA3]	-31.355 (134.108)	-0.234	> 1 [0.815]	[-294.203, 231.492]
Neural Timescale	Group Var	1.000 (-)	--	-- [-]	[-, -]
Neural Timescale	Group Var	132356.821 (-)	--	-- [-]	[-, -]
Branching Factor	Intercept	0.991 (0.026)	37.981	< 0.001 [< 0.001]	[0.940, 1.042]
Branching Factor	C(performance_cat, Treatment(reference='0.0'))[T.0.5]	0.001 (0.005)	0.305	> 1 [0.760]	[-0.008, 0.011]
Branching Factor	C(performance_cat, Treatment(reference='0.0'))[T.1.0]	-0.001 (0.004)	-0.290	> 1 [0.771]	[-0.008, 0.006]
Branching Factor	area[CA3]	-0.011 (0.009)	-1.295	> 1 [0.195]	[-0.028, 0.006]
Branching Factor	C(performance_cat, Treatment(reference='0.0'))[T.0.5]:area[CA3]	-0.025 (0.012)	-2.087	0.332 [0.037]	[-0.049, -0.002]
Branching Factor	C(performance_cat, Treatment(reference='0.0'))[T.1.0]:area[CA3]	-0.020 (0.010)	-2.042	0.370 [0.041]	[-0.038, -0.001]
Branching Factor	Group Var	1.000 (-)	--	-- [-]	[-, -]
Branching Factor	Group Var	0.001 (-)	--	-- [-]	[-, -]

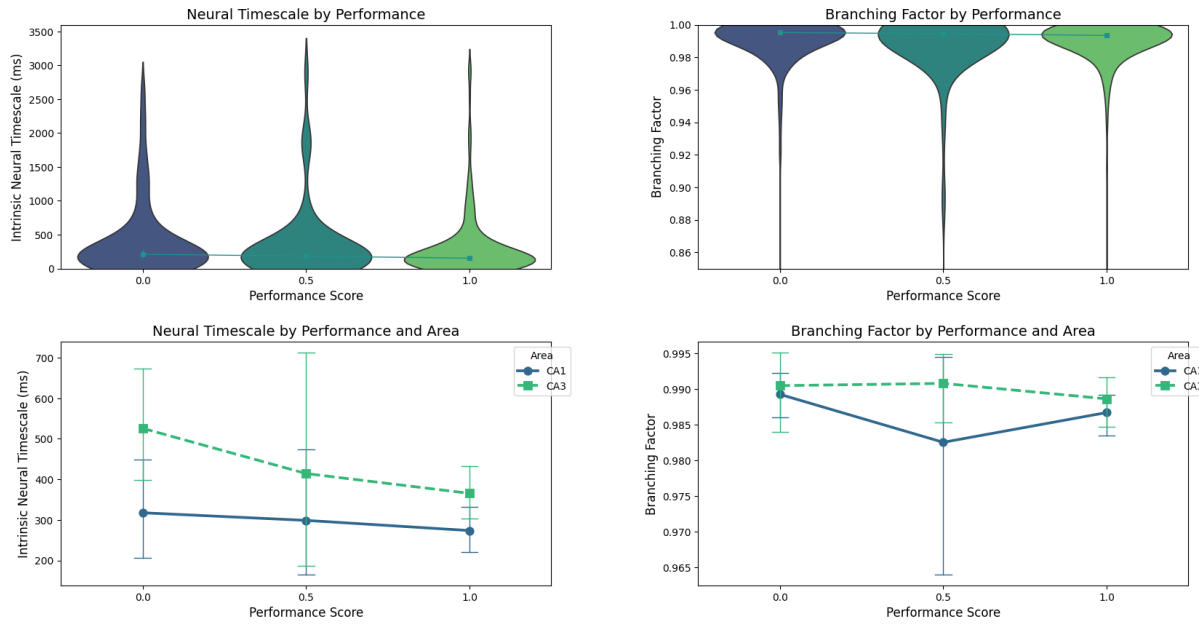
Animal: egyptian vulture



Within-Task Analysis Results for Animal egyptian vulture

Measure	Predictor	Coefficient (SE)	z-value	p-value (Bonferroni-corrected)	CI 95% [uncorrected]
Neural Timescale	Intercept	153.654 (383.551)	0.401	> 1 [0.689]	[-598.092, 905.401]
Neural Timescale	C(performance_cat, Treatment(reference='0.0')) T.0.5]	55.675 (71.409)	0.780	> 1 [0.436]	[-84.285, 195.635]
Neural Timescale	C(performance_cat, Treatment(reference='0.0')) T.1.0]	61.922 (43.800)	1.414	> 1 [0.157]	[-23.924, 147.769]
Neural Timescale	area[T.CA3]	79.285 (54.770)	1.448	> 1 [0.148]	[-28.063, 186.632]
Neural Timescale	C(performance_cat, Treatment(reference='0.0')) T.0.5]:area[T.CA3]	-135.304 (104.994)	-1.289	> 1 [0.198]	[-341.088, 70.480]
Neural Timescale	C(performance_cat, Treatment(reference='0.0')) T.1.0]:area[T.CA3]	-62.880 (64.815)	-0.970	> 1 [0.332]	[-189.916, 64.155]
Neural Timescale	Group Var	1.000 (-)	--	-- [-]	[-, -]
Neural Timescale	Group Var	145749.429 (-)	--	-- [-]	[-, -]
Branching Factor	Intercept	0.982 (0.035)	27.730	< 0.001 [<< 0.001]	[0.912, 1.051]
Branching Factor	C(performance_cat, Treatment(reference='0.0')) T.0.5]	-0.006 (0.007)	-0.942	> 1 [0.346]	[-0.019, 0.007]
Branching Factor	C(performance_cat, Treatment(reference='0.0')) T.1.0]	0.001 (0.004)	0.137	> 1 [0.891]	[-0.007, 0.008]
Branching Factor	area[T.CA3]	-0.015 (0.005)	-2.869	0.037 [0.004]	[-0.024, -0.005]
Branching Factor	C(performance_cat, Treatment(reference='0.0')) T.0.5]:area[T.CA3]	0.012 (0.010)	1.196	> 1 [0.232]	[-0.007, 0.031]
Branching Factor	C(performance_cat, Treatment(reference='0.0')) T.1.0]:area[T.CA3]	0.005 (0.006)	0.844	> 1 [0.399]	[-0.007, 0.017]
Branching Factor	Group Var	1.000 (-)	--	-- [-]	[-, -]
Branching Factor	Group Var	0.001 (-)	--	-- [-]	[-, -]

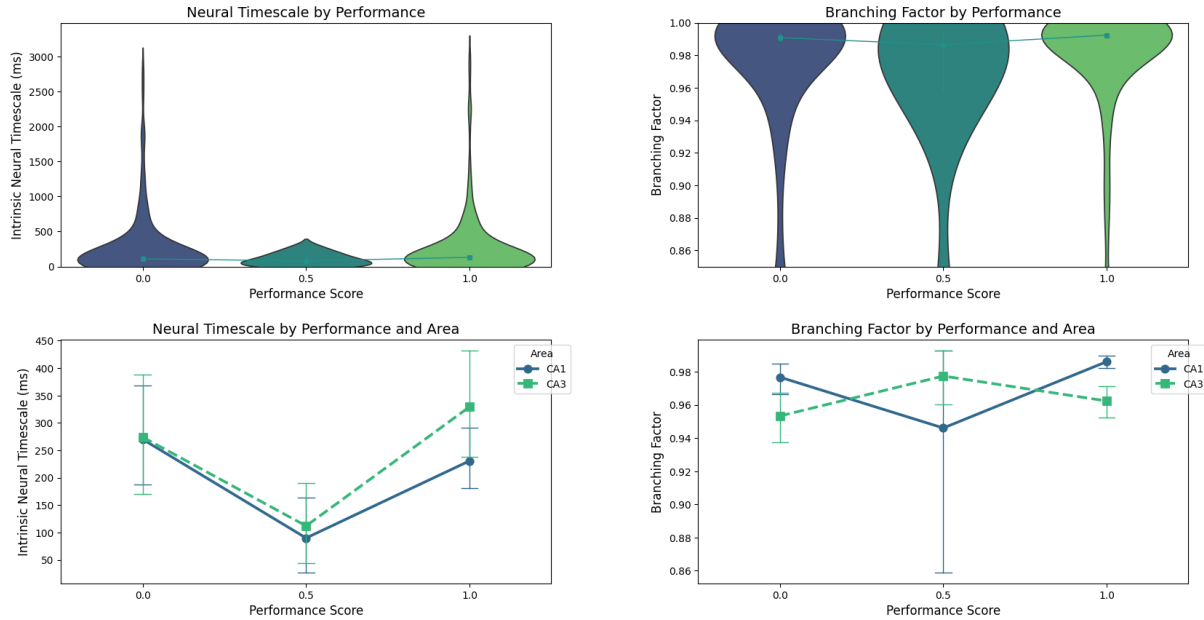
Animal: bon



Within-Task Analysis Results for Animal bon

Measure	Predictor	Coefficient (SE)	z-value	p-value [Bonferroni-corrected] [uncorrected]	CI 95%
Neural Timescale	Intercept	317.715 (505.229)	0.629	> 1 [0.529]	[−672.516, 1307.945]
Neural Timescale	C(performance_cat, Treatment(reference='0.0')) T.0.5]	-18.754 (120.241)	-0.156	> 1 [0.876]	[−254.422, 216.914]
Neural Timescale	C(performance_cat, Treatment(reference='0.0')) T.1.0]	-43.841 (71.149)	-0.616	> 1 [0.538]	[−183.290, 95.609]
Neural Timescale	area[T.CA3]	208.118 (90.042)	2.311	0.187 [0.021]	[31.640, 384.597]
Neural Timescale	C(performance_cat, Treatment(reference='0.0')) T.0.5]:area[T.CA3]	-92.664 (168.051)	-0.551	> 1 [0.581]	[−422.038, 236.710]
Neural Timescale	C(performance_cat, Treatment(reference='0.0')) T.1.0]:area[T.CA3]	-116.375 (101.504)	-1.147	> 1 [0.252]	[−315.319, 82.569]
Neural Timescale	Group Var	1.000 (−)	--	-- [−]	[−, −]
Neural Timescale	Group Var	251267.956 (−)	--	-- [−]	[−, −]
Branching Factor	Intercept	0.989 (0.023)	42.287	< 0.001 [< 0.001]	[0.943, 1.035]
Branching Factor	C(performance_cat, Treatment(reference='0.0')) T.0.5]	-0.007 (0.006)	-1.205	> 1 [0.228]	[−0.018, 0.004]
Branching Factor	C(performance_cat, Treatment(reference='0.0')) T.1.0]	-0.003 (0.003)	-0.772	> 1 [0.440]	[−0.009, 0.004]
Branching Factor	area[T.CA3]	0.001 (0.004)	0.293	> 1 [0.770]	[−0.007, 0.009]
Branching Factor	C(performance_cat, Treatment(reference='0.0')) T.0.5]:area[T.CA3]	0.007 (0.008)	0.903	> 1 [0.367]	[−0.008, 0.022]
Branching Factor	C(performance_cat, Treatment(reference='0.0')) T.1.0]:area[T.CA3]	0.001 (0.005)	0.148	> 1 [0.883]	[−0.009, 0.010]
Branching Factor	Group Var	1.000 (−)	--	-- [−]	[−, −]
Branching Factor	Group Var	0.001 (−)	--	-- [−]	[−, −]

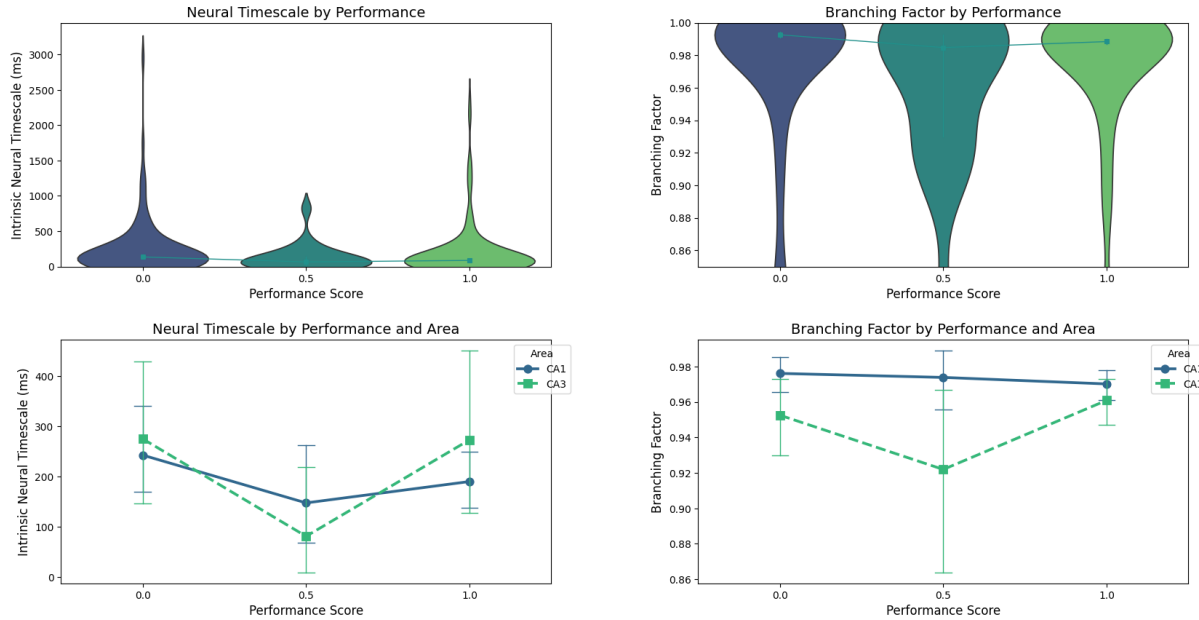
Animal: Cor



Within-Task Analysis Results for Animal Cor

Measure	Predictor	Coefficient (SE)	z-value	p-value [Bonferroni-corrected] [uncorrected]	CI 95%
Neural Timescale	Intercept	270.003 (459.872)	0.587	> 1 [0.557]	[-631.331, 1171.336]
Neural Timescale	C(performance_cat, Treatment(reference='0.0'))[T.0.5]	-180.101 (234.055)	-0.769	> 1 [0.442]	[-638.840, 278.638]
Neural Timescale	C(performance_cat, Treatment(reference='0.0'))[T.1.0]	-39.351 (64.655)	-0.609	> 1 [0.543]	[-166.073, 87.371]
Neural Timescale	area[T.CA3]	4.060 (74.673)	0.054	> 1 [0.957]	[-142.296, 150.416]
Neural Timescale	C(performance_cat, Treatment(reference='0.0'))[T.0.5]:area[T.CA3]	18.048 (304.355)	0.059	> 1 [0.953]	[-578.477, 614.574]
Neural Timescale	C(performance_cat, Treatment(reference='0.0'))[T.1.0]:area[T.CA3]	94.581 (93.891)	1.007	> 1 [0.314]	[-89.442, 278.604]
Neural Timescale	Group Var	1.000 (20468011.635)	0.000	> 1 [1.000]	[-40116564.640, 40116566.640]
Neural Timescale	Group Var	208934.672 (-)	--	-- [-]	[-, -]
Branching Factor	Intercept	0.977 (0.048)	20.417	< 0.001 [< 0.001]	[0.883, 1.070]
Branching Factor	C(performance_cat, Treatment(reference='0.0'))[T.0.5]	-0.031 (0.024)	-1.259	> 1 [0.208]	[-0.078, 0.017]
Branching Factor	C(performance_cat, Treatment(reference='0.0'))[T.1.0]	0.009 (0.007)	1.391	> 1 [0.164]	[-0.004, 0.023]
Branching Factor	area[T.CA3]	-0.023 (0.008)	-3.013	0.023 [0.003]	[-0.039, -0.008]
Branching Factor	C(performance_cat, Treatment(reference='0.0'))[T.0.5]:area[T.CA3]	0.055 (0.032)	1.729	0.754 [0.084]	[-0.007, 0.117]
Branching Factor	C(performance_cat, Treatment(reference='0.0'))[T.1.0]:area[T.CA3]	-0.000 (0.010)	-0.031	> 1 [0.976]	[-0.019, 0.019]
Branching Factor	Group Var	1.000 (20468013.718)	0.000	> 1 [1.000]	[-40116568.723, 40116570.723]
Branching Factor	Group Var	0.002 (-)	--	-- [-]	[-, -]

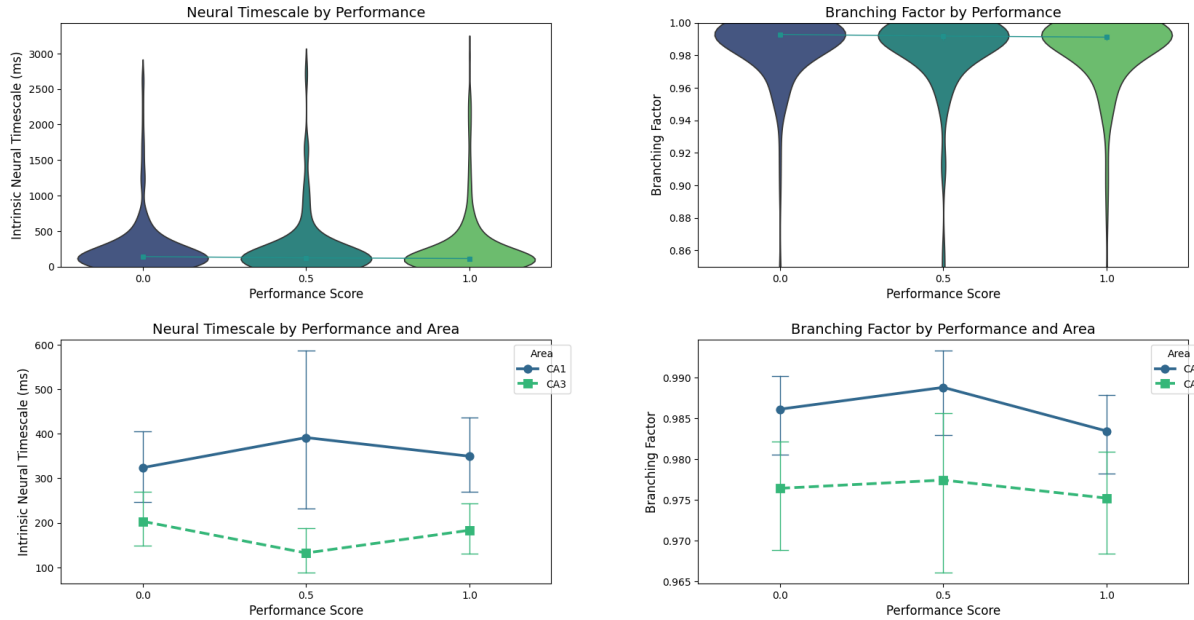
Animal: cha



Within-Task Analysis Results for Animal cha

Measure	Predictor	Coefficient (SE)	z-value	p-value [Bonferroni-corrected] [uncorrected]	CI 95%
Neural Timescale	Intercept	242.261 (386.089)	0.627	> 1 [0.530]	[-514.459, 998.980]
Neural Timescale	C(performance_cat, Treatment(reference='0.0'))[T.0.5]	-95.145 (111.663)	-0.852	> 1 [0.394]	[-314.002, 123.711]
Neural Timescale	C(performance_cat, Treatment(reference='0.0'))[T.1.0]	-52.599 (56.104)	-0.938	> 1 [0.348]	[-162.561, 57.363]
Neural Timescale	area[T.CA3]	32.422 (80.984)	0.400	> 1 [0.689]	[-126.303, 191.146]
Neural Timescale	C(performance_cat, Treatment(reference='0.0'))[T.0.5]:area[T.CA3]	-98.896 (215.607)	-0.459	> 1 [0.646]	[-521.478, 323.685]
Neural Timescale	C(performance_cat, Treatment(reference='0.0'))[T.1.0]:area[T.CA3]	50.545 (104.281)	0.485	> 1 [0.628]	[-153.842, 254.932]
Neural Timescale	Group Var	1.000 (23726566.406)	0.000	> 1 [1.000]	[-46503214.633, 46503216.633]
Neural Timescale	Group Var	147102.974 (-)	--	-- [-]	[-, -]
Branching Factor	Intercept	0.976 (0.049)	19.891	< 0.001 [< 0.001]	[0.880, 1.072]
Branching Factor	C(performance_cat, Treatment(reference='0.0'))[T.0.5]	-0.002 (0.014)	-0.159	> 1 [0.873]	[-0.030, 0.026]
Branching Factor	C(performance_cat, Treatment(reference='0.0'))[T.1.0]	-0.006 (0.007)	-0.833	> 1 [0.405]	[-0.020, 0.008]
Branching Factor	area[T.CA3]	-0.024 (0.010)	-2.291	0.198 [0.022]	[-0.044, -0.003]
Branching Factor	C(performance_cat, Treatment(reference='0.0'))[T.0.5]:area[T.CA3]	-0.028 (0.027)	-1.034	> 1 [0.301]	[-0.082, 0.025]
Branching Factor	C(performance_cat, Treatment(reference='0.0'))[T.1.0]:area[T.CA3]	0.014 (0.013)	1.082	> 1 [0.279]	[-0.012, 0.040]
Branching Factor	Group Var	1.000 (23726566.635)	0.000	> 1 [1.000]	[-46503215.081, 46503217.081]
Branching Factor	Group Var	0.002 (-)	--	-- [-]	[-, -]

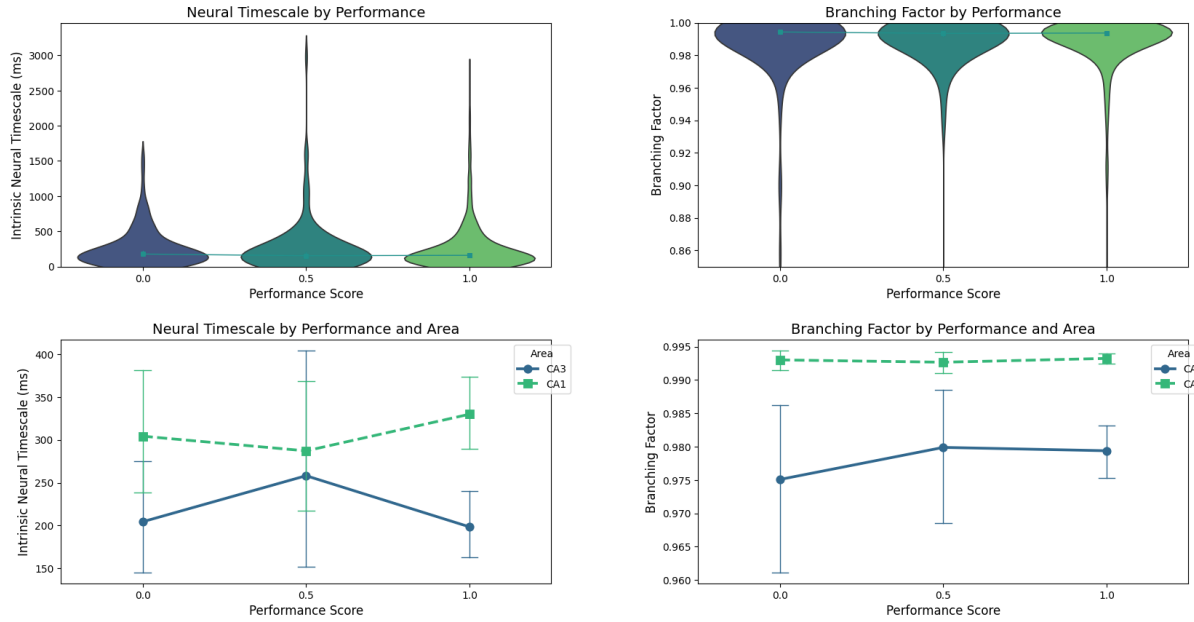
Animal: con



Within-Task Analysis Results for Animal con

Measure	Predictor	Coefficient (SE)	z-value	p-value [Bonferroni-corrected] [uncorrected]	CI 95%
Neural Timescale	Intercept	323.981 (423.880)	0.764	> 1 [0.445]	[−506.808, 1154.769]
Neural Timescale	C(performance_cat, Treatment(reference='0.0')) T.0.5]	67.613 (77.296)	0.875	> 1 [0.382]	[−83.885, 219.111]
Neural Timescale	C(performance_cat, Treatment(reference='0.0')) T.1.0]	25.668 (51.397)	0.499	> 1 [0.617]	[−75.069, 126.405]
Neural Timescale	area[T.CA3]	-120.735 (54.601)	-2.211	0.243 [0.027]	[−227.752, -13.718]
Neural Timescale	C(performance_cat, Treatment(reference='0.0')) T.0.5]:area[T.CA3]	-138.693 (107.722)	-1.288	> 1 [0.198]	[−349.823, 72.437]
Neural Timescale	C(performance_cat, Treatment(reference='0.0')) T.1.0]:area[T.CA3]	-45.600 (73.873)	-0.617	> 1 [0.537]	[−190.389, 99.190]
Neural Timescale	Group Var	1.000 (−)	--	-- [−]	[−, −]
Neural Timescale	Group Var	178270.239 (−)	--	-- [−]	[−, −]
Branching Factor	Intercept	0.986 (0.033)	30.055	< 0.001 [< 0.001]	[0.922, 1.050]
Branching Factor	C(performance_cat, Treatment(reference='0.0')) T.0.5]	0.003 (0.006)	0.447	> 1 [0.655]	[−0.009, 0.014]
Branching Factor	C(performance_cat, Treatment(reference='0.0')) T.1.0]	-0.003 (0.004)	-0.674	> 1 [0.500]	[−0.010, 0.005]
Branching Factor	area[T.CA3]	-0.010 (0.004)	-2.297	0.194 [0.022]	[−0.018, −0.001]
Branching Factor	C(performance_cat, Treatment(reference='0.0')) T.0.5]:area[T.CA3]	-0.002 (0.008)	-0.200	> 1 [0.842]	[−0.018, 0.015]
Branching Factor	C(performance_cat, Treatment(reference='0.0')) T.1.0]:area[T.CA3]	0.001 (0.006)	0.258	> 1 [0.797]	[−0.010, 0.013]
Branching Factor	Group Var	1.000 (−)	--	-- [−]	[−, −]
Branching Factor	Group Var	0.001 (−)	--	-- [−]	[−, −]

Animal: dav

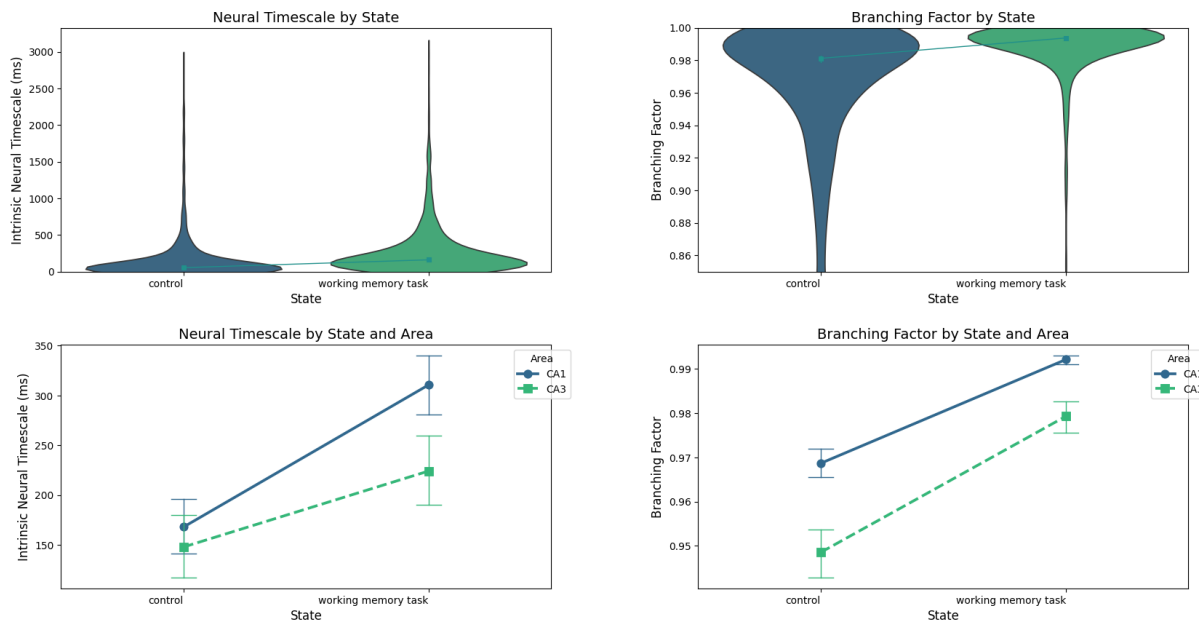


Within-Task Analysis Results for Animal dav

Measure	Predictor	Coefficient (SE)	z-value	p-value	
				(Bonferroni-corrected)	[uncorrected]
Neural Timescale	Intercept	304.335 (345.476)	0.881	> 1 [0.376]	[−372.785, 981.456]
Neural Timescale	C(performance_cat, Treatment(reference='0.0'))[T.0.5]	-17.142 (59.825)	-0.287	> 1 [0.774]	[−134.396, 100.112]
Neural Timescale	C(performance_cat, Treatment(reference='0.0'))[T.1.0]	25.659 (46.063)	0.557	> 1 [0.577]	[−64.622, 115.940]
Neural Timescale	area[T.CA3]	-99.892 (65.544)	-1.524	> 1 [0.127]	[−228.356, 28.571]
Neural Timescale	C(performance_cat, Treatment(reference='0.0'))[T.0.5]:area[T.CA3]	70.877 (92.452)	0.767	> 1 [0.443]	[−110.326, 252.079]
Neural Timescale	C(performance_cat, Treatment(reference='0.0'))[T.1.0]:area[T.CA3]	-31.651 (72.229)	-0.438	> 1 [0.661]	[−173.217, 109.915]
Neural Timescale	Group Var	1.000 (−)	--	-- [−]	[−, −]
Neural Timescale	Group Var	117672.643 (−)	--	-- [−]	[−, −]
Branching Factor	Intercept	0.993 (0.024)	41.217	< 0.001 [< 0.001]	[0.946, 1.040]
Branching Factor	C(performance_cat, Treatment(reference='0.0'))[T.0.5]	-0.000 (0.004)	-0.083	> 1 [0.934]	[−0.009, 0.008]
Branching Factor	C(performance_cat, Treatment(reference='0.0'))[T.1.0]	0.000 (0.003)	0.071	> 1 [0.944]	[−0.006, 0.007]
Branching Factor	area[T.CA3]	-0.018 (0.005)	-3.923	< 0.001 [< 0.001]	[−0.027, −0.009]
Branching Factor	C(performance_cat, Treatment(reference='0.0'))[T.0.5]:area[T.CA3]	0.005 (0.006)	0.800	> 1 [0.424]	[−0.007, 0.018]
Branching Factor	C(performance_cat, Treatment(reference='0.0'))[T.1.0]:area[T.CA3]	0.004 (0.005)	0.810	> 1 [0.418]	[−0.006, 0.014]
Branching Factor	Group Var	1.000 (−)	--	-- [−]	[−, −]
Branching Factor	Group Var	0.001 (−)	--	-- [−]	[−, −]

Between-Task individual animal analysis

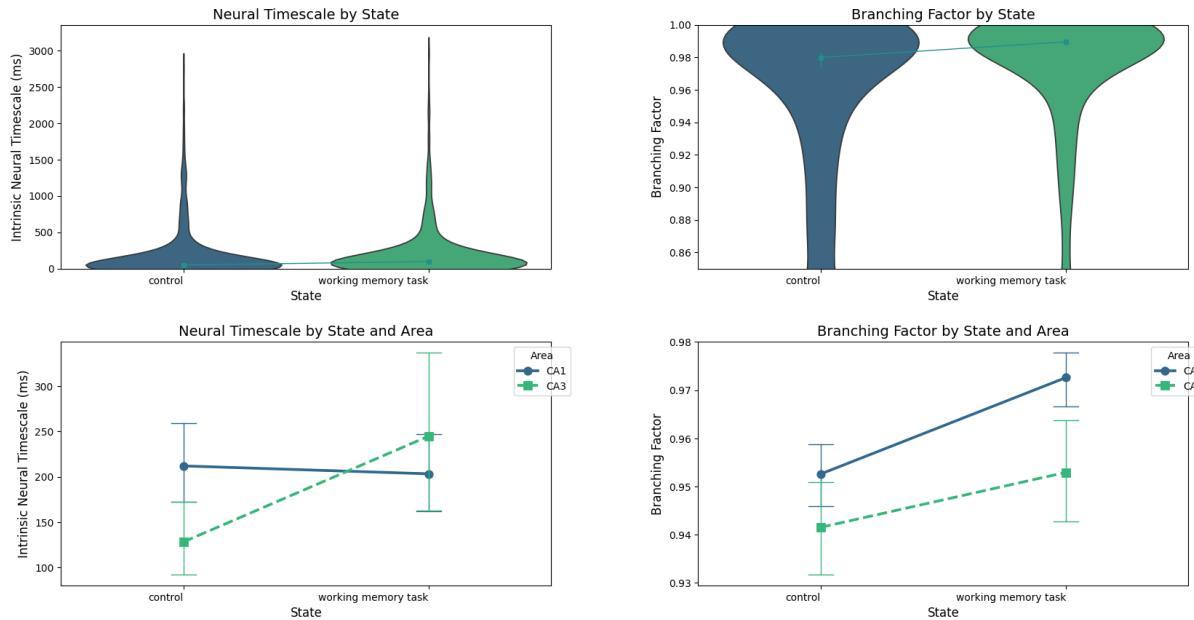
Animal: dav



Between-Task Analysis Results for Animal dav

Measure	Predictor	Coefficient (SE)	z-value	p-value (Bonferroni-corrected) [uncorrected]	CI 95%
Neural Timescale	Intercept	168.025 (336.011)	0.500	> 1 [0.617]	[-490.544, 826.593]
Neural Timescale	state[T.working memory task]	142.577 (20.297)	7.025	< 0.001 [< 0.001]	[102.797, 182.358]
Neural Timescale	area[T.CA3]	-20.079 (21.427)	-0.937	> 1 [0.349]	[-62.075, 21.918]
Neural Timescale	state[T.working memory task]:area[T.CA3]	-66.366 (31.176)	-2.129	0.366 [0.033]	[-127.469, -5.263]
Neural Timescale	Group Var	1.000 (8108389.534)	0.000	> 1 [1.000]	[-15892150.459, 15892152.459]
Neural Timescale	Group Var	112710.442 (-)	--	-- [--]	[--, --]
Branching Factor	Intercept	0.969 (0.039)	25.081	< 0.001 [< 0.001]	[0.893, 1.044]
Branching Factor	state[T.working memory task]	0.023 (0.002)	10.049	< 0.001 [< 0.001]	[0.019, 0.028]
Branching Factor	area[T.CA3]	-0.020 (0.002)	-8.175	< 0.001 [< 0.001]	[-0.025, -0.015]
Branching Factor	state[T.working memory task]:area[T.CA3]	0.007 (0.004)	2.039	0.456 [0.041]	[0.000, 0.014]
Branching Factor	Group Var	1.000 (8108495.532)	0.000	> 1 [1.000]	[-15892358.211, 15892360.211]
Branching Factor	Group Var	0.001 (-)	--	-- [--]	[--, --]

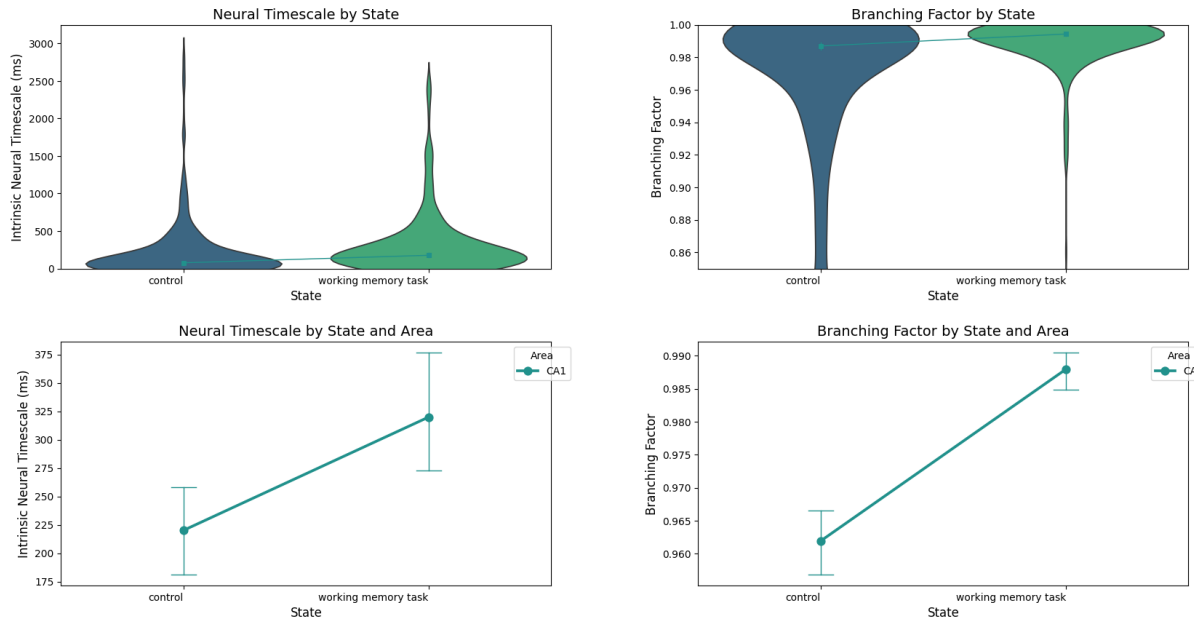
Animal: cha



Between-Task Analysis Results for Animal cha

Measure	Predictor	Coefficient (SE)	z-value	p-value (Bonferroni-corrected) [uncorrected]	CI 95%
Neural Timescale	Intercept	211.993 (365.118)	0.581	> 1 [0.561]	[-503.625, 927.612]
Neural Timescale	state[T.working memory task]	-8.708 (30.310)	-0.287	> 1 [0.774]	[-68.115, 50.698]
Neural Timescale	area[T.CA3]	-83.946 (35.621)	-2.357	0.203 [0.018]	[-153.763, -14.130]
Neural Timescale	state[T.working memory task]:area[T.CA3]	125.581 (55.263)	2.272	0.254 [0.023]	[17.267, 233.894]
Neural Timescale	Group Var	1.000 (-)	--	-- [--]	[--, --]
Neural Timescale	Group Var	132899.959 (-)	--	-- [--]	[--, --]
Branching Factor	Intercept	0.953 (0.055)	17.224	< 0.001 [< 0.001]	[0.844, 1.061]
Branching Factor	state[T.working memory task]	0.020 (0.005)	4.356	< 0.001 [< 0.001]	[0.011, 0.029]
Branching Factor	area[T.CA3]	-0.011 (0.005)	-2.052	0.442 [0.040]	[-0.022, -0.000]
Branching Factor	state[T.working memory task]:area[T.CA3]	-0.009 (0.008)	-1.028	> 1 [0.304]	[-0.025, 0.008]
Branching Factor	Group Var	1.000 (-)	--	-- [--]	[--, --]
Branching Factor	Group Var	0.003 (-)	--	-- [--]	[--, --]

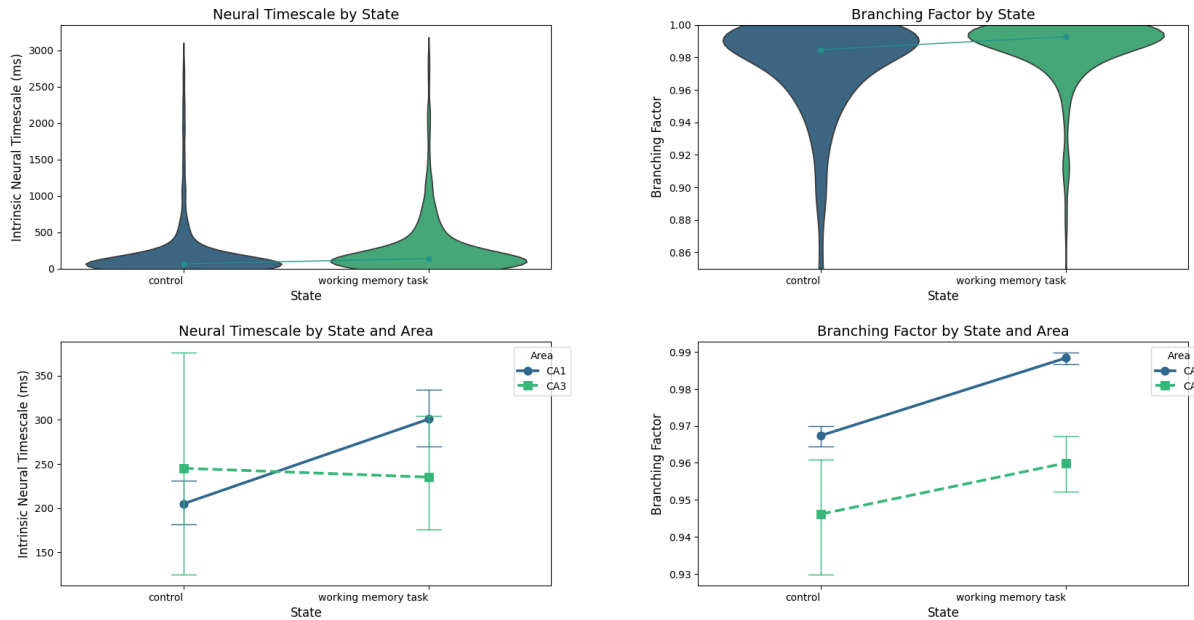
Animal: mil



Between-Task Analysis Results for Animal mil

Measure	Predictor	Coefficient (SE)	z-value	p-value (Bonferroni-corrected) [uncorrected]	CI 95%
Neural Timescale	Intercept	220.117 (411.866)	0.534	> 1 [0.593]	[-587.127, 1027.360]
Neural Timescale	state[T.working memory task]	99.722 (31.750)	3.141	0.019 [0.002]	[37.493, 161.951]
Neural Timescale	Group Var	1.000 (--)	--	-- [--]	[--, --]
Neural Timescale	Group Var	169252.742 (--)	--	-- [--]	[--, --]
Branching Factor	Intercept	0.962 (0.044)	21.705	< 0.001 [<> 0.001]	[0.875, 1.049]
Branching Factor	state[T.working memory task]	0.026 (0.003)	7.608	< 0.001 [<> 0.001]	[0.019, 0.033]
Branching Factor	Group Var	1.000 (--)	--	-- [--]	[--, --]
Branching Factor	Group Var	0.002 (--)	--	-- [--]	[--, --]

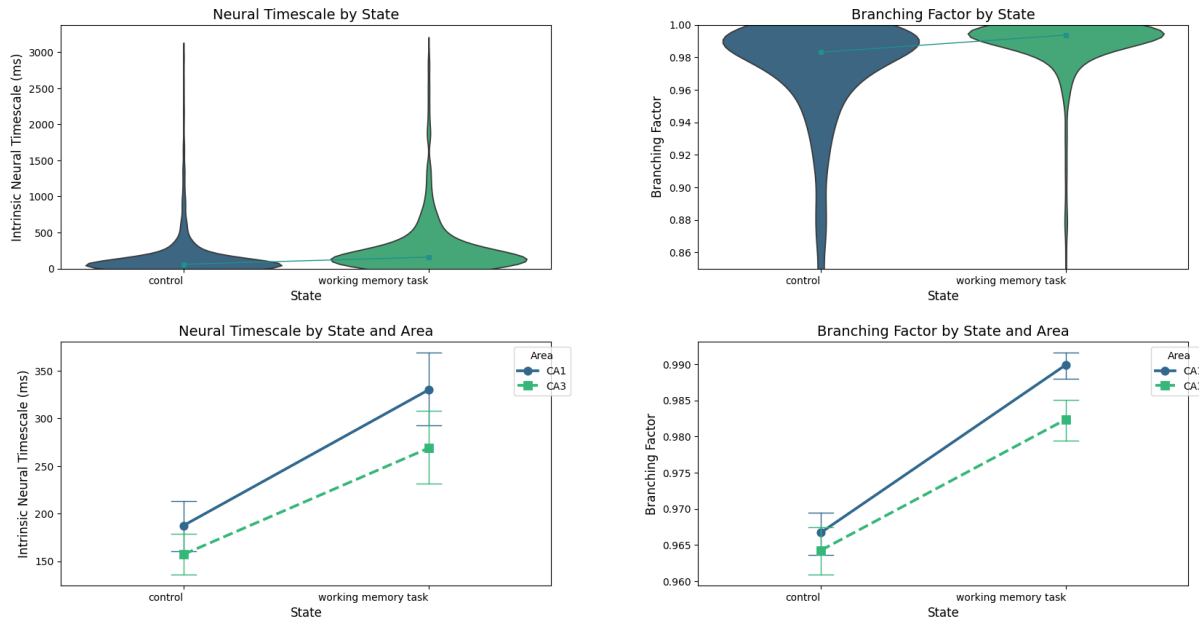
Animal: gov



Between-Task Analysis Results for Animal gov

Measure	Predictor	Coefficient (SE)	z-value	p-value (Bonferroni-corrected) [uncorrected]	CI 95%
Neural Timescale	Intercept	204.857 (425.236)	0.482	> 1 [0.630]	[-628.590, 1038.304]
Neural Timescale	state[T.working memory task]	95.830 (21.265)	4.506	< 0.001 [<> 0.001]	[54.151, 137.509]
Neural Timescale	area[T.CA3]	40.172 (56.352)	0.713	> 1 [0.476]	[-70.276, 150.620]
Neural Timescale	state[T.working memory task]:area[T.CA3]	-105.852 (66.962)	-1.581	> 1 [0.114]	[-237.095, 25.391]
Neural Timescale	Group Var	1.000 (10234005.940)	0.000	> 1 [1.000]	[-20058282.060, 20058284.060]
Neural Timescale	Group Var	180661.102 (--)	--	--	[--, --]
Branching Factor	Intercept	0.967 (0.040)	24.180	< 0.001 [<> 0.001]	[0.889, 1.046]
Branching Factor	state[T.working memory task]	0.021 (0.002)	10.488	< 0.001 [<> 0.001]	[0.017, 0.025]
Branching Factor	area[T.CA3]	-0.021 (0.005)	-4.004	< 0.001 [<> 0.001]	[-0.032, -0.011]
Branching Factor	state[T.working memory task]:area[T.CA3]	-0.007 (0.006)	-1.138	> 1 [0.255]	[-0.020, 0.005]
Branching Factor	Group Var	1.000 (10234337.754)	0.000	> 1 [1.000]	[-20058932.404, 20058934.404]
Branching Factor	Group Var	0.002 (--)	--	--	[--, --]

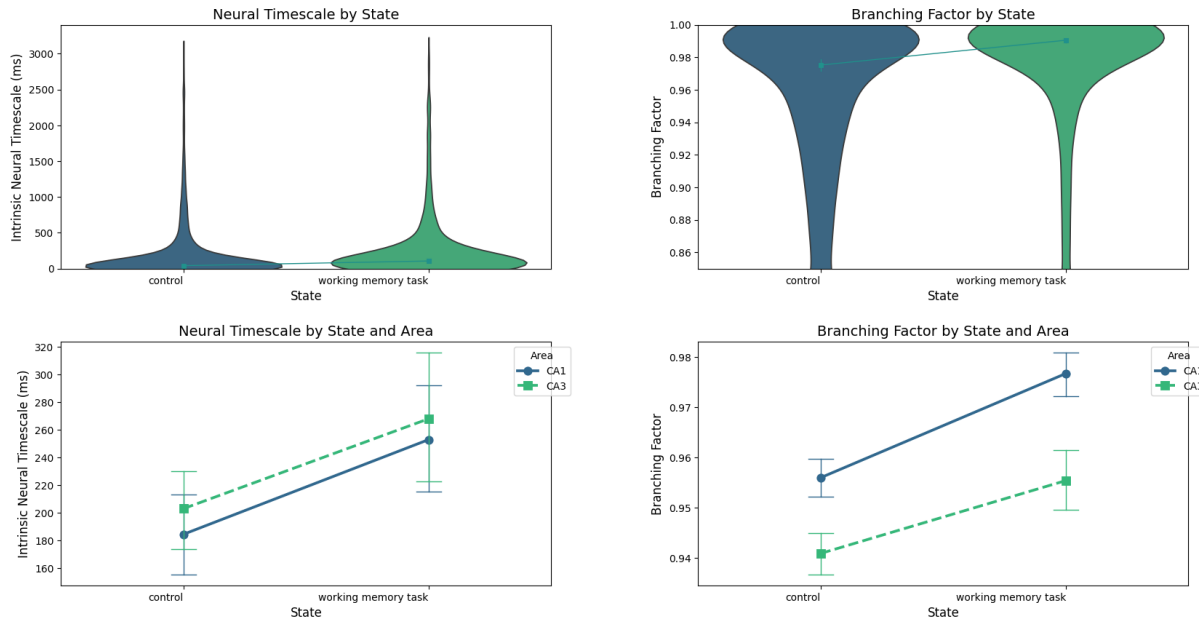
Animal: ten



Between-Task Analysis Results for Animal ten

Measure	Predictor	Coefficient (SE)	z-value	p-value (Bonferroni-corrected) [uncorrected]	CI 95%
Neural Timescale	Intercept	187.478 (376.928)	0.497	> 1 [0.619]	[-551.288, 926.244]
Neural Timescale	state[T.working memory task]	142.478 (22.707)	6.275	< 0.001 [<< 0.001]	[97.973, 186.984]
Neural Timescale	area[T.CA3]	-30.294 (19.027)	-1.592	> 1 [0.111]	[-67.586, 6.999]
Neural Timescale	state[T.working memory task]:area[T.CA3]	-30.894 (31.920)	-0.968	> 1 [0.333]	[-93.457, 31.669]
Neural Timescale	Group Var	1.000 (--)	--	-- [--]	[--, --]
Neural Timescale	Group Var	141886.998 (--)	--	-- [--]	[--, --]
Branching Factor	Intercept	0.967 (0.039)	24.732	< 0.001 [<< 0.001]	[0.890, 1.043]
Branching Factor	state[T.working memory task]	0.023 (0.002)	9.842	< 0.001 [<< 0.001]	[0.019, 0.028]
Branching Factor	area[T.CA3]	-0.002 (0.002)	-1.241	> 1 [0.215]	[-0.006, 0.001]
Branching Factor	state[T.working memory task]:area[T.CA3]	-0.005 (0.003)	-1.537	> 1 [0.124]	[-0.012, 0.001]
Branching Factor	Group Var	1.000 (--)	--	-- [--]	[--, --]
Branching Factor	Group Var	0.002 (--)	--	-- [--]	[--, --]

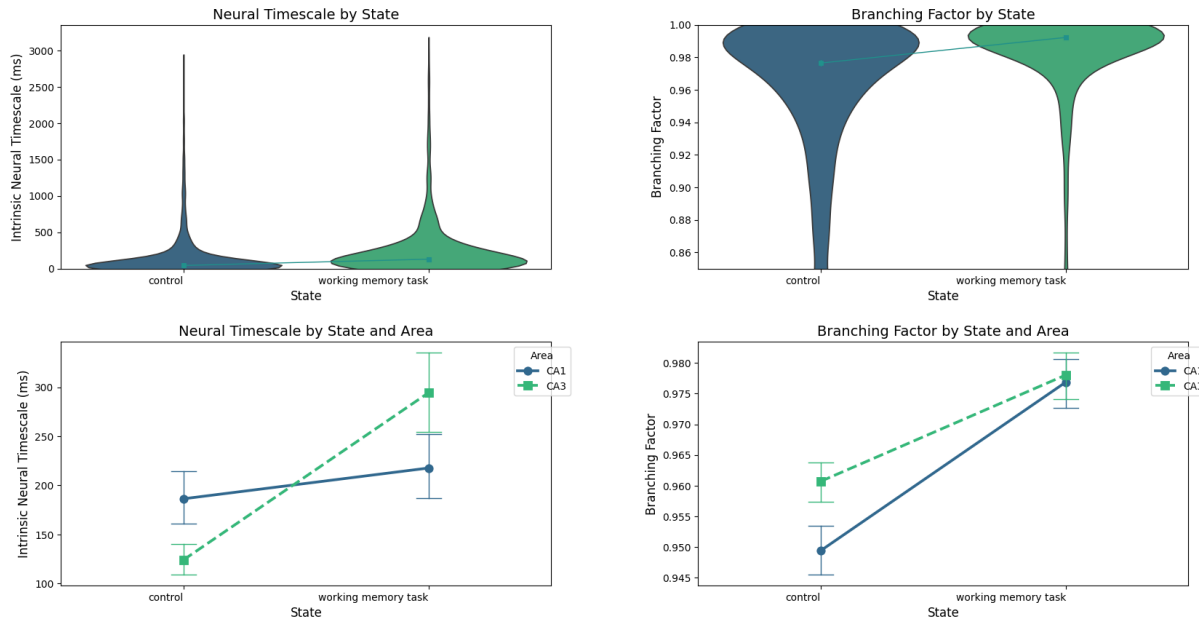
Animal: Cor



Between-Task Analysis Results for Animal Cor

Measure	Predictor	Coefficient (SE)	z-value	p-value (Bonferroni-corrected) [uncorrected]	CI 95%
Neural Timescale	Intercept	184.597 (419.227)	0.440	> 1 [0.660]	[-637.073, 1006.268]
Neural Timescale	state[T.working memory task]	68.421 (26.680)	2.564	0.114 [0.010]	[16.129, 120.714]
Neural Timescale	area[T.CA3]	18.540 (21.281)	0.871	> 1 [0.384]	[-23.171, 60.250]
Neural Timescale	state[T.working memory task]:area[T.CA3]	-3.470 (36.974)	-0.094	> 1 [0.925]	[-75.937, 68.998]
Neural Timescale	Group Var	1.000 (-)	--	-- [-]	[-, -]
Neural Timescale	Group Var	175501.440 (-)	--	-- [-]	[-, -]
Branching Factor	Intercept	0.956 (0.056)	16.930	< 0.001 [<> 0.001]	[0.845, 1.067]
Branching Factor	state[T.working memory task]	0.021 (0.004)	5.775	< 0.001 [<> 0.001]	[0.014, 0.028]
Branching Factor	area[T.CA3]	-0.015 (0.003)	-5.270	< 0.001 [<> 0.001]	[-0.021, -0.009]
Branching Factor	state[T.working memory task]:area[T.CA3]	-0.006 (0.005)	-1.252	> 1 [0.211]	[-0.016, 0.004]
Branching Factor	Group Var	1.000 (-)	--	-- [-]	[-, -]
Branching Factor	Group Var	0.003 (-)	--	-- [-]	[-, -]

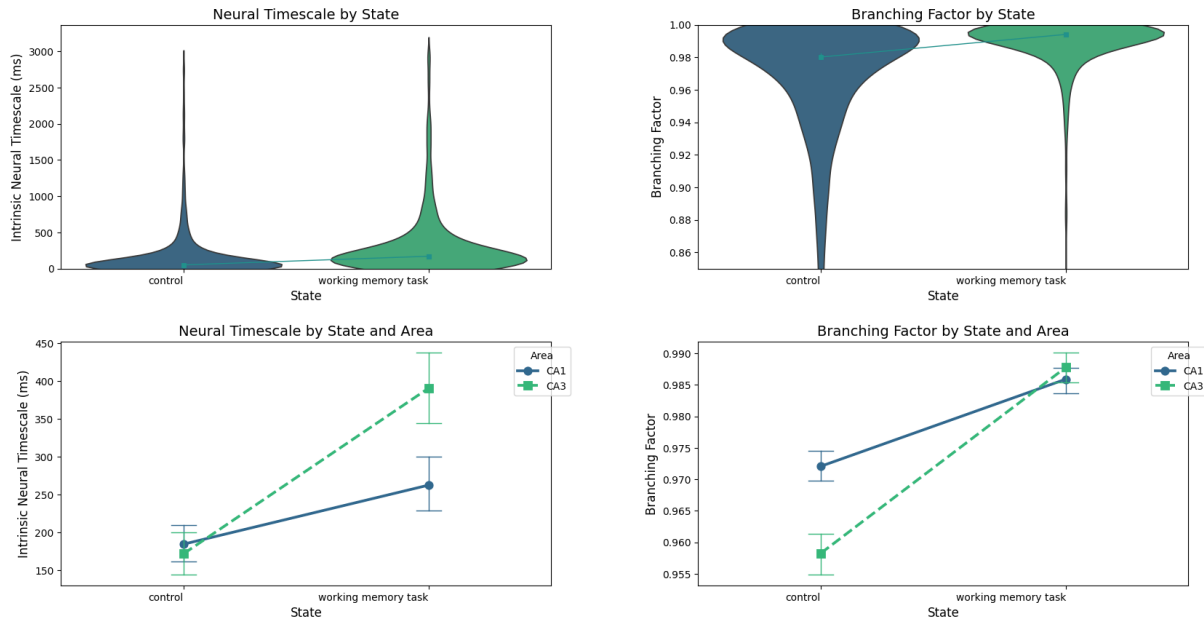
Animal: fra



Between-Task Analysis Results for Animal fra

Measure	Predictor	Coefficient (SE)	z-value	p-value (Bonferroni-corrected) [uncorrected]	CI 95%
Neural Timescale	Intercept	186.364 (343.291)	0.543	> 1 [0.587]	[-486.475, 859.202]
Neural Timescale	state[T.working memory task]	-31.349 (21.292)	1.472	> 1 [0.141]	[-10.383, 73.081]
Neural Timescale	area[T.CA3]	-62.218 (17.805)	-3.494	0.005 [< 0.001]	[-97.114, -27.321]
Neural Timescale	state[T.working memory task]:area[T.CA3]	139.008 (29.625)	4.692	< 0.001 [< 0.001]	[80.944, 197.072]
Neural Timescale	Group Var	1.000 (-)	--	--	[--, --]
Neural Timescale	Group Var	117690.435 (-)	--	--	[--, --]
Branching Factor	Intercept	0.949 (0.048)	19.672	< 0.001 [< 0.001]	[0.855, 1.044]
Branching Factor	state[T.working memory task]	0.027 (0.003)	9.181	< 0.001 [< 0.001]	[0.022, 0.033]
Branching Factor	area[T.CA3]	0.011 (0.003)	4.515	< 0.001 [< 0.001]	[0.006, 0.016]
Branching Factor	state[T.working memory task]:area[T.CA3]	-0.010 (0.004)	-2.435	0.164 [0.015]	[-0.018, -0.002]
Branching Factor	Group Var	1.000 (-)	--	--	[--, --]
Branching Factor	Group Var	0.002 (-)	--	--	[--, --]

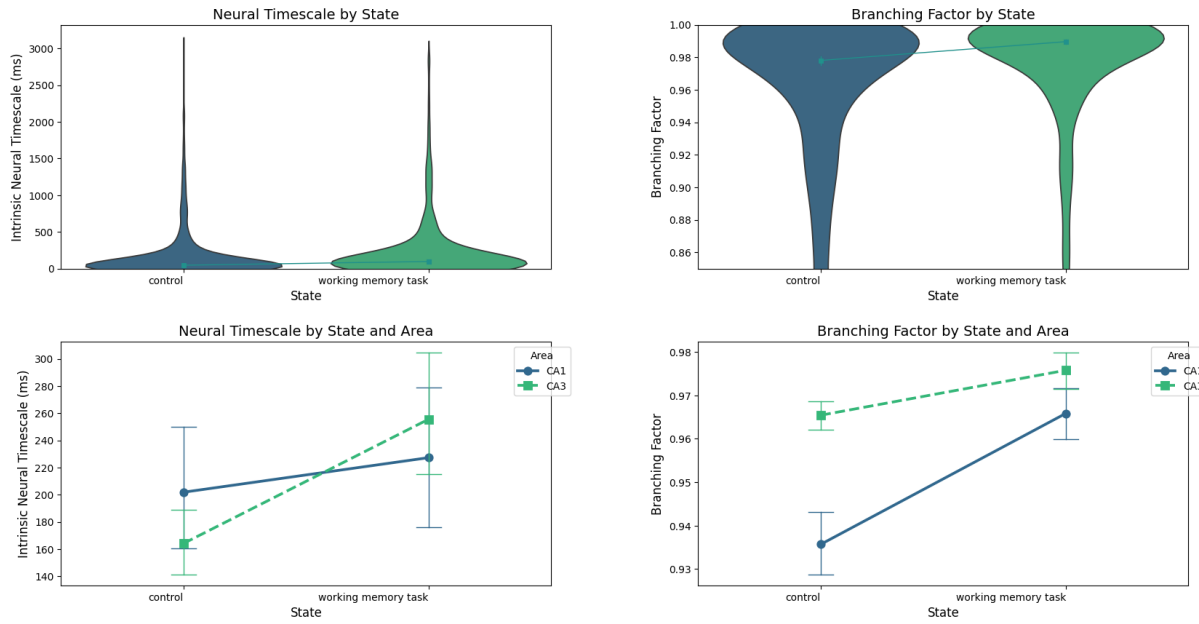
Animal: bon



Between-Task Analysis Results for Animal bon

Measure	Predictor	Coefficient (SE)	z-value	p-value (Bonferroni-corrected) [uncorrected]	CI 95%
Neural Timescale	Intercept	184.448 (407.971)	0.452	> 1 [0.651]	[-615.162, 984.057]
Neural Timescale	state[T.working memory task]	78.048 (23.375)	3.339	0.009 [< 0.001]	[32.234, 123.862]
Neural Timescale	area[T.CA3]	-12.663 (20.479)	-0.618	> 1 [0.536]	[-52.802, 27.476]
Neural Timescale	state[T.working memory task]:area[T.CA3]	140.871 (33.095)	4.257	< 0.001 [< 0.001]	[76.005, 205.737]
Neural Timescale	Group Var	1.000 (--)	--	--	[--, --]
Neural Timescale	Group Var	166226.769 (--)	--	--	[--, --]
Branching Factor	Intercept	0.972 (0.036)	27.235	< 0.001 [< 0.001]	[0.902, 1.042]
Branching Factor	state[T.working memory task]	0.014 (0.002)	6.765	< 0.001 [< 0.001]	[0.010, 0.018]
Branching Factor	area[T.CA3]	-0.014 (0.002)	-7.711	< 0.001 [< 0.001]	[-0.017, -0.010]
Branching Factor	state[T.working memory task]:area[T.CA3]	0.016 (0.003)	5.420	< 0.001 [< 0.001]	[0.010, 0.021]
Branching Factor	Group Var	1.000 (--)	--	--	[--, --]
Branching Factor	Group Var	0.001 (--)	--	--	[--, --]

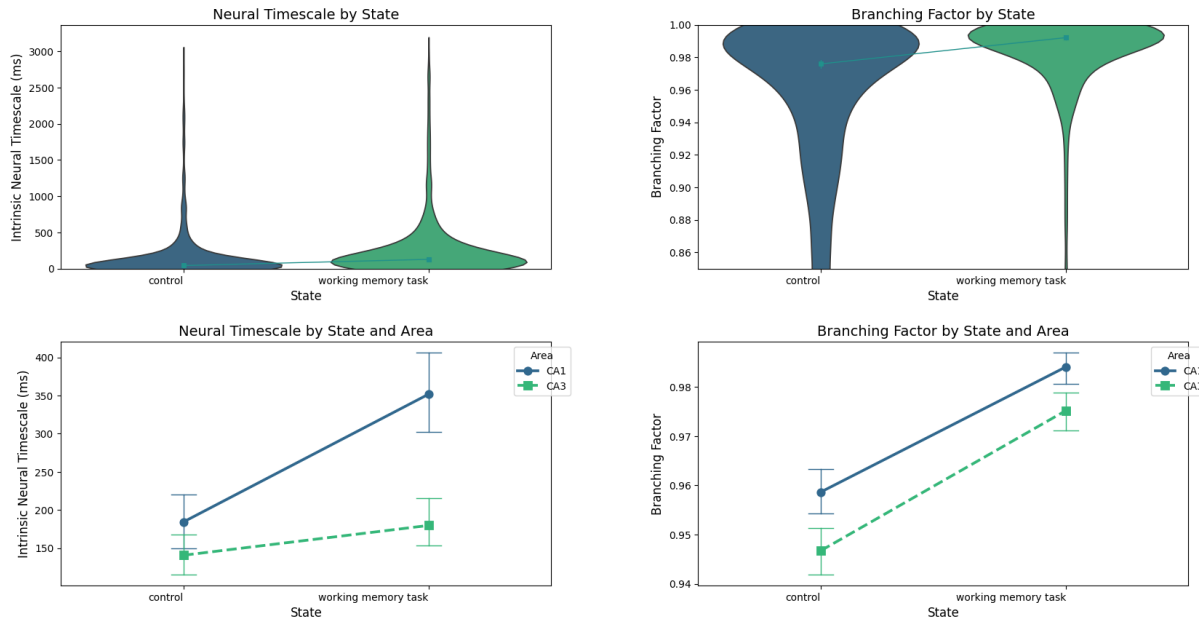
Animal: dud



Between-Task Analysis Results for Animal dud

Measure	Predictor	Coefficient (SE)	z-value	p-value (Bonferroni-corrected) [uncorrected]	CI 95%
Neural Timescale	Intercept	201.852 (381.806)	0.529	> 1 [0.597]	[-546.473, 950.178]
Neural Timescale	state[T.working memory task]	25.444 (31.381)	0.811	> 1 [0.417]	[-36.061, 86.949]
Neural Timescale	area[T.CA3]	-37.710 (25.802)	-1.462	> 1 [0.144]	[-88.280, 12.861]
Neural Timescale	state[T.working memory task]:area[T.CA3]	66.003 (40.993)	1.610	> 1 [0.107]	[-14.341, 146.347]
Neural Timescale	Group Var	1.000 (--)	--	-- [--]	[--, --]
Neural Timescale	Group Var	145335.342 (--)	--	-- [--]	[--, --]
Branching Factor	Intercept	0.936 (0.048)	19.389	< 0.001 [< 0.001]	[0.841, 1.030]
Branching Factor	state[T.working memory task]	0.030 (0.004)	7.599	< 0.001 [< 0.001]	[0.022, 0.038]
Branching Factor	area[T.CA3]	0.030 (0.003)	9.115	< 0.001 [< 0.001]	[0.023, 0.036]
Branching Factor	state[T.working memory task]:area[T.CA3]	-0.020 (0.005)	-3.821	0.001 [< 0.001]	[-0.030, -0.010]
Branching Factor	Group Var	1.000 (--)	--	-- [--]	[--, --]
Branching Factor	Group Var	0.002 (--)	--	-- [--]	[--, --]

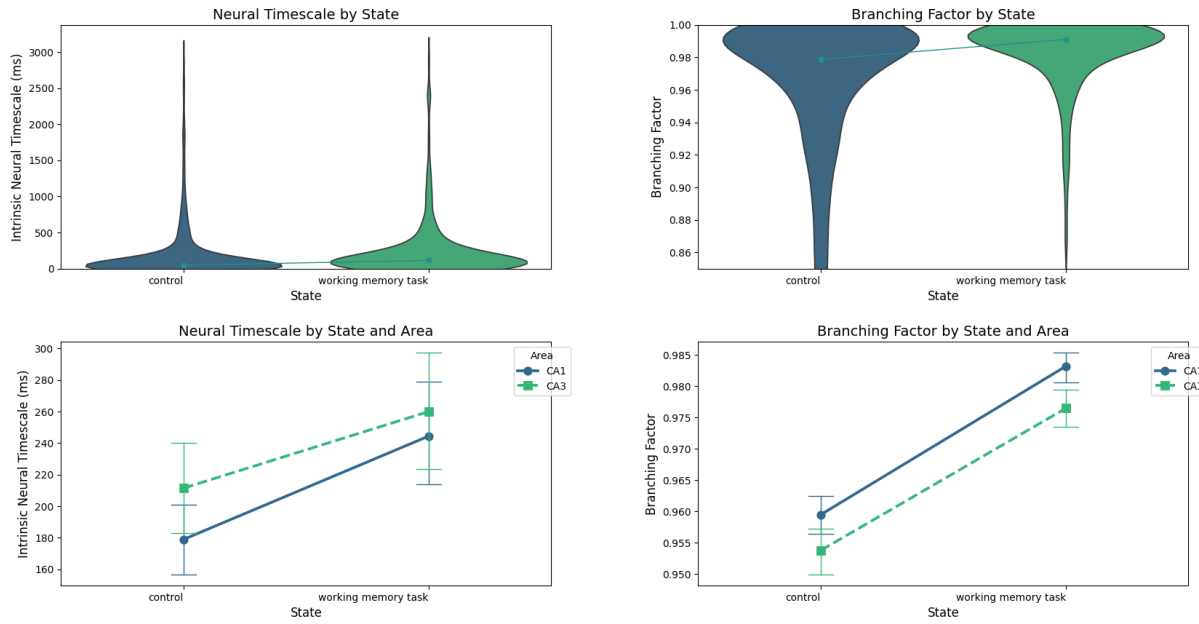
Animal: con



Between-Task Analysis Results for Animal con

Measure	Predictor	Coefficient (SE)	z-value	p-value (Bonferroni-corrected) [uncorrected]	CI 95%
Neural Timescale	Intercept	184.447 (387.617)	0.476	> 1 [0.634]	[-575.269, 944.162]
Neural Timescale	state[T.working memory task]	167.357 (26.033)	6.429	< 0.001 [< 0.001]	[116.333, 218.381]
Neural Timescale	area[T.CA3]	-43.729 (23.996)	-1.822	0.752 [0.068]	[-90.759, 3.302]
Neural Timescale	state[T.working memory task]:area[T.CA3]	-128.320 (36.591)	-3.507	0.005 [< 0.001]	[-200.037, -56.602]
Neural Timescale	Group Var	1.000 (-)	--	-- [--]	[--, --]
Neural Timescale	Group Var	149948.906 (-)	--	-- [--]	[--, --]
Branching Factor	Intercept	0.959 (0.046)	20.856	< 0.001 [< 0.001]	[0.869, 1.049]
Branching Factor	state[T.working memory task]	0.025 (0.003)	8.234	< 0.001 [< 0.001]	[0.019, 0.031]
Branching Factor	area[T.CA3]	-0.012 (0.003)	-4.190	< 0.001 [< 0.001]	[-0.017, -0.006]
Branching Factor	state[T.working memory task]:area[T.CA3]	0.003 (0.004)	0.703	> 1 [0.482]	[-0.005, 0.012]
Branching Factor	Group Var	1.000 (-)	--	-- [--]	[--, --]
Branching Factor	Group Var	0.002 (-)	--	-- [--]	[--, --]

Animal: egyptian vulture



Between-Task Analysis Results for Animal egyptian vulture

Measure	Predictor	Coefficient (SE)	z-value	p-value (Bonferroni-corrected) [uncorrected]	CI 95%
Neural Timescale	Intercept	178.888 (411.694)	0.435	> 1 [0.664]	[-628.018, 985.794]
Neural Timescale	state[T.working memory task]	65.517 (21.820)	3.003	0.029 [0.003]	[22.751, 108.284]
Neural Timescale	area[T.CA3]	32.533 (18.271)	1.781	0.825 [0.075]	[-3.278, 68.344]
Neural Timescale	state[T.working memory task]:area[T.CA3]	-16.964 (30.984)	-0.548	> 1 [0.584]	[-77.692, 43.763]
Neural Timescale	Group Var	1.000 (6968237.313)	0.000	> 1 [1.000]	[-13657493.169, 13657495.169]
Neural Timescale	Group Var	169334.316 (--)	--	-- [-]	--, --
Branching Factor	Intercept	0.959 (0.046)	20.863	< 0.001 [<> 0.001]	[0.869, 1.050]
Branching Factor	state[T.working memory task]	0.024 (0.002)	9.724	< 0.001 [<> 0.001]	[0.019, 0.028]
Branching Factor	area[T.CA3]	-0.006 (0.002)	-2.795	0.057 [0.005]	[-0.010, -0.002]
Branching Factor	state[T.working memory task]:area[T.CA3]	-0.001 (0.003)	-0.290	> 1 [0.772]	[-0.008, 0.006]
Branching Factor	Group Var	1.000 (6968365.148)	0.000	> 1 [1.000]	[-13657743.721, 13657745.721]
Branching Factor	Group Var	0.002 (--)	--	-- [-]	--, --